JUSTUS-LIEBIG-
UNIVERSITÄT
GIESSEN

London Dispersion:
From Molecular Balances to Organic Synthesis

Kumulative Dissertation

zur Erlangung des akademischen Grades

„Doctor rerum naturalium“

– Dr. rer. nat. –

Eingereicht am Fachbereich Biologie und Chemie der

Justus-Liebig-Universität Gießen

Vorgelegt von

Marvin Hans-Julian Domanski

Angefertigt im Zeitraum von Juni 2022 bis August 2026

Erstgutachter: Prof. Dr. Peter R. Schreiner, PhD

Zweitgutachter: Prof. Dr. Richard Göttlich

Ich kann | Ich will | **Ich werde**

Ich erkläre: Ich habe die vorgelegte Dissertation selbstständig und ohne unerlaubte fremde Hilfe und nur mit den Hilfen angefertigt, die ich in der Dissertation angegeben habe. Alle Textstellen, die wörtlich oder sinngemäß aus veröffentlichten Schriften entnommen sind, und alle Angaben, die auf mündlichen Auskünften beruhen, sind als solche kenntlich gemacht. Ich stimme einer evtl. Überprüfung meiner Dissertation durch eine Antiplagiat-Software zu. Bei den von mir durchgeführten und in der Dissertation erwähnten Untersuchungen habe ich die Grundsätze guter wissenschaftlicher Praxis, wie sie in der „Satzung der Justus-Liebig-Universität Gießen zur Sicherung guter wissenschaftlicher Praxis“ niedergelegt sind, eingehalten.

Angaben zu auf künstlicher Intelligenz (KI) basierender Hilfen wie ChatGPT oder SchulKI von OpenAI oder Gemini von Google zur Erstellung meiner Dissertation (Zutreffendes angekreuzt): ☐ Ich habe bei der Erstellung dieses Textes kein KI-Tool verwendet.

☒ Ich habe ein KI-Tool in den folgenden Bereichen eingesetzt (Mehrfachnennungen möglich):

- ☐ Ideen finden, meine Kreativität anregen
- ☐ Verstehen von Konzepten, Recherche von Fakten und Definitionen
- ☒ Optimierung eines von mir verfassten Textes
- ☐ Erstellen ganzer Textpassagen nach meinen Vorgaben

Folgende KI-Tools habe ich verwendet, damit aufgeführte Teile meines Textes von dem Tool wie folgt profitiert haben:

Ich habe das KI-Tool ChatGPT (OpenAI) genutzt um vereinzelt vorformulierte Textabschnitte sprachlich zu optimieren.

_____ _____

Datum Unterschrift

Table of Contents

Zusammenfassung vi

Abstract vii

Publikationsliste viii

Konferenzbeiträge ix

1. Introduction 1

1.1 London Dispersion 2

1.2 London Dispersion Persists in Solution 5

1.3 Cyclooctatetraene as Molecular Balance 7

1.4 Additivity of London Dispersion Interactions 10

1.5 London Dispersion as Stereochemical Determinant 11

1.6 Steric Attraction not Steric Hindrance Makes a Better Catalyst 13

1.7 Dispersion Energy Donors Enhance Reactivity and Selectivity 19

1.8 The Johnson−Corey−Chaykovsky Epoxidation 20

1.9 References 23

2. Publications 31

2.1 London Dispersion Favors Sterically Hindered Diarylthiourea Conformers in Solution 31

2.2 Assessing Benzene Dimer Interactions in Solution With a Molecular Balance 41

2.3 Quantifying Anisole Dimer Interactions in Solution with a Molecular Balance 49

2.4 London Dispersion Favors *Cis* Selectivity in the Johnson−Corey−Chaykovsky Epoxidation 57

3. Danksagung 71

Zusammenfassung

London’sche Dispersionswechselwirkungen sind als attraktiver Bestandteil der van-der-Waals-Wechselwirkungen in der Chemie allgegenwärtig. Sie stellen eine wesentliche Triebkraft für die Aggregation von Molekülen dar und können darüber hinaus die Struktur, Stabilität und Selektivität chemischer Systeme maßgeblich beeinflussen.

Ziel dieser Arbeit ist es zu zeigen, wie sich London’sche Dispersionswechselwirkungen durch die gezielte Kombination geeigneter Molekülfragmente verstärken lassen, welchen Einfluss das Lösungsmittel auf diese Wechselwirkungen ausübt und inwieweit bereits etablierte chemische Reaktionen diese Kräfte unbewusst nutzen oder bislang unzureichend berücksichtigen. Darüber hinaus wird untersucht, wie die Berücksichtigung von Dispersionswechselwirkungen unser Verständnis von Reaktionsmechanismen erweitern und in einzelnen Fällen sogar neu definieren kann.

In der ersten Forschungsarbeit stand die gezielte Verstärkung und Quantifizierung von London’schen Dispersionswechselwirkungen im Mittelpunkt. Hierzu wurden Diphenylthioharnstoffe mit Dispersionsenergie-Donoren in *meta*-Position untersucht, wodurch das bis dahin wenig beachtete *syn-syn*-Konformer stabilisiert werden konnte. Mithilfe von Tieftemperatur-NMR-Spektroskopie und quantenchemischen Methoden wurden die Beiträge verschiedener Substituenten zur Konformationsstabilisierung und die Stärke der zugrunde liegenden Dispersionswechselwirkungen quantifiziert.

Die zweite Publikation untersucht den Einfluss von Lösungsmitteln auf schwache nichtkovalente Wechselwirkungen. Mithilfe einer Cyclooctatetraen-(COT)-basierten molekularen Waage wurde zunächst das einfachste aromatische System, das Benzoldimer, betrachtet. Anschließend wurde in der dritten Publikation beobachtet, wie sich der Lösungsmitteleinfluss durch die Einführung polarer Gruppen verändert.

Abschließend wurde in der vierten Publikation gezeigt, wie die gewonnenen Erkenntnisse genutzt werden können, um etablierte Reaktionsmechanismen kritisch zu hinterfragen. Am Beispiel der Johnson–Corey–Chaykovsky-Epoxidierung konnte nachgewiesen werden, dass die beobachtete Selektivität nicht primär durch sterische Abstoßung bestimmt wird, wie lange angenommen, sondern maßgeblich durch attraktive London’sche Dispersionswechselwirkungen zwischen sterisch anspruchsvollen Substituenten beeinflusst wird.

Abstract

London dispersion interactions are a ubiquitous attractive component of van der Waals interactions in chemistry. They represent a key driving force for molecular aggregation and can significantly influence the structure, stability, and selectivity of chemical systems.

The aim of this work is to demonstrate how London dispersion interactions can be enhanced through the targeted combination of molecular fragments, what influence the solvent exerts on these interactions, and to what extent established chemical reactions already exploit or insufficiently account for these forces. Furthermore, it is investigated how considering dispersion interactions can extend our understanding of reaction mechanisms and, in some cases, even redefine them.

In the first research article, the targeted enhancement and quantification of London dispersion interactions was the central focus. Diphenylthioureas with dispersion energy donors in the *meta*-position were investigated, which enabled stabilization of the previously little-studied *syn–syn* conformer. Using low-temperature NMR spectroscopy and quantum chemical methods, the contributions of different substituents to conformational stabilization and the strength of the underlying dispersion interactions were quantified.

The second publication investigates the influence of solvents on weak noncovalent interactions between aromatic moieties. Using a cyclooctatetraene (COT)-based molecular balance, the simplest aromatic system, the benzene dimer, was first considered. In the third publication, it was subsequently observed how the solvent effect changes upon introduction of polar groups.

Finally, the fourth publication shows how the obtained insights can be used to critically re-evaluate established reaction mechanisms. In the case of the Johnson–Corey–Chaykovsky epoxidation, it was demonstrated that the observed selectivity is not primarily governed by steric repulsion, as long assumed, but is instead significantly influenced by attractive London dispersion interactions between sterically demanding substituents.

Publikationsliste

Lars Rummel, Marvin H. J. Domanski, Heike Hausmann, Jonathan Becker, and Peter R. Schreiner, London Dispersion Favors Sterically Hindered Diarylthiourea Conformers in Solution, *Angew. Chem. Int. Ed.* **2022**, *61*, e202204393; *Angew. Chem.* **2022**, *134*, e202204393. **DOI:** 10.1002/anie.202204393

Niklas Broel, Johanna V. Stein, Franziska V. Wengner, Marvin H. J. Domanski, Tatyana Zhuk and Martin Gand, Dryinones: Structure Elucidation of Red Colorants from Submerged Cultures of Pleurotus dryinus, *J. Nat. Prod.* **2025**, 88, 2602–2609. **DOI:** 10.1021/acs.jnatprod.5c00926

Marvin H. J. Domanski, Michael Fuhrmann and Peter R. Schreiner, London Dispersion as a Design Element in Molecular Catalysis, *J. Am. Chem. Soc.* **2025**, *147*, 29611–29623. **DOI:** 10.1021/jacs.5c09212

Marvin H. J. Domanski, Michael Fuhrmann, Nils F. Hacket, Heike Hausmann, and Peter R. Schreiner, Assessing Benzene Dimer Interactions in Solution With a Molecular Balance**,** *Chem. Eur. J.* **2026**, 32, *e71126*. **DOI:** 10.1002/chem.71126

Marvin H. J. Domanski, Saskia N. Krug, Heike Hausmann, and Peter R. Schreiner, Quantifying Anisole Dimer Interactions in Solution with a Molecular Balance, *Eur. J. Org. Chem.*, **2026**, *29*, e70649. **DOI:** 10.1002/ejoc.70649

Marvin H. J. Domanski, Lars Rummel, Saskia N. Krug, Heike Hausmann, Ephrath Solel, and Peter R. Schreiner, London Dispersion Favors *Cis* Selectivity in the Johnson–Corey–Chaykovsky Epoxidation *J. Org. Chem.* **2026**, 91, 4829–4841. **DOI:** 10.1021/acs.joc.6c00154

Konferenzbeiträge

Vortragspräsentation

Lars Rummel, Marvin H. J. Domanski, Heike Hausmann, Jonathan Becker, and Peter R. Schreiner, London Dispersion Favors Sterically Hindered Diarylthiourea Conformers in Solution, Bunsen-Tagung, Gießen, Deutschland, 2022.

Posterpräsentation

Marvin H. J. Domanski, Lars Rummel, and Peter R. Schreiner, London Dispersion in Organic Synthesis, The van der Waals – London Discussion, Straßburg, Frankreich 2023.

Posterpräsentation

Marvin H. J. Domanski, Lars Rummel, Ephrath Solel, Heike Hausmann, Saskia N. Krug and Peter R. Schreiner, Dispersion Favors *cis*-Selectivity in the Johnson-Corey-Chaykovsky Epoxidation, 3rd International Conference on Noncovalent Interactions, Belgrad, Serbien, 2024.

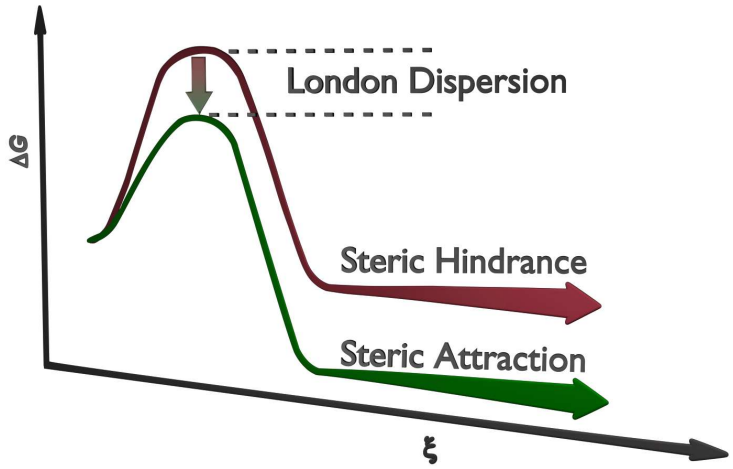
Vortragspräsentation

Marvin H. J. Domanski, Michael Fuhrmann, Nils F. Hacket, Heike Hausmann, Peter R. Schreiner, Assessing the Benzene Dimer in Solution, Physical Organic Chemistry Conference GRC, Holderness, USA, 2025.

Posterpräsentation

Marvin H. J. Domanski and Peter R. Schreiner, *London Dispersion:* From Molecular Balances to Application in Organic Synthesis, Armin-de-Meijere-Gedenksymposium, Göttingen, Deutschland, 2026.

1. Introduction



Abstract

This Perspective describes the role of London dispersion (LD) interactions as a key factor controlling chemical selectivity. LD arises from the correlated motion of electrons, leading to subtle yet significant stabilization (“steric attraction”), and counterbalances, together with other noncovalent interactions, Pauli exchange repulsion (“steric hindrance”). While chemists have largely relied on the latter to rationalize selectivities in catalyzed reactions, we emphasize here the role LD plays as a key design element in chemical reactions, in particular, for catalyst development.

***Reference*:**

Marvin H. J. Domanski, Michael Fuhrmann and Peter R. Schreiner, *J. Am. Chem. Soc.* **2025**, *147*, 29611–29623.

DOI: 10.1021/jacs.5c09212

Reproduced (or adapted) with permission from © 2026 American Chemical Society.

1.1 London Dispersion

London dispersion (LD) is a fundamental quantum mechanical phenomenon arising from electron correlation in atoms and molecules.[1] A common “visualization” is to think of electron movements causing very small imbalances in electron density, resulting in short-lived dipoles (Fig. 1). In turn, these transient dipoles induce dipoles in neighboring atoms, resulting in attractive interactions that are universally present across all matter.[2]

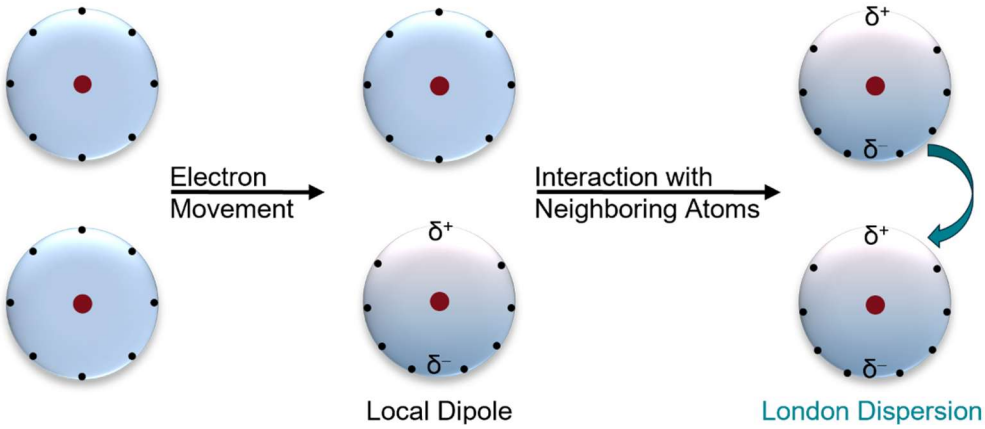


Figure 1. Schematic illustration of London Dispersion.

The theoretical foundation for LD was first established by London and Eisenschitz in 1930.[1,3] The term “dispersion” derives from optical dispersion, reflecting the connection between London's theoretical description of these interactions and the frequency-dependent response of matter to electromagnetic radiation. Their work provided a mathematical description of these interactions, demonstrating that the dispersion energy follows an r^{-6} dependence, which is now commonly represented by equation 1.[4–9]

$$E_{LD} = -\frac{C_6}{r^6} \tag{1}$$

C_6, the dipole-dipole dispersion coefficient, is determined by the polarizability α and ionization energy I of the interacting partners. The negative sign highlights the attractive nature of LD, with its strength rapidly decreasing as distance r increases. Larger system sizes exhibit greater polarizability α (Fig. 2) and therefore interact stronger via LD.[10] This has led to the notion of dispersion energy donors (DED) and mutual acceptors which follow this trend.[11–13]

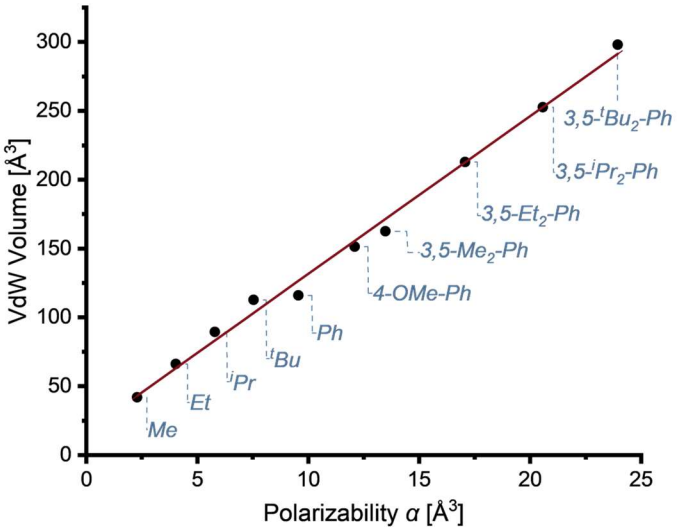


Figure 2. Relationship between van der Waals volume and polarizability *α* for selected molecules.

In the past decade, LD has been increasingly recognized but not yet used as a routine design element to control chemical reactivity, in particular, for catalyst design. One reason may be that, in contrast to approximately formulated Pauli repulsion (eq. 2), LD has no analogue that would reflect human experience, and it is much easier to conceptualize steric repulsion rather than steric attraction. Pauli repulsion is always positive (thus repulsive) and generally much stronger at short distances due to its r^{-12} dependence.[14–17]

$$E_{\text{Pauli}} = \frac{C_{12}}{r^{12}} \qquad (2)$$

These factors likely explain why chemists have traditionally relied on steric arguments, such as those in the Cram model where the stereochemical outcome of nucleophilic addition to carbonyls is exclusively explained via steric repulsion (predominantly of alkyl groups).[18] However, Pauli repulsion only dominates at very short distances, typically below ~2.5 Å for hydrocarbons. Beyond that, its influence declines rapidly, and LD becomes the prevailing interaction. This shift in relative importance is visualized in the characteristic shape of the simplified van der Waals-potential shown in Figure 3[16] and is the very reason why we discuss equilibrium structures.

While London's insights were groundbreaking, the significance of LD interactions remained largely overlooked for many decades. These interactions were often dismissed as "too weak" to influence molecular behavior meaningfully. Many practicing chemists argued that such weak interactions would not be relevant in solution because solute-solvent interactions should override such seemingly faint forces.

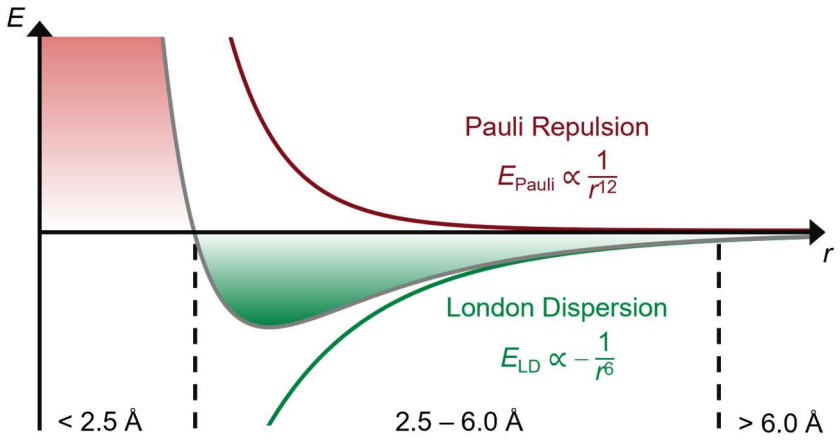


Figure 3. Schematic illustration between LD (green) and Pauli repulsion (red) depending on distance *r*. Resulting binding potential curve in gray.

This dismissal is especially surprising, given that LD helps explain fundamental chemical properties, such as the increasing boiling points, the difference in isomerization energies of linear and branched alkanes,[19] as well as *π*-*π* stacking structures in graphite and graphene and the attraction between *σ* and *π* systems.[20–22] In computational chemistry the early implementations of density functional theory (DFT) also dismissed the dispersion component[23] and it was to a good part the correction of this deficiency[24–28] that paved the way to analyze the role LD actually plays. Hence, the implementation of LD drastically improved the accuracy of affordable DFT and other approaches to be able to study increasingly larger molecules[29,30] (for which LD becomes increasingly relevant, *vide supra*), and put the proper physics back into the theoretical modeling.[31–33] Dispersion-corrected quantum chemical methods fall into three broad categories: (i) empirical corrections (DFT-D*n*), where atom-pairwise dispersion terms are added to conventional DFT energies;[34] (ii) nonlocal functionals (vdW-DF), which incorporate dispersion directly into the exchange-correlation functional via nonlocal correlation terms;[35] (iii) density-based methods (many-body dispersion),[36] which derive dispersion interactions from the electron density and atomic properties.[37] These approaches differ in cost, accuracy, and applicability,[36,38] but all share the goal of restoring missing long-range correlation to otherwise dispersion-uncorrected functionals.[39] Additionally, computational tools became available to visualize LD and other noncovalent interactions (NCIs).[40–42]

1.2 London Dispersion Persists in Solution

Molecular balances can be designed to probe LD interactions[43] through two thermodynamically accessible and spectroscopically discernible states: a “folded” state, where the interacting groups are in close proximity and an “unfolded” state, where they are spatially separated, thereby preventing their direct interaction (Fig. 4).

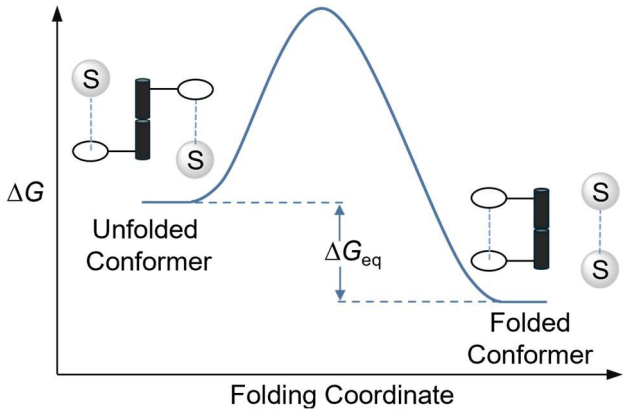


Figure 4. Concept of a two-state molecular torsion balance to determine LD interactions in solution.

The equilibrium between these states often provides a good measure of the interaction strength, with stronger NCIs shifting the balance toward the folded state.[44–46] Among the various designs, torsional balances have been particularly useful in isolating and quantifying LD interactions.[43,45–47] One of the first, and most prominent examples was published in 1994 by Wilcox and coworkers, who utilized an aryl-ester balance to study alkyl-arene interactions in solution (Fig. 5).

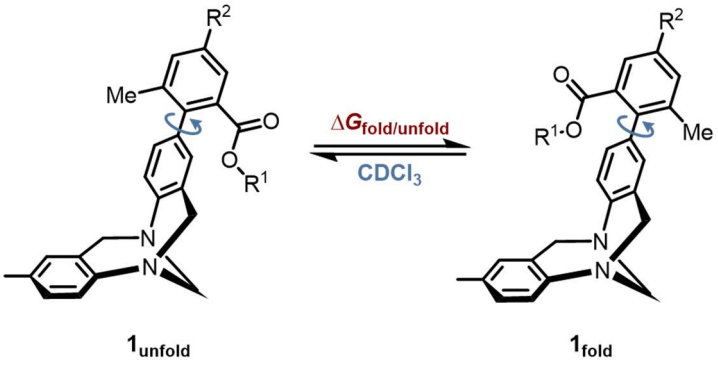


Figure 5. Wilcox-Balance for investigation of alkyl-arene interactions.

The rotation around the aryl-aryl bond is slow enough to distinguish between both conformations by ^{1}H NMR spectroscopy. While a methyl ester does not show any preference towards conformer **1**$_{\mathbf{unfold}}$ or **1**$_{\mathbf{fold}}$, as the distance towards the aryl group was too great, a larger *tert*-butyl residue was observed to shift the equilibrium to the more crowded conformer **1**$_{\mathbf{fold}}$, due to attractive CH-π contacts.[18] As only specific

interactions could be captured and the choice of solvent was only limited to chloroform, the results had to be taken with caution.

One prominent observation was that all interactions are weaker, compared to their gas phase counterpart. In solution there are additional interacting partners (solvent molecules, or dimers), which in turn, can compete with LD interactions. Chen and coworkers investigated this further by studying substituted pyridines **2, 3**, and their proton-bound dimers **4** in both the gas phase and dichloromethane (CH_2Cl_2) solution (Fig. 6). They found that LD interactions in CH_2Cl_2 solution were approximately 70% weaker than in the gas phase.[48] Follow-up studies expanded this view and included additional polar and nonpolar aprotic solvents.[49]

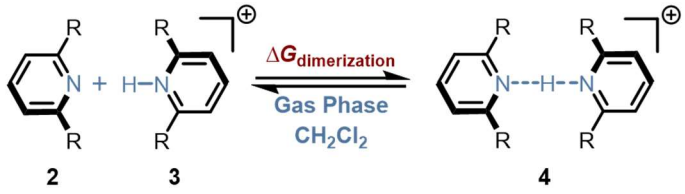


Figure 6. Interaction of pyridine-based proton dimers to investigate LD in the gas phase and in solution.

Cockroft and coworkers investigated how solvent interactions influence LD in polyaromatic stacking.[50] While gas-phase computations at ωB97X-D/def2-TZVP predicted significant stabilization (up to −6.4 kcal mol^{-1}) of the folded conformer **5$_{fold}$** by LD, solution-phase experiments consistently favored the unfolded structure **5$_{unfold}$** (Fig. 7). The smallest stabilization of **5$_{fold}$** in solution was observed for substituents such as R = 1-naphthyl (**5-1-Np**), with a measured Gibbs free energy of $\Delta G_{fold/unfold}$ = +1.1 kcal mol^{-1}. The population of **5$_{fold}$** in solution increases with the size of R, whose volume and ability for LD increases concomitantly. Pyrene (**5-Pyr**) increases the ratio of the closed conformer **5$_{fold}$** through LD by 1.0 kcal mol^{-1} to a total Gibbs free energy of $\Delta G_{fold/unfold}$ = +0.1 kcal mol^{-1}.

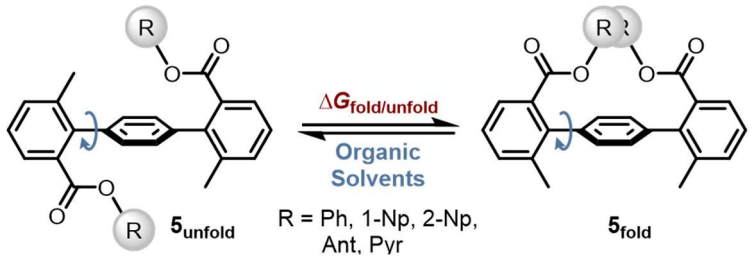


Figure 7. Molecular torsion balance to quantify stacking interactions between polyaromatic residues in solution.

In addition, the authors found a correlation between the degree of folding and the bulk solvent polarizability (*P*). Solvents with high bulk solvent polarizability, maximized with a solvent like CS_2, showed a reduced preference for **5$_{fold}$**, while solvents with low polarizability, like CH_2Cl_2, enhanced the population of the folded conformer **5$_{fold}$**.[50] One limitation of these balances is that they are substituted with heteroatoms, leading to local bond dipoles that will have, *inter alia*, coulombic interactions with the solvent; separating these from LD can be quite challenging.

1.3 Cyclooctatetraene as Molecular Balance

To minimize additional interactions introduced by heteroatoms in molecular balance systems, fully hydrocarbon-based scaffolds can be employed instead. One prominent example is cyclooctatetraene (**COT**). [51,52] **COT** was first synthesized by Willstätter and Waser in 1911 during efforts to access benzene-like molecules (Fig. 8).[53] However, in contrast to benzene, **COT** did not exhibit aromatic characteristics, but showed reactivity typical of localized double bonds instead.[53]

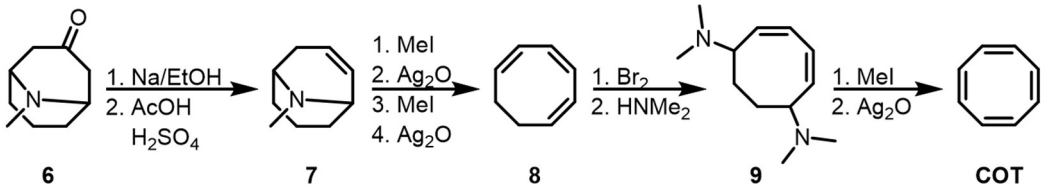


Figure 8. First synthesis of cyclooctatetraene by Willstätter in 1911.

While the original synthesis provided the first access to **COT** and enabled the initial investigation of its properties, the overall route was highly inefficient. A major breakthrough was subsequently achieved by Walter Reppe and co-workers, who developed a considerably more efficient synthesis through the cyclization of acetylene **10** using nickel cyanide under high pressure on large scale (Fig. 9).[54]

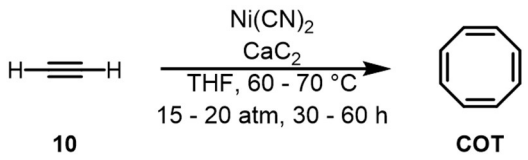


Figure 9. Large scale synthesis of cyclooctatetraene by Reppe in 1948.

Several decades later, Paquette and Streitwieser revisited the **COT** system and focused on substituted **COT** derivatives, which were among the first systems to be employed for the investigation of noncovalent interactions in solution.[55–58] In contrast to conventional torsion balances, the interconversion between the **1,4-** and **1,6-**isomers

of **COT** does not proceed through rotation around a single bond. Instead, conformational exchange occurs via a double bond shift (DBS) with first spectroscopic evidence already in 1962.[59] Computational studies conducted in the 1990s and early 2000s verified this mechanism.[58,60–62]

The interconversion of both the **1,4-** and **1,6-COT** isomers into their respective mirror images proceeds through a planar ring-inversion transition state (**TS_{RI}**, **TS_{RI}'**), in which the double bonds remain localized (Fig. 10). In the case of **1,6-COT**, the mirror images possess C_s symmetry and are therefore identical and spectroscopically indistinguishable. In contrast, the mirror images of **1,4-COT** exhibit C_2 symmetry and are chiral.

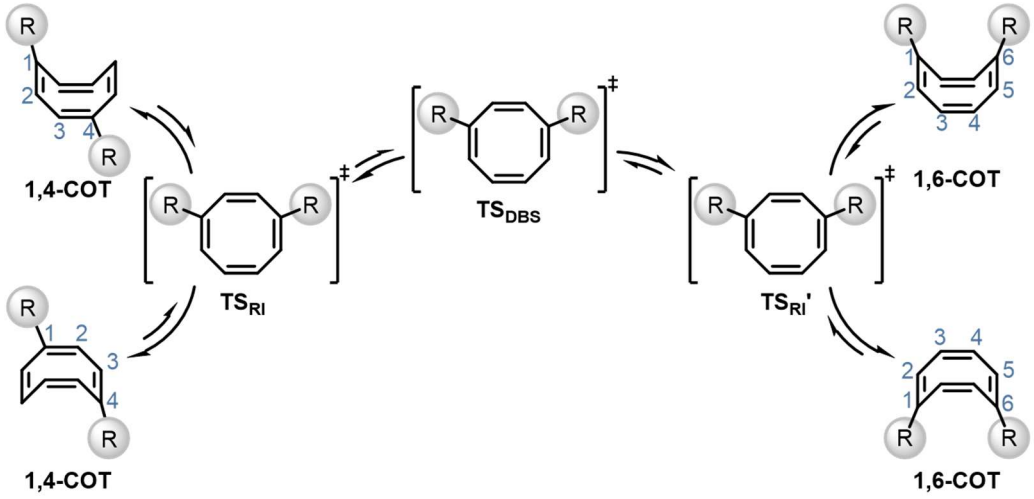


Figure 10. Double bond valance shift (DBS) and ring inversion (RI) of cyclooctatetraene.

Interconversion between the two ring-inversion transition states occurs through an additional transition state involving double-bond delocalization. This process is generally associated with a substantially higher activation barrier, typically ranging from ΔG = 13 to 23 kcal mol^{-1}, depending on the substitution pattern of the **COT** scaffold. Consequently, careful control of the equilibration temperature is essential to ensure complete conformational equilibration in experimental studies.

In 2020, Schümann and co-workers under the supervision of prof. Schreiner employed the **1,4-/1,6-COT** equilibrium as a molecular balance to quantify London dispersion interactions between saturated hydrocarbon substituents. Initial studies focused on *tert*-butyl groups,[63] which were later expanded to include larger DEDs such as adamantyl and diamantyl substituents (Fig. 11).[64] In these systems, the folded **1,6-COT** is stabilized by LD between the hydrocarbon substituents, thereby enabling the direct quantification of their energetic contributions in solution.



Figure 11. Equilibrium between **1,4-** and **1,6-COT** as a molecular balance to quantify LD in solution.

In contrast to the seminal molecular balance studies by Wilcox and Cockroft, which employed heteroatom-containing scaffolds,[50,65] the solvent dependence observed for the **COT**-based systems was considerably less pronounced.[63] For instance, in chlorinated solvents the conformational equilibrium broadly followed the polarizability of the solvent, with less polarizable solvents favoring the folded **1,6-COT** conformer to a greater extent. Nevertheless, the overall solvent-induced changes in equilibrium remained comparatively small, indicating that dispersion-driven stabilization in these hydrocarbon-only systems is less susceptible to solvent changes.[63,64]

Since then, the **COT**-based molecular balance has been applied extensively in a variety of studies investigating weak noncovalent interactions. For example, the system has been employed to quantify attractive interactions between silyl ether substituents as well as to probe the hydrogen-bonding interactions present geometrically confined water dimers.[66–68]

One goal is to determine whether the comparatively weak solvent dependence observed for saturated hydrocarbon substituents also applies to aromatic moieties such as phenyl groups. Furthermore, we were interested in understanding how these interactions are affected by the introduction of a heteroatom directly into the aromatic substituent, rather than into the molecular balance backbone itself.

1.4 Additivity of London Dispersion Interactions

In the previously discussed systems, the energetic contributions arising from LD typically range from approximately −0.1 to −1.0 kcal mol^{-1}, depending on the nature of the interacting substituents. However, in most of these studies the primary objective was not the maximization of dispersion interactions themselves, but rather their quantification and isolation within well-defined molecular environments.

Importantly, London dispersion interactions are, to a first approximation, pairwise additive.[33] Consequently, a given substituent is not restricted to interacting with only a single interaction partner, but instead experiences attractive interactions with its entire surrounding molecular environment over a range of intermolecular distances. The cumulative effect of these individually weak interactions can therefore lead to substantial overall stabilization energies in appropriately designed systems.

One of the most striking demonstrations of the additive nature of LD is found in the prime example of all-*meta*-*tert*-butyl-hexaphenylethane. In 1900, Gomberg attempted to synthesize parent hexaphenylethane via the dimerization of two trityl radicals (the first reported organic radical at the time), but the highly symmetric S_6-structure proved unattainable.[69–73] The argument for this instability was the apparent phenyl-phenyl repulsion. Notwithstanding this reasoning, Kahr and coworkers demonstrated the unexpected stability of all-*meta*-*tert*-butyl-hexaphenylethane for which they could even provide an X-ray structure analysis.[74] The question why the parent molecule does not exist –because it is sterically too hindered – while a closely related derivative that is obviously much more sterically crowded does exist, had apparently not been in focus at the time. Decades later a theoretical study suggested that the all-*meta*-*tert*-butyl groups actually are responsible for the stability of this highly crowded Gomberg system through mutually attractive intramolecular LD interactions (Fig. 12).[73]

NMR spectroscopic experiments confirmed this finding by observing all-*meta*-*tert*-butyl-hexaphenylethane also in solution.[75–77] Counterintuitively, the bulky substituents are responsible for the stability of this molecules despite high steric encumbrance. This conclusion is supported by the incorporation of even larger groups in the *meta*-positions such as adamantyl, which amplify LD interactions, leading to even higher stabilization.[76] Furthermore, the substitution pattern shows that the *meta*-substituents do not only interact with each other, but also with the opposing phenyl rings, as indicated by the green isosurfaces in Fig. 12[40,78,79] resulting in additional interactions.

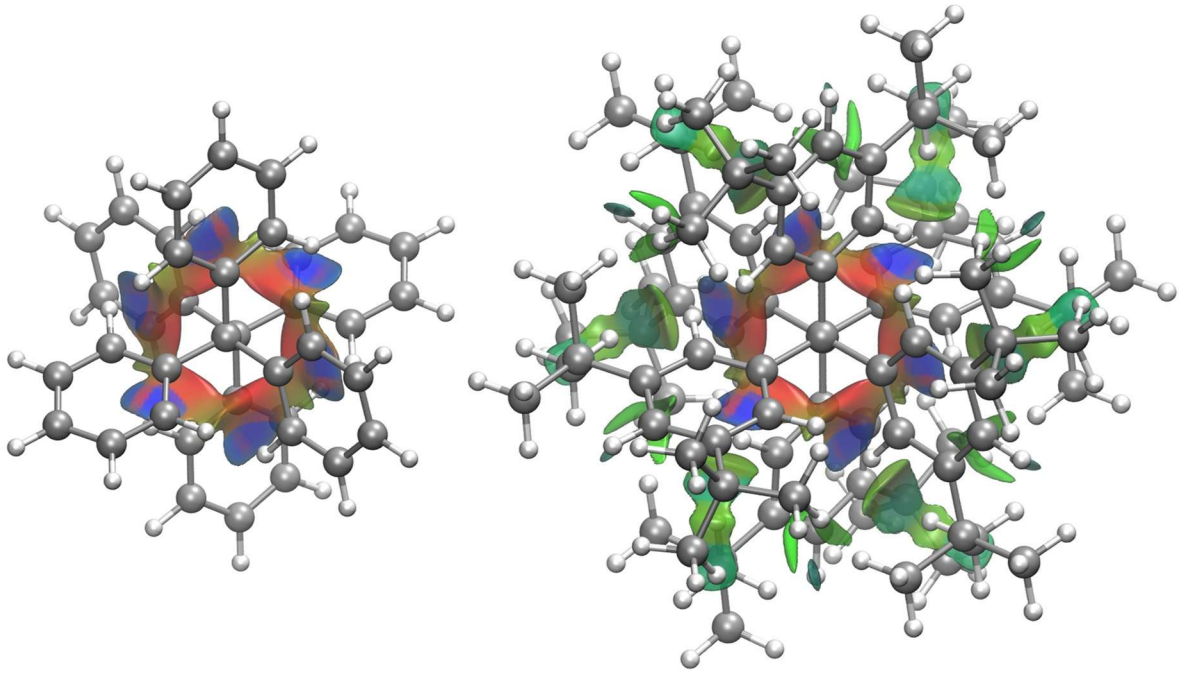


Figure 12. NCI plots of unsubstituted hexaphenylethane (left) and the *tert*-butyl substituted derivative (right) viewed along the central carbon-carbon bond. Blue isosurfaces show strong attraction, red isosurfaces show repulsion, while the substituted derivative benefits from stabilizing LD contacts (green isosurfaces).

Based on this, one of our goals is to systematically investigate, quantify, and ultimately maximize the interaction between *meta*-substituted benzene moieties using a molecular balance that allows easy synthesis of multiple structures.

1.5 London Dispersion as Stereochemical Determinant

The use of LD as a stereochemical determinant is under active investigation. In non-catalytic processes, such as the [4+2] cycloaddition of benzynes to furans[80] and the [2+2] cyclodimerization of substituted benzynes **11** and **12** (Fig. 13),[81] LD significantly impacts regioselectivity. In both cases, the proximal product $\mathbf{13}_{\mathbf{fold}}$, where two substituents are on same side, benefits from LD stabilization relative to the distal product $\mathbf{13}_{\mathbf{unfold}}$. With weak DEDs such as methyl groups, the [2+2] cyclodimerization provides a 1.1:1 ratio, only slightly favoring the proximal product $\mathbf{13}_{\mathbf{fold}}$. As the DED strength increases (via size and polarizability),[82] the product ratio changes in favor of the proximal (more hindered) product $\mathbf{13}_{\mathbf{fold}}$. *Tert*-Butyl groups increase the proximal product $\mathbf{13}_{\mathbf{fold}}$ ratio to 16:1 and adamantyl groups even to >20:1.[81]

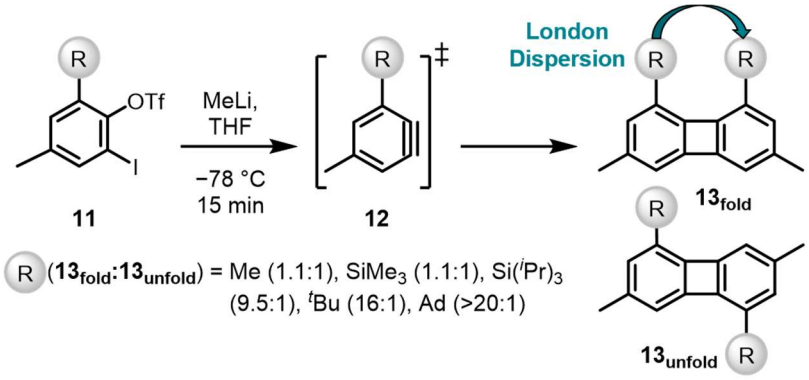


Figure 13. [2+2] Cyclodimerization of substituted benzynes. The proximal product is stabilized by LD interaction between the R groups. The selectivity of the reaction increases with the ability of R functioning as stronger dispersion energy donors (DEDs) with increasing size and polarizability.

All stereoselective catalyzed reactions must be executed under kinetic conditions because a non-equilibrium product mixture is desired. The difference in energy of the corresponding transition states is responsible for the product distribution and hence stereoselection. Lowering one transition structure, for example, through LD, will significantly change the product distribution even in nonequilibrium processes.[83,84] For example, the direct impact of LD on a transition structure was demonstrated with the mechanism and selectivities of photochemical dearomative cycloadditions of quinolines **14** with alkenes (Fig. 14).[85] After reversible radical addition, the reaction proceeds through a selectivity-determining radical recombination, favoring the *endo* product **15.** While methyl substituents **16a** lower the transition state energy by 0.7 kcal mol^{-1}, *tert*-butyl groups **16b** increase this value to 1.8 kcal mol^{-1}, which the authors attributed to LD.[85]

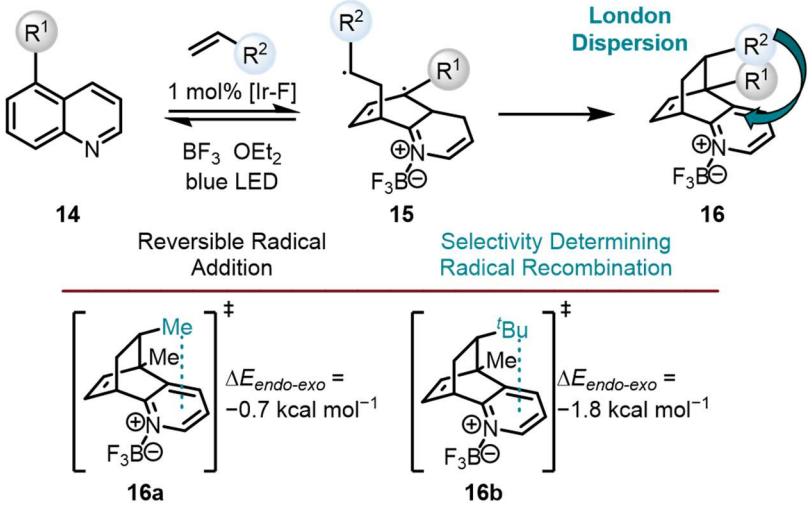


Figure 14. Schematic dearomative cycloaddition of quinolines and alkenes (top). Suggested transition structure of the radical recombination for the *endo* product (bottom).

1.6 Steric Attraction not Steric Hindrance Makes a Better Catalyst

Unfortunately, LD is still often neglected in the structure-activity relationships between catalysts and substrates.[12] However, it is essential to consider *all* NCIs, repulsive and attractive, to achieve a meaningful and physically sound understanding of a catalytic mechanism to design better catalysts.[86–91]

With the motivation to demonstrate the importance of LD in catalysis we elaborated on the versatile Corey–Bakshi–Shibata (CBS) reduction of prochiral ketones **17** with oxazaborolidine-based catalysts achieving high selectivity and high yields (Fig. 15).[92–97] The mechanism proposed by Corey in 1992 assumes that stereocontrol arises *exclusively* through steric repulsion between the substituent R on the catalyst **19** and a small R_S as well as a large R_L on the ketone substrate.

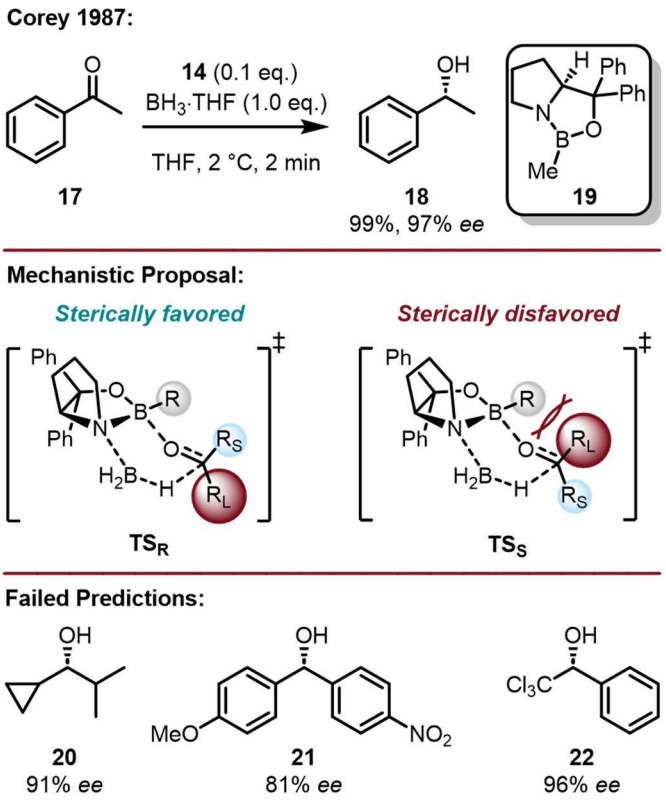


Figure 15. Corey–Bakshi–Shibata (CBS) reduction of acetophenone (top), proposed mechanism for the CBS reduction (middle), and selectivities of CBS reductions Corey's model failed to predict (bottom).

In this Cram-based model, the enantiodiscrimination is suggested to originate from a boat-like transition state in which the smaller substituent R_S faces R on boron to minimize steric repulsion, while the sterically demanding R_L points in the opposite direction **TS_R**. However, several mechanistic findings indicate that Corey's model is

incomplete and cannot deliver a satisfying explanation for the observed selectivities in several reductions; it is also not suitable to rationally improve the catalyst structure. For example, trichloroacetophenone reacts to the corresponding *R*-alcohol **22** with high enantioselectivity, which indicates that the large phenyl group faces the boron substituent R **TS$_S$**. Furthermore, the reduction of cyclopropyl isopropyl ketone, bearing two substituents of very similar steric size, provided an *ee* of 91% in favor of the *R*-enantiomer **20**.[96] The same holds true for the reduction of *p*-methoxy-*p*'-nitrobenzophenone, where again two substituents of similar size provide an *ee* of 81%.[96] Hence, steric repulsion alone cannot be taken as a rationale for the observed enantioselectivities.

Early computational work by Liotta et al. utilizing the MNDO semiempirical approach indicated that the hydride transfer in the CBS reduction proceeds in a chair-like TS rather than the initially proposed boat conformation.[98] Therefore, the phenyl substituents on the carbinol backbone align parallel with R_L to minimize steric repulsion. Liotta's results are further supported by Meyer investigating the role of steric repulsion in the transition structure of the borane reduction step via kinetic isotope effects.[99] He observed only a slight contribution of steric repulsion when bulky ketones were employed, which manifests itself in inverse ^{2}H kinetic isotope effects. However, this requires the reduction of acetophenone to proceed via the chair-like TS in which the boron substituent R only exerts little influence on the transition structure.[100,101] A more recent theoretical study by Lachtar et al. demonstrated a more diversified view of NCIs influencing the TS of the oxazaborolidine catalyzed reduction of ketimines.[102] However, the employed B3LYP/6-31G(d,p) computations do not include LD corrections and thus neglect major parts of these key NCIs when replacing phenyl groups of the catalyst by hydrogen.

These findings (Fig. 16) demonstrate the importance of LD in understanding the mechanism of the CBS reduction by employing LD and solvent corrections at the B3LYP-D3(BJ)/6−311G(d,p)SMD(THF) level of theory. First, the computationally obtained LD-corrected free energies of 13.7 kcal mol^{-1} for **TS1$_R$** and 15.7 kcal mol^{-1} for **TS1$_S$** match the experimental finding that the reaction proceeds at room temperature, in contrast to the energies of 29.8 kcal mol^{-1} and 31.7 kcal mol^{-1}, respectively, without the LD correction. The DLPNO-CCSD(T)/cc-pVTZ single-point energies using DFT-optimized **TS1$_R$** and **TS1$_S$** geometries are provided in brackets for comparison and underline the importance of LD. Furthermore, the computed free

energy of the hydride transfer (−2.0 kcal mol^{-1}) is consistent with previously determined experimental $\Delta\Delta G^{\ddagger}$ (−2.2 kcal mol^{-1}).[93] Note that the **TS1$_R$** and **TS1$_S$** geometries adopt chair-like conformations that are 3.8 kcal mol^{-1} lower in energy than the boat-like transition states initially proposed by Corey et al. Here, the lone pair of the ketone binds to the catalyst that faces the *smaller* substituent R_S in an *anti*-fashion to the electron-rich substituent as described by Corey. However, steric hydrogen-hydrogen repulsion is *not* discernible in the NCI plot analysis. On the other hand, stabilizing *σ-π* LD interactions favor **TS1R**. Decomposing the interaction energies of both transition structures into physically meaningful components with the help of symmetry-adapted perturbation theory (SAPT)[103,104] analysis further underlines these findings.

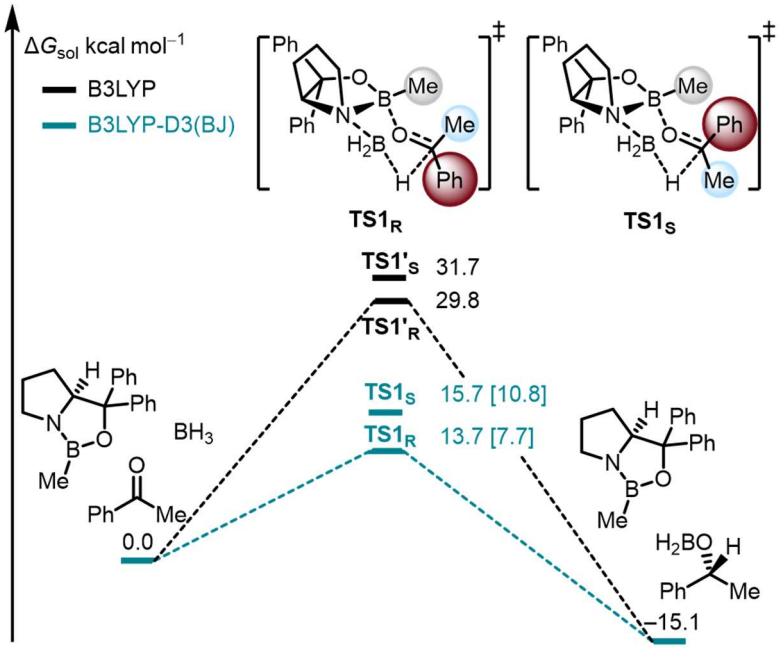


Figure 16. Potential energy surface of the CBS reduction of acetophenone at 2 °C. Free energies ($\Delta G_{275\,K}$) computed at B3LYP-D3(BJ)/6-311+G(d,p)-SMD(THF)//B3LYP-D3(BJ)/6-311Gd,p). Pathways with (teal) and without (black) dispersion correction. Energies in brackets are based on DLPNO-CCSD(T)/cc-pVTZ single-point energies (corrected for DFT-ZPVE).[105]

The experimental results strongly support the computations. For example, electron-deficient and poorly polarizable substituents (3,5-CF_3-C_6H_6 and C_6F_6) on the carbinol backbone gave very low *ee* or even racemic product mixtures in the reduction of acetophenone resulting from reduced LD interactions between substrate and catalyst. On the contrary, bulky and highly polarizable phenyl substituents on the catalyst maximize the *ee*s in the acetophenone reduction. More importantly, for the most challenging substrate butanone, the *ee*s increase with increasing DED-polarizability

(Fig. 17). Note that all catalysts depicted in Figure 17 perform *better* than those initially proposed by Corey et al. Competitive reduction experiments employing 3,3-dimethylbutan-2-one (pinacolone) and 2-pentanone counterintuitively show faster conversion of the sterically *more* hindered neopentyl substrate. This clearly demonstrates that increased steric bulk does not hamper the reaction rates, in fact, the opposite is the case: the reaction proceeds faster when DEDs are implemented in catalyst and substrate.

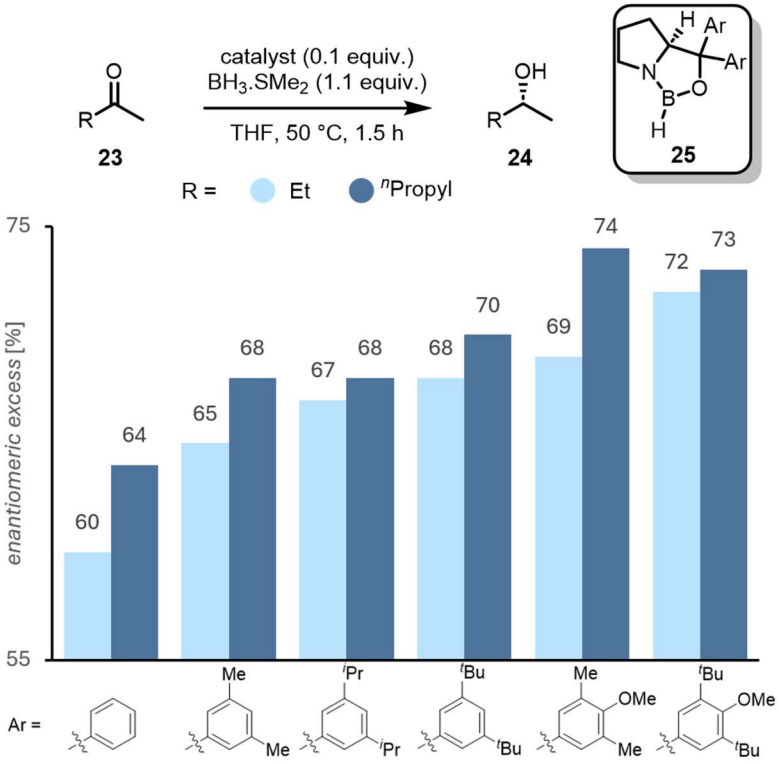


Figure 17. CBS reduction of butanone and 2-pentanone employing various DED-bearing catalysts.

Even the well-established Houk-List model[106] for understanding the stereochemical outcome of proline catalyzed inter- and intra-molecular aldol, Mannich, and Michael reactions, among others, had to be refined after taking into account LD interactions.[107] The D3 correction at B3LYP/6-31G(d), initially used by Houk et al.[106] changes the relative energies of the stereochemistry-determining transition structures by up to 3.0 kcal mol^{-1} when benzaldehyde **26** or isobutanal are employed in the proline-catalyzed aldol reaction with cyclohexanone (Fig. 18).[107] Four different stereochemical possibilities arise from the corresponding diastereomeric TSs **29-32**, with the *anti*-configuration being the energetically most preferred leading to the experimentally observed (*S*,*R*) aldol product **33**. For the reaction with benzaldehyde, the D3 correction between the energetically lowest (*S*,*R*) and (*S*,*S*) TSs accounts for

2.3 kcal mol^{-1} and a $\Delta\Delta G^{\ddagger}_{298\,K}$ between both competing TSs of 3.0 kcal mol^{-1} resulting in a population of the (*S*,*R*) isomer of 99.3% (B3LYP-D3/TZVP/SCRF=DMSO) reproducing the experimentally observed *ee* values. This strikingly large energy difference may come as a surprise but impressively demonstrates how large the impact of LD interactions even for small molecules or groups can be. That is, the Houk-List model can lead to large quantitative deviations and, in some cases, fails qualitatively as is the case in the proline-catalyzed reaction of acetone and pyrrole-2-carboxaldehyde. Strikingly, the inclusion of LD turns the initially computed 96% *ee* into an almost racemic product mixture prediction.[107]

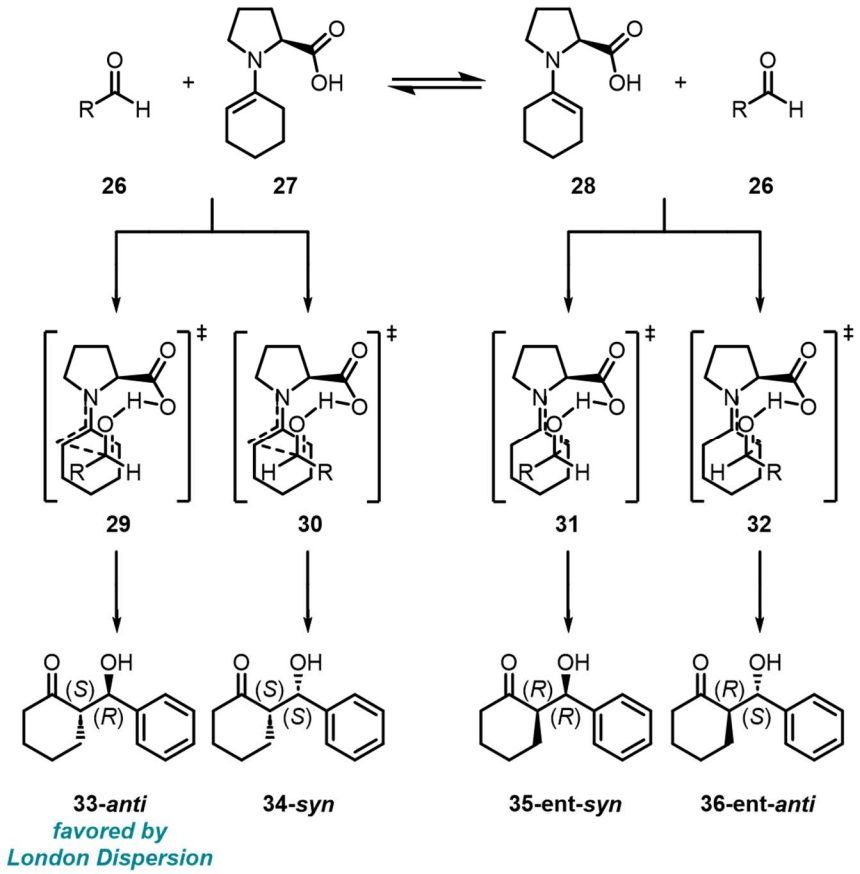


Figure 18. The Houk-List model for the proline catalyzed aldol reaction of cyclohexanone with aldehydes.[106,107]

Similarly, a preliminary analysis was put forth by the MacMillan group when they first introduced phenylalanine-derived imidazolidinone in the first highly enantioselective organocatalytic Diels-Alder reaction of iminium ions with dienes in 2000 (Fig. 19).[108] Rationalizing their remarkable results, the group argued that the selective formation of the (*E*)-iminium isomer **39** arises from avoiding steric clashes between the olefin substrate and the geminal methyl substituents on the imidazolidinone and the benzyl

group of the catalyst framework sterically shielding the *re* face of the iminium dienophile. Therefore, only the *si* face was suggested to remain exposed for the cycloaddition. In 2004, the Houk group supported this proposal computationally through investigating alkylation reactions of pyrroles developed by the MacMillan group[109] with B3LYP/ 6-31G(d) computations, which, however, do not account for LD interactions and lack polarization of the hydrogen atoms. This widely accepted MacMillan-Houk model was challenged by Grimme comparing fourteen X-ray crystal structures[110,111] with LD-corrected DFT (*e.g.*, B3LYP-D/def-QZVP-gf) geometries.[112] The computed relative energies with and without LD correction revealed a difference in stabilization energies of 2.6 kcal mol^{-1} in favor of the (+)-*sc* conformation in which the benzyl moiety faces the geminal *methyl groups* on the catalyst backbone, in line with X-ray crystal structure[110,111] data of the corresponding iminium salts of the catalysts. The computed conformational energies between (+)-*sc* and (−)-*sc* vary in a small range of ±2.0 kcal mol^{-1} for various typical substituents in the C(2) position of the heterocycle, which lies in the energetic span of the LD interactions. The benzyl group provides the steric shielding of the iminium *π*-system via a "*windshield-wiper*" effect freely rotating at ambient temperatures due to the low rotational barriers between the conformers. Therefore, it is necessary to account for LD in the computational model.[39,112]

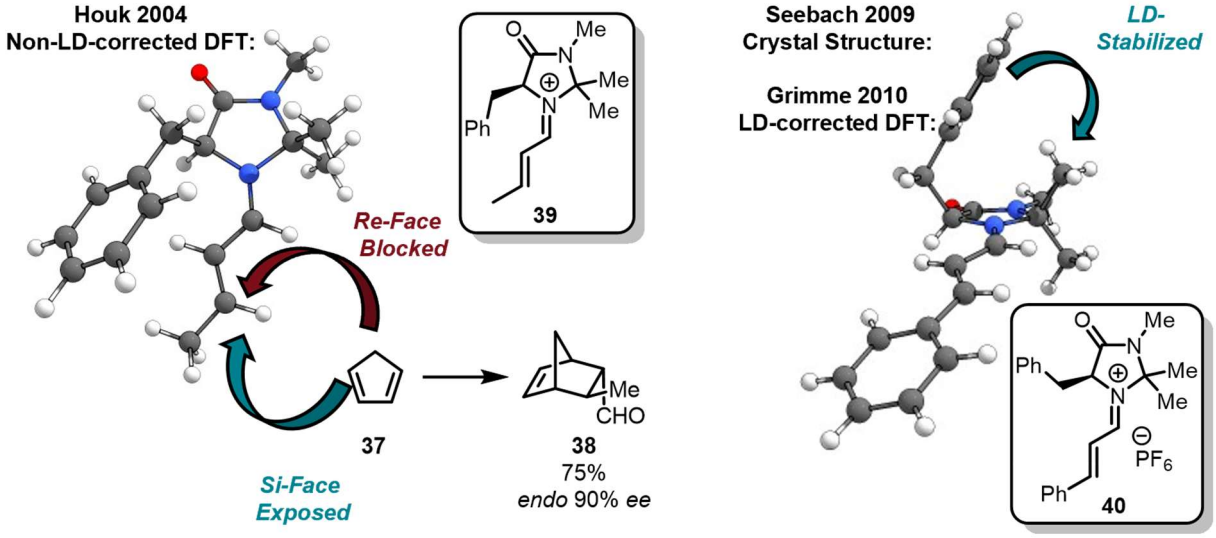


Figure 19. MacMillan's imidazolidinone catalyst in the initially proposed (−)-*sc* (top) and the LD corrected (+)-*sc* (bottom) conformation.

1.7 Dispersion Energy Donors Enhance Reactivity and Selectivity

Incorporation of bulky aliphatic or aromatic moieties in catalytic motifs has been good practice for decades under the assumption that these groups are sterically active in the sense that they "shield" parts of the interaction space from reacting. The notion of these groups being sterically attractive in their functions as DEDs, however, has only scarcely been recognized. Since the pioneering work of Akiyama[113] and Terada[114] in 2004 on chiral phosphoric acid catalysts (CPAs), chemists regularly implemented highly substituted aromatic substituents in 3,3'-position of the BINOL backbone to achieve high enantioselectivities. Well-known examples include MacMillan's –$Si(Ph)_3$[115] and List's TRIP[116,117] substituted CPAs providing exceptional enantioselectivities in reductive transfer hydrogenations of imines, enals, and enones. But how can these catalysts be so general even though they are used in quite different transformations? An obvious rationale would be steric shielding of either the *re*- or the *si*- face of the chiral catalyst-substrate adduct as the MacMillan group proposed.[115] However, the mechanism of the CPA-catalyzed transfer hydrogenation was extensively studied by Gschwind[118–122] and Goodman[123,124] experimentally and computationally (Fig. 20). The CPA catalyst and the *E*- or *Z*-imine form a binary hydrogen bond-assisted ion pair **44** followed by the binding of the Hantzsch ester **45**. In this ternary adduct **46**, enantioselectivity arises from the bottom or top side directed hydride transfer of the Hantzsch ester to the *E*- or *Z*-imine providing four different transition structures.[118–122] Computations indicate that the lowest energy TSs includes the *Z*-imine **43** and hydride transfer directed to the bottom side leading to the experimentally obtained enantioselectivities. Furthermore, the imine isomerization is slow compared to the hydride transfer, facilitating enantiocontrol of the reaction via increased population of the *Z*-imine. The Gschwind group found that the strategic positioning of *tert*-butyl groups as DEDs on the imine starting material led to a stabilization of the *Z*-isomer by around 1.0 kcal mol^{-1} and demonstrated that its preference is preserved in the binary and ternary CPA adducts.[125] Counterintuitively, additional decoration of the CPA with intrinsically bulky DEDs did not lead to increased steric repulsion between catalyst and imine, rather, it added favorable LD interactions in the binding event of the catalyst and substrate leading to almost exclusive population of the desired *Z*-imine and excellent enantioselectivities.[125]

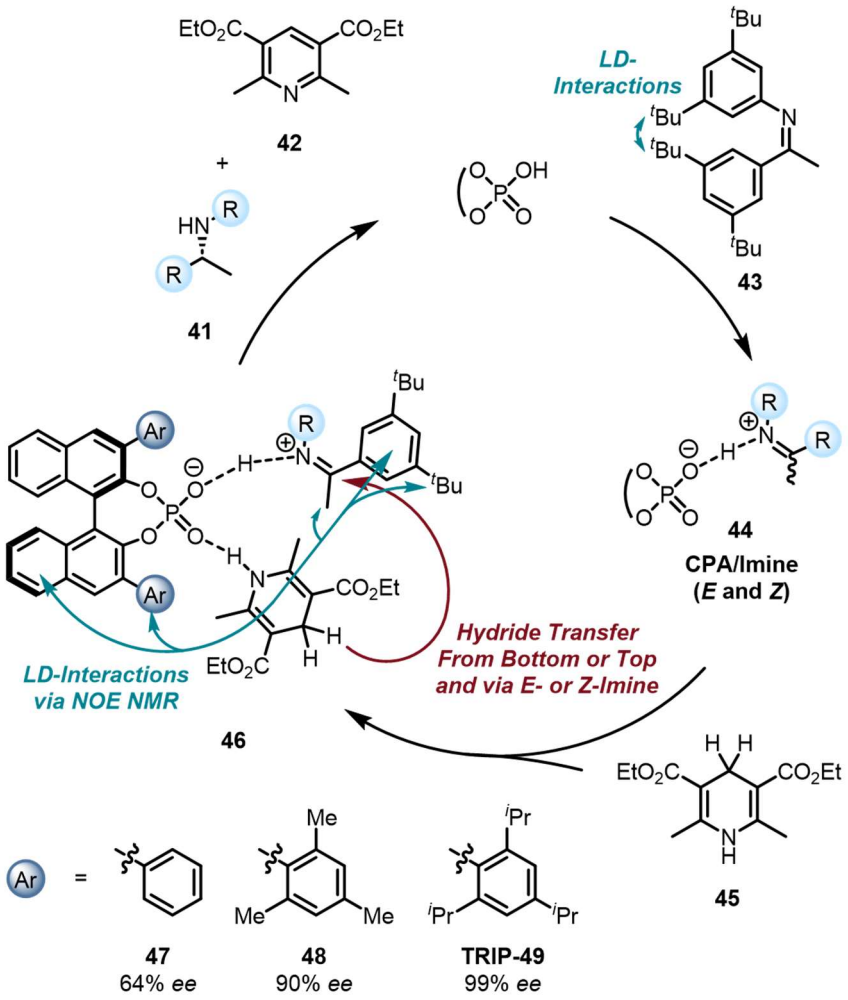


Figure 20. Mechanism of the CPA-catalyzed transfer hydrogenation of imines with Hantzsch esters.[125]

1.8 The Johnson−Corey−Chaykovsky Epoxidation

As demonstrated in several examples discussed above, London dispersion interactions can significantly influence the outcome and selectivity of chemical reactions. Nevertheless, many reactions, particularly older examples, are still primarily rationalized on the basis of steric repulsion alone. One prominent example is the Johnson–Corey–Chaykovsky epoxidation, which was first described by Johnson in 1961.[126] During investigations of the reaction between benzaldehyde and dimethylsulfonium fluorenylide, Johnson observed the formation of the corresponding epoxide rather than the expected Wittig-type olefination product.[126]

Subsequently, Corey and Chaykovsky further developed the reaction by improving the reaction conditions and identifying more suitable sulfonium and sulfoxonium ylides for epoxidation reactions,[127–129] ultimately giving rise to the now commonly used name Johnson–Corey–Chaykovsky reaction.

The current consensus is that after a pre-equilibrium deprotonation with base to generate the ylide from sulfonium salt **50-R^1**, the ylide adds nucleophilically to the aldehyde **51-R^2** in the rate-determining step.[130–135] Subsequent bond rotation around the central C-C bond results the *syn*- or *anti*-betaine, followed by stereospecific elimination of sulfide to yield the *cis*- or *trans*-epoxide (Fig. 21).

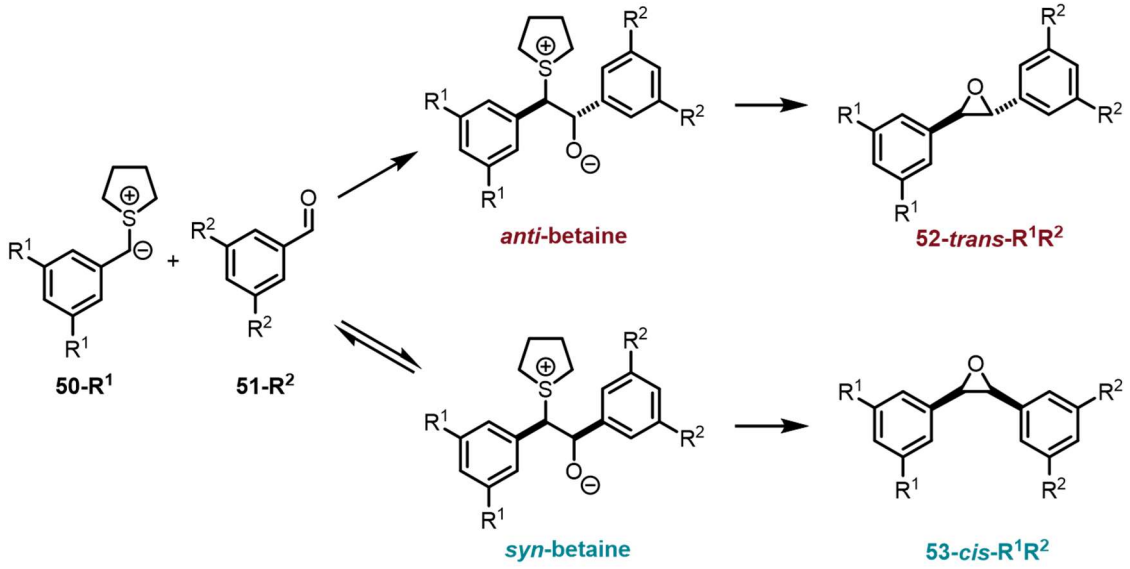


Figure 21. Currently accepted reaction sequence of the Johnson-Corey-Chaykovsky-epoxidation.

The origin of the diastereoselectivity lies in the reversibility of the *syn*-betaine formation on the one hand and the irreversibility of the *anti*-betaine formation (from cross-over experiments)[136] on the other. Based on the mechanistic studies, Aggarwal proposed that the stereo control is mainly governed by the reversibility of the initial betaine formation proposed four key factors for the selectivity.[133]

1 **Carbonyl stability:** More stable carbonyl compounds increase reversibility by favoring the starting material over the betaine intermediate.

2 **Ylide stability:** More stabilized ylides similarly increase reversibility, leading to enhanced diastereocontrol.

3 **Steric effects:** Increased steric congestion disfavors formation of the betaine intermediate and slows rotation around the central bond, resulting in greater reversibility and higher diastereocontrol.

4 **Charge solvation:** Solvation of the charged betaine intermediate by counterions such as lithium facilitates bond rotation, lowers reversibility, and consequently reduces diastereocontrol.

As most mechanistic investigations of the Johnson–Corey–Chaykovsky reaction are still based on the computational study by Aggarwal and co-workers from 2002, it is important to consider the limitations of the employed methodology. The calculations were performed at the B3LYP/6-311+G**//B3LYP/6-31G* level of theory using a continuum solvation model and relied on relative electronic energies without inclusion of zero-point vibrational energy corrections.[133] While state-of-the-art at the time, this approach no longer meets modern standards for accurately describing subtle energetic differences.[137]

More importantly, conventional B3LYP lacks an explicit treatment of long-range electron correlation and therefore cannot adequately account for London dispersion interactions.[23] This is particularly relevant, as the computed energy differences between competing reaction pathways and transition states are often only 1–3 kcal mol^{-1}. Although some degree of error compensation may be expected for electronically similar structures, this assumption is unlikely to hold true when dispersion interactions differ substantially between the *cis* and *trans* pathways as the relative distance between substituents changes. Inspection of the reported transition-state geometries reveals intermolecular distances that generally exceed 3 Å.[133] At such distances, steric repulsion is expected to be less dominant, whereas attractive London dispersion interactions can become significant.[13]

In our final study, we therefore want to revisit this paradigm both computationally and experimentally. By introducing increasingly bulky substituents on the aromatic rings, we aimed to probe the contribution of London dispersion interactions to the stereochemical outcome of the reaction and compare the observed selectivities with the interaction trends determined independently from molecular balance experiments.

1.9 References

[1] R. Eisenschitz, F. London, Über das Verhältnis der van der Waalsschen Kräfte zu den homöopolaren Bindungskräften *Z. Phys.* **1930**, *60*, 491–527.

[2] D. G. Truhlar, Dispersion Forces: Neither Fluctuating Nor Dispersing *J. Chem. Educ.* **2019**, *96*, 1671–1675.

[3] F. London, Zur Theorie und Systematik der Molekularkräfte *Z. Phys.* **1930**, *63*, 245–279.

[4] C. T. Wang, On the Nature of Molecular Force *Z. Phys.* **1927**, *28*, 663–666.

[5] F. London, The general theory of molecular forces *Trans. Faraday Soc.* **1937**, *33*, 8b.

[6] H. B. G. Casimir, D. Polder, The Influence of Retardation on the London-van der Waals Forces *Phys. Rev.* **1948**, *73*, 360–372.

[7] J. O. Hirschfelder, J. W. Linnett, The Energy of Interaction between Two Hydrogen Atoms *J. Chem. Phys.* **1950**, *18*, 130–142.

[8] A. D. McLachlan, Retarded Dispersion Forces in Dielectrics at Finite Temperatures *Proc. R. Soc. Lond.* **1963**, *274*, 80–90.

[9] Y. Andersson, D. C. Langreth, B. I. Lundqvist, van der Waals Interactions in Density-Functional Theory *Phys. Rev. Lett.* **1996**, *76*, 102–105.

[10] Y. Yang, K. U. Lao, D. M. Wilkins, A. Grisafi, M. Ceriotti, R. A. DiStasio, Quantum mechanical static dipole polarizabilities in the QM7b and AlphaML showcase databases *Sci. Data* **2019**, *6*, 1–10.

[11] S. Grimme, R. Huenerbein, S. Ehrlich, On the Importance of the Dispersion Energy for the Thermodynamic Stability of Molecules *ChemPhysChem* **2011**, *12*, 1258–1261.

[12] J. P. Wagner, P. R. Schreiner, London Dispersion in Molecular Chemistry—Reconsidering Steric Effects *Angew. Chem. Int. Ed.* **2015**, *54*, 12274–12296.

[13] L. Rummel, P. R. Schreiner, Advances and Prospects in Understanding London Dispersion Interactions in Molecular Chemistry *Angew. Chem. Int. Ed.* **2024**, *63*, e202316364.

[14] W. Pauli, Über den Zusammenhang des Abschlusses der Elektronengruppen im Atom mit der Komplexstruktur der Spektren *Z. Phys.* **1925**, *31*, 765–783.

[15] W. Heitler, F. London, Wechselwirkung neutraler Atome und homöopolare Bindung nach der Quantenmechanik *Z. Phys.* **1927**, *44*, 455–472.

[16] J. E. Lennard-Jones, Cohesion *Proc. Phys. Soc.* **1931**, *43*, 461–482.

[17] J. C. Slater, A Simplification of the Hartree-Fock Method *Phys. Rev.* **1951**, *81*, 385–390.

[18] D. J. Cram, F. A. A. Elhafez, Studies in Stereochemistry. X. The Rule of “Steric Control of Asymmetric Induction” in the Syntheses of Acyclic Systems *J. Am. Chem. Soc.* **1952**, *74*, 5828–5835.

[19] K. S. Pitzer, E. Catalano, Electronic correlation in molecules. III. The paraffin hydrocarbons *J. Am. Chem. Soc.* **1956**, *78*, 4844–4846.

[20] A. A. Fokin, D. Gerbig, P. R. Schreiner, σ/σ- and π/π-Interactions Are Equally Important: Multilayered Graphanes *J. Am. Chem. Soc.* **2011**, *133*, 20036–20039.

[21] T. Janowski, P. Pulay, A Benchmark Comparison of σ/σ and π/π Dispersion: the Dimers of Naphthalene and Decalin, and Coronene and Perhydrocoronene *J. Am. Chem. Soc.* **2012**, *134*, 17520–17525.

[22] C. Wang, Y. Mo, J. P. Wagner, P. R. Schreiner, E. D. Jemmis, D. Danovich, S. Shaik, The Self-Association of Graphane Is Driven by London Dispersion and Enhanced Orbital Interactions *J. Chem. Theory Comput.* **2015**, *11*, 1621–1630.

[23] S. Kristyán, P. Pulay, Can (semi)local density functional theory account for the London dispersion forces? *Chem. Phys. Lett* **1994**, *229*, 175–180.

[24] M. P. Hodges, A. J. Stone, A new representation of the dispersion interaction *Mol. Phys.* **2000**, *98*, 275–286.

[25] A. Jiemchooroj, B. E. Sernelius, P. Norman, C6 dipole-dipole dispersion coefficients for the n-alkanes: Test of an additivity procedure *Phys. Rev. A* **2004**, *69*, 044701.

[26] S. Grimme, Accurate description of van der Waals complexes by density functional theory including empirical corrections *J. Comput. Chem.* **2004**, *25*, 1463–1473.

[27] A. D. Becke, E. R. Johnson, A density-functional model of the dispersion interaction *J. Chem. Phys.* **2005**, *123*, 154101.

[28] A. D. Becke, E. R. Johnson, Exchange-hole dipole moment and the dispersion interaction: High-order dispersion coefficients *J. Chem. Phys.* **2006**, *124*, 014104.

[29] A. J. Du, S. C. Smith, Van der Waals-corrected density functional theory: benchmarking for hydrogen–nanotube and nanotube–nanotube interactions *Nanotechnology* **2005**, *16*, 2118–2123.

[30] J. Antony, S. Grimme, Density functional theory including dispersion corrections for intermolecular interactions in a large benchmark set of biologically relevant molecules *Phys. Chem. Chem. Phys.* **2006**, *8*, 5287–5293.

[31] S. Grimme, Density functional theory with London dispersion corrections *WIREs Comp. Mol. Sci.* **2011**, *1*, 211–228.

[32] S. Grimme, A. Hansen, J. G. Brandenburg, C. Bannwarth, Dispersion-Corrected Mean-Field Electronic Structure Methods *Chem. Rev.* **2016**, *116*, 5105–5154.

[33] S. Grimme, P. R. Schreiner, The Role of London Dispersion Interactions in Modern Chemistry *Acc. Chem. Res.* **2024**, *57*, 2233–2233.

[34] Q. Wu, W. Yang, Empirical correction to density functional theory for van der Waals interactions *J. Chem. Phys.* **2002**, *116*, 515–524.

[35] M. Dion, H. Rydberg, E. Schröder, D. C. Langreth, B. I. Lundqvist, Van der Waals Density Functional for General Geometries *Phys. Rev. Lett.* **2004**, *92*, 246401.

[36] J. Hermann, A. Tkatchenko, Density Functional Model for van der Waals Interactions: Unifying Many-Body Atomic Approaches with Nonlocal Functionals *Phys. Rev. Lett.* **2020**, *124*, 146401.

[37] A. Tkatchenko, M. Scheffler, Accurate Molecular Van Der Waals Interactions from Ground-State Electron Density and Free-Atom Reference Data *Phys. Rev. Lett.* **2009**, *102*, 073005.

[38] N. Mardirossian, M. Head-Gordon, Thirty years of density functional theory in computational chemistry: an overview and extensive assessment of 200 density functionals *Mol. Phys.* **2017**, *115*, 2315–2372.

[39] S. Grimme, A. Hansen, J. G. Brandenburg, C. Bannwarth, Dispersion-Corrected Mean-Field Electronic Structure Methods *Chem. Rev.* **2016**, *116*, 5105–5154.

[40] J. Contreras-García, E. R. Johnson, S. Keinan, R. Chaudret, J.-P. Piquemal, D. N. Beratan, W. Yang, NCIPLOT: A Program for Plotting Noncovalent Interaction Regions *J. Chem. Theory Comput.* **2011**, *7*, 625–632.

[41] A. S. Mahadevi, G. N. Sastry, Cooperativity in Noncovalent Interactions *Chem. Rev.* **2016**, *116*, 2775–2825.

[42] T. Lu, Visualization Analysis of Covalent and Noncovalent Interactions in Real Space *Angew. Chem. Int. Ed.* **2025**, e202504895.

[43] I. K. Mati, S. L. Cockroft, Molecular balances for quantifying non-covalent interactions *Chem. Soc. Rev.* **2010**, *39*, 4195–4205.

[44] M. Ōki, Unusually High Barriers to Rotation Involving the Tetrahedral Carbon Atom *Angew. Chem. Int. Ed.* **1976**, *15*, 87–93.

[45] M. A. Strauss, H. A. Wegner, Molecular Systems for the Quantification of London Dispersion Interactions *Eur. J. Org. Chem.* **n.d.**, *2019*, 295–302.

[46] A. E. Aliev, W. B. Motherwell, Some Recent Advances in the Design and Use of Molecular Balances for the Experimental Quantification of Intramolecular Noncovalent Interactions of π Systems *Chem. Eur. J.* **2019**, *25*, 10516–10530.

[47] M. Petroselli, P. Ballester, Molecular Balances as Physical Organic Chemistry Tools to Quantify Non-Covalent Interactions *Chem. Eur. J.* **2025**, *31*, e202404351.

[48] R. Pollice, M. Bot, I. J. Kobylianskii, I. Shenderovich, P. Chen, Attenuation of London Dispersion in Dichloromethane Solutions *J. Am. Chem. Soc.* **2017**, *139*, 13126–13140.

[49] R. Pollice, F. Fleckenstein, I. Shenderovich, P. Chen, Compensation of London Dispersion in the Gas Phase and in Aprotic Solvents *Angew. Chem. Int. Ed.* **2019**, *58*, 14281–14288.

[50] A. Elmi, K. M. Bąk, S. L. Cockroft, Solvent Attenuation of London Dispersion in Polycyclic Aromatic Stacking *Angew. Chem. Int. Ed.* **2024**, *63*, e202412056.

[51] N. L. Allinger, M. Frierson, F. A. Van-Catledge, The importance of van der Waals attractions in determining the equilibrium between 1,4- and 1,6-dialkylcyclooctatetraenes *J. Am. Chem. Soc.* **1982**, *104*, 4592–4593.

[52] J. E. Anderson, P. A. Kirsch, Structural equilibria determined by attractive steric interactions. 1,6-Dialkylcyclooctatetraenes and their bond-shift and ring inversion investigated by dynamic NMR spectroscopy and molecular mechanics calculations *J. Chem. Soc., Perkin Trans. 2* **1992**, 1951.

[53] R. Willstätter, E. Waser, Über Cyclo-octatetraen *Ber. Dtsch. Chem. Ges.* **1911**, *44*, 3423–3445.

[54] W. Reppe, O. Schlichting, K. Klager, T. Toepel, Cyclisierende Polymerisation von Acetylen I Über Cyclooctatetraen *Justus Liebigs Annalen der Chemie* **1948**, *560*, 1–92.

[55] L. A. Paquette, S. V. Ley, R. H. Meisinger, R. K. Russell, M. Oku, Directed syntheses of the isomeric dimethylcyclooctatetraenes and a study of their polarographic and alkali metal reduction *J. Am. Chem. Soc.* **1974**, *96*, 5806–5815.

[56] M. H. Lyttle, A. Jr. Streitwieser, R. Q. Kluttz, Unusual equilibrium between 1,4- and 1,6-di-tert-butylcyclooctatetraenes *J. Am. Chem. Soc.* **1981**, *103*, 3232–3233.

[57] L. A. Paquette, G. J. Hefferon, R. Samodral, Y. Hanzawa, Bond fixation in annulenes. 14. Synthesis of and bond shifting equilibrium between 1,4- and 1,6-di-tert-butylcyclooctatetraenes *J. Org. Chem.* **1983**, *48*, 1262–1266.

[58] M. H. Lyttle, A. Streitwieser, M. J. Miller, 1,5-Disubstituted cyclooctatetraenes *J. Org. Chem.* **1989**, *54*, 2331–2335.

[59] F. A. L. Anet, The Rate of Bond Change in Cycloöctatetraene *J. Am. Chem. Soc.* **1962**, *84*, 671–672.

[60] J. L. Andrés, O. Castaño, A. Morreale, R. Palmeiro, R. Gomperts, Potential energy surface of cyclooctatetraene *J. Chem. Phys.* **1998**, *108*, 203–207.

[61] C. Conesa, H. S. Rzepa, PM3 and ab initio studies of the C 8 H 8 potential energy surface. Thermal isomerism of syn - and anti -tricyclo[4.2.0.0 2,5]octa-3,7-dienes† *J. Chem. Soc. Perkin Trans. 2* **1998**, *0*, 857–862.

[62] O. Castaño, R. Palmeiro, L. M. Frutos, J. Luisandrés, Role of bifurcation in the bond shifting of cyclooctatetraene *J. Comput. Chem.* **2002**, *23*, 732–736.

[63] J. M. Schümann, J. P. Wagner, A. K. Eckhardt, H. Quanz, P. R. Schreiner, Intramolecular London Dispersion Interactions Do Not Cancel in Solution *J. Am. Chem. Soc.* **2021**, *143*, 41–45.

[64] J. M. Schümann, L. Ochmann, J. Becker, A. Altun, I. Harden, G. Bistoni, P. R. Schreiner, Exploring the Limits of Intramolecular London Dispersion Stabilization with Bulky Dispersion Energy Donors in Alkane Solution *J. Am. Chem. Soc.* **2023**, *145*, 2093–2097.

[65] S. Paliwal, S. Geib, C. S. Wilcox, Molecular Torsion Balance for Weak Molecular Recognition Forces. Effects of "Tilted-T" Edge-to-Face Aromatic Interactions on Conformational Selection and Solid-State Structure *J. Am. Chem. Soc.* **1994**, *116*, 4497–4498.

[66] L. Rummel, H. F. König, H. Hausmann, P. R. Schreiner, Silyl Groups Are Strong Dispersion Energy Donors *J. Org. Chem.* **2022**, *87*, 13168–13177.

[67] H. F. König, L. Rummel, H. Hausmann, J. Becker, J. M. Schümann, P. R. Schreiner, Gauging the Steric Effects of Silyl Groups with a Molecular Balance *J. Org. Chem.* **2022**, *87*, 4670–4679.

[68] H. F. König, H. Hausmann, P. R. Schreiner, Assessing the Experimental Hydrogen Bonding Energy of the Cyclic Water Dimer Transition State with a Cyclooctatetraene-Based Molecular Balance *J. Am. Chem. Soc.* **2022**, *144*, 16965–16973.

[69] M. Gomberg, Triphenylmethyl, ein Fall von dreiwerthigem Kohlenstoff *Ber. Dtsch. Chem. Ges.* **1900**, *33*, 3150–3163.

[70] M. Gomberg, An Instance of Trivalent Carbon: Triphenylmethyl. *J. Am. Chem. Soc.* **1900**, *22*, 757–771.

[71] H. Lankamp, W. Th. Nauta, C. MacLean, A new interpretation of the monomer-dimer equilibrium of triphenylmethyl- and alkylsubstituted-diphenyl methyl-radicals in solution *Tetrahedron Lett.* **1968**, *9*, 249–254.

[72] M. Stein, W. Winter, A. Rieker, Hexakis(2,6-di-tert-butyl-4-biphenylyl)ethane—The First Unbridged Hexaarylethane *Angew. Chem. Int. Ed.* **1978**, *17*, 692–694.

[73] S. Grimme, P. R. Schreiner, Steric Crowding Can Stabilize a Labile Molecule: Solving the Hexaphenylethane Riddle *Angew. Chem. Int. Ed.* **2011**, *50*, 12639–12642.

[74] Bart. Kahr, Donna. Van Engen, Kurt. Mislow, Length of the ethane bond in hexaphenylethane and its derivatives *J. Am. Chem. Soc.* **1986**, *108*, 8305–8307.

[75] S. Rösel, C. Balestrieri, P. R. Schreiner, Sizing the role of London dispersion in the dissociation of all-meta tert-butyl hexaphenylethane *Chem. Sci.* **2017**, *8*, 405–410.

[76] S. Rösel, J. Becker, W. D. Allen, P. R. Schreiner, Probing the Delicate Balance between Pauli Repulsion and London Dispersion with Triphenylmethyl Derivatives *J. Am. Chem. Soc.* **2018**, *140*, 14421–14432.

[77] S. Rösel, P. R. Schreiner, Computational Chemistry as a Conceptual Game Changer: Understanding the Role of London Dispersion in Hexaphenylethane Derivatives (Gomberg Systems) *Isr. J. Chem.* **2022**, *62*, e202200002.

[78] W. Humphrey, A. Dalke, K. Schulten, VMD: Visual molecular dynamics *J. Mol. Graph.* **1996**, *14*, 33–38.

[79] R. Laplaza, F. Peccati, R. A. Boto, C. Quan, A. Carbone, J.-P. Piquemal, Y. Maday, J. Contreras-García, NCIPLOT and the analysis of noncovalent interactions using the reduced density gradient *WIREs Comput. Mol. Sci.* **2021**, *11*, e1497.

[80] H. Aikawa, Y. Takahira, M. Yamaguchi, Synthesis of 1,8-di(1-adamantyl)naphthalenes as single enantiomers stable at ambient temperatures *Chem. Commun.* **2011**, *47*, 1479–1481.

[81] T. Ikawa, Y. Yamamoto, A. Heguri, Y. Fukumoto, T. Murakami, A. Takagi, Y. Masuda, K. Yahata, H. Aoyama, Y. Shigeta, H. Tokiwa, S. Akai, Could London Dispersion Force Control Regioselective (2 + 2) Cyclodimerizations of Benzynes? YES: Application to the Synthesis of Helical Biphenylenes *J. Am. Chem. Soc.* **2021**, *143*, 10853–10859.

[82] E. Solel, M. Ruth, P. R. Schreiner, London Dispersion Helps Refine Steric A-Values: Dispersion Energy Donor Scales *J. Am. Chem. Soc.* **2021**, *143*, 20837–20848.

[83] J. E. Leffler, Parameters for the Description of Transition States *Science* **1953**, *117*, 340–341.

[84] G. S. Hammond, A Correlation of Reaction Rates *J. Am. Chem. Soc.* **1955**, *77*, 334–338.

[85] R. Guo, S. Adak, P. Bellotti, X. Gao, W. W. Smith, S. N. Le, J. Ma, K. N. Houk, F. Glorius, S. Chen, M. K. Brown, Photochemical Dearomative Cycloadditions of Quinolines and Alkenes: Scope and Mechanism Studies *J. Am. Chem. Soc.* **2022**, *144*, 17680–17691.

[86] R. R. Knowles, E. N. Jacobsen, Attractive noncovalent interactions in asymmetric catalysis: Links between enzymes and small molecule catalysts *Proc. Natl. Acad. Sci. USA* **2010**, *107*, 20678–20685.

[87] R. C. Wende, A. Seitz, D. Niedek, S. M. M. Schuler, C. Hofmann, J. Becker, P. R. Schreiner, The Enantioselective Dakin–West Reaction *Angew. Chem. Int. Ed.* **2016**, *55*, 2719–2723.

[88] E. Procházková, A. Kolmer, J. Ilgen, M. Schwab, L. Kaltschnee, M. Fredersdorf, V. Schmidts, R. C. Wende, P. R. Schreiner, C. M. Thiele, Uncovering Key Structural Features of an Enantioselective Peptide-Catalyzed Acylation Utilizing Advanced NMR Techniques *Angew. Chem. Int. Ed.* **2016**, *55*, 15754–15759.

[89] A. J. Neel, M. J. Hilton, M. S. Sigman, F. D. Toste, Exploiting non-covalent π interactions for catalyst design *Nature* **2017**, *543*, 637–646.

[90] G. Lu, R. Y. Liu, Y. Yang, C. Fang, D. S. Lambrecht, S. L. Buchwald, P. Liu, Ligand–Substrate Dispersion Facilitates the Copper-Catalyzed Hydroamination of Unactivated Olefins *J. Am. Chem. Soc.* **2017**, *139*, 16548–16555.

[91] F. D. Toste, M. S. Sigman, S. J. Miller, Pursuit of Noncovalent Interactions for Strategic Site-Selective Catalysis *Acc. Chem. Res.* **2017**, *50*, 609–615.

[92] E. J. Corey, R. K. Bakshi, S. Shibata, C.-P. Chen, V. K. Singh, A Stable and Easily Prepared Catalyst for the Enantioselective Reduction of Ketones. Applications to Multistep Syntheses *J. Am. Chem. Soc.* **1987**, *109*, 7925–7926.

[93] E. J. Corey, R. K. Bakshi, S. Shibata, Highly enantioselective borane reduction of ketones catalyzed by chiral oxazaborolidines. Mechanism and synthetic implications *J. Am. Chem. Soc.* **1987**, *109*, 5551–5553.

[94] E. J. Corey, S. Shibata, R. K. Bakshi, An efficient and catalytically enantioselective route to (S)-(-)-phenyloxirane *J. Org. Chem.* **1988**, *53*, 2861–2863.

[95] E. J. Corey, R. K. Bakshi, A new system for catalytic enantioselective reduction of achiral ketones to chiral alcohols. Synthesis of chiral α-hydroxy acids *Tetrahedron Lett.* **1990**, *31*, 611–614.

[96] E. J. Corey, C. J. Helal, Novel electronic effects of remote substituents on the oxazaborolidine-catalyzed enantioselective reduction of ketones *Tetrahedron Lett.* **1995**, *36*, 9153–9156.

[97] E. J. Corey, J. O. Link, A new chiral catalyst for the enantioselective synthesis of secondary alcohols and deuterated primary alcohols by carbonyl reduction *Tetrahedron Lett.* **1989**, *30*, 6275–6278.

[98] D. K. Jones, D. C. Liotta, I. Shinkai, D. J. Mathre, Origins of the enantioselectivity observed in oxazaborolidine-catalyzed reductions of ketones *J. Org. Chem.* **1993**, *58*, 799–801.

[99] M. P. Meyer, Nonbonding Interactions and Stereoselection in the Corey-Bakshi-Shibata Reduction *Org. Lett.* **2009**, *101*, 4338–4341.

[100] T. Giagou, M. P. Meyer, Kinetic Isotope Effects in Asymmetric Reactions *Chem. Eur. J.* **2010**, *16*, 10616–10628.

[101] H. Zhu, D. J. O'Leary, M. P. Meyer, Stereoselection in the Corey–Bakshi–Shibata Reduction: Insight from Kinetic Isotope Effects and Transition-Structure Modeling *Angew. Chem. Int. Ed.* **2012**, *51*, 11890–11893.

[102] Z. Lachtar, A. Khorief Nacereddine, A. Djerourou, Understanding the origin of the enantioselectivity and the mechanism of the asymmetric reduction of ketimine generated from acetophenone with oxazaborolidine catalyst *Struct. Chem.* **2020**, *31*, 253–261.

[103] K. Szalewicz, Symmetry-adapted perturbation theory of intermolecular forces *WIREs Comput. Mol. Sci.* **2012**, *2*, 254–272.

[104] T. M. Parker, L. A. Burns, R. M. Parrish, A. G. Ryno, C. D. Sherrill, Levels of symmetry adapted perturbation theory (SAPT). I. Efficiency and performance for interaction energies *J. Chem. Phys.* **2014**, *140*, 094106.

[105] C. Eschmann, L. Song, P. R. Schreiner, London Dispersion Interactions Rather than Steric Hindrance Determine the Enantioselectivity of the Corey–Bakshi–Shibata Reduction *Angew. Chem. Int. Ed.* **2021**, *60*, 4823–4832.

[106] S. Bahmanyar, K. N. Houk, H. J. Martin, B. List, Quantum Mechanical Predictions of the Stereoselectivities of Proline-Catalyzed Asymmetric Intermolecular Aldol Reactions *J. Am. Chem. Soc.* **2003**, *125*, 2475–2479.

[107] A. Armstrong, R. A. Boto, P. Dingwall, J. Contreras-García, M. J. Harvey, N. J. Mason, H. S. Rzepa, The Houk–List transition states for organocatalytic mechanisms revisited *Chem. Sci.* **2014**, *5*, 2057–2071.

[108] K. A. Ahrendt, C. J. Borths, D. W. C. MacMillan, New Strategies for Organic Catalysis: The First Highly Enantioselective Organocatalytic Diels−Alder Reaction *J. Am. Chem. Soc.* **2000**, *122*, 4243–4244.

[109] R. Gordillo, J. Carter, K. N. Houk, Theoretical Explorations of Enantioselective Alkylation Reactions of Pyrroles and Indoles Organocatalyzed by Chiral Imidazolidinones *Adv. Synth. Catal.* **2004**, *346*, 1175–1185.

[110] U. Grošelj, D. Seebach, D. M. Badine, W. B. Schweizer, A. K. Beck, I. Krossing, P. Klose, Y. Hayashi, T. Uchimaru, Structures of the Reactive Intermediates in Organocatalysis with Diarylprolinol Ethers *Helv. Chim. Acta* **2009**, *92*, 1225–1259.

[111] J. B. Brazier, G. Evans, T. J. K. Gibbs, S. J. Coles, M. B. Hursthouse, J. A. Platts, N. C. O. Tomkinson, Solution Phase, Solid State, and Theoretical Investigations on the MacMillan Imidazolidinone *Org. Lett.* **2009**, *11*, 133–136.

[112] D. Seebach, U. Grošelj, W. B. Schweizer, S. Grimme, C. Mück-Lichtenfeld, Experimental and Theoretical Conformational Analysis of 5-Benzylimidazolidin-4-one Derivatives – a “Playground” for Studying Dispersion Interactions and a “Windshield-Wiper” Effect in Organocatalysis *Helv. Chim. Acta* **2010**, *93*, 1–16.

[113] T. Akiyama, J. Itoh, K. Yokota, K. Fuchibe, Enantioselective Mannich-type reaction catalyzed by a chiral Brønsted acid *Angew. Chem. Int. Ed.* **2004**, *43*, 1566–1568.

[114] D. Uraguchi, M. Terada, Chiral Brønsted Acid-Catalyzed Direct Mannich Reactions via Electrophilic Activation *J. Am. Chem. Soc.* **2004**, *126*, 5356–5357.

[115] R. I. Storer, D. E. Carrera, Y. Ni, D. W. C. MacMillan, Enantioselective Organocatalytic Reductive Amination *J. Am. Chem. Soc.* **2006**, *128*, 84–86.

[116] N. J. A. Martin, B. List, Highly Enantioselective Transfer Hydrogenation of α,β-unasturated Ketones *J. Am. Chem. Soc.* **2006**, *128*, 13368–13369.

[117] M. Mahlau, B. List, Asymmetric counteranion-directed catalysis (ACDC): A remarkably general approach to enantioselective synthesis *Isr. J. Chem.* **2012**, *52*, 630–638.

[118] P. Renzi, J. Hioe, R. M. Gschwind, Decrypting Transition States by Light: Photoisomerization as a Mechanistic Tool in Brønsted Acid Catalysis *J. Am. Chem. Soc.* **2017**, *139*, 6752–6760.

[119] N. Sorgenfrei, J. Hioe, J. Greindl, K. Rothermel, F. Morana, N. Lokesh, R. M. Gschwind, NMR Spectroscopic Characterization of Charge Assisted Strong Hydrogen Bonds in Brønsted Acid Catalysis *J. Am. Chem. Soc.* **2016**, *138*, 16345–16354.

[120] J. Greindl, J. Hioe, N. Sorgenfrei, F. Morana, R. M. Gschwind, Brønsted Acid Catalysis—Structural Preferences and Mobility in Imine/Phosphoric Acid Complexes *J. Am. Chem. Soc.* **2016**, *138*, 15965–15971.

[121] K. Rothermel, M. Melikian, J. Hioe, J. Greindl, J. Gramüller, M. Žabka, N. Sorgenfrei, T. Hausler, F. Morana, R. M. Gschwind, Internal acidity scale and reactivity evaluation of chiral phosphoric acids with different 3,3′-substituents in Brønsted acid catalysis *Chem. Sci.* **2019**, *10*, 10025–10034.

[122] M. Melikian, J. Gramüller, J. Hioe, J. Greindl, R. M. Gschwind, Brønsted acid catalysis – the effect of 3,3′-substituents on the structural space and the stabilization of imine/phosphoric acid complexes *Chem. Sci.* **2019**, *10*, 5226–5234.

[123] L. Simón, J. M. Goodman, Theoretical Study of the Mechanism of Hantzsch Ester Hydrogenation of Imines Catalyzed by Chiral BINOL-Phosphoric Acids *J. Am. Chem. Soc.* **2008**, *130*, 8741–8747.

[124] J. P. Reid, J. M. Goodman, Goldilocks Catalysts: Computational Insights into the Role of the 3,3′ Substituents on the Selectivity of BINOL-Derived Phosphoric Acid Catalysts *J. Am. Chem. Soc.* **2016**, *138*, 7910–7917.

[125] J. Gramüller, M. Franta, R. M. Gschwind, Tilting the Balance: London Dispersion Systematically Enhances Enantioselectivities in Brønsted Acid Catalyzed Transfer Hydrogenation of Imines *J. Am. Chem. Soc.* **2022**, *144*, 19861–19871.

[126] A. W. Johnson, R. B. LaCount, The Chemistry of Ylids. VI. Dimethylsulfonium Fluorenylide—A Synthesis of Epoxides1 *J. Am. Chem. Soc.* **1961**, *83*, 417–423.

[127] E. J. Corey, M. Chaykovsky, Dimethylsulfonium methylide, a reagent for selective oxirane synthesis from aldehydes and ketones *J. Am. Chem. Soc.* **1962**, *84*, 3782–3783.

[128] E. J. Corey, M. Chaykovsky, Dimethylsulfoxonium Methylide *J. Am. Chem. Soc.* **1962**, *84*, 867–868.

[129] E. J. Corey, M. Chaykovsky, Dimethyloxosulfonium Methylide ((CH3)2SOCH2) and Dimethylsulfonium Methylide ((CH3)2SCH2). Formation and Application to Organic Synthesis *J. Am. Chem. Soc.* **1965**, *87*, 1353–1364.

[130] F. Volatron, O. Eisenstein, Theoretical study of the reactivity of phosphonium and sulfonium ylides with carbonyl groups *J. Am. Chem. Soc.* **1984**, *106*, 6117–6119.

[131] F. Volatron, O. Eisenstein, Wittig versus Corey-Chaykovsky Reaction. Theoretical study of the reactivity of phosphonium methylide and sulfonium methylide with formaldehyde *J. Am. Chem. Soc.* **1987**, *109*, 1–14.

[132] M. K. Lindvall, A. M. Koskinen, Origins of Stereoselectivity in the Corey-Chaykovsky Reaction. Insights from Quantum Chemistry *J. Org. Chem.* **1999**, *64*, 4596–4606.

[133] V. K. Aggarwal, J. N. Harvey, J. Richardson, Unraveling the Mechanism of Epoxide Formation from Sulfur Ylides and Aldehydes *J. Am. Chem. Soc.* **2002**, *124*, 5747–5756.

[134] D. R. Edwards, P. Montoya-Peleaz, C. M. Crudden, Experimental Investigation into the Mechanism of the Epoxidation of Aldehydes with Sulfur Ylides *Org. Lett.* **2007**, *9*, 5481–5484.

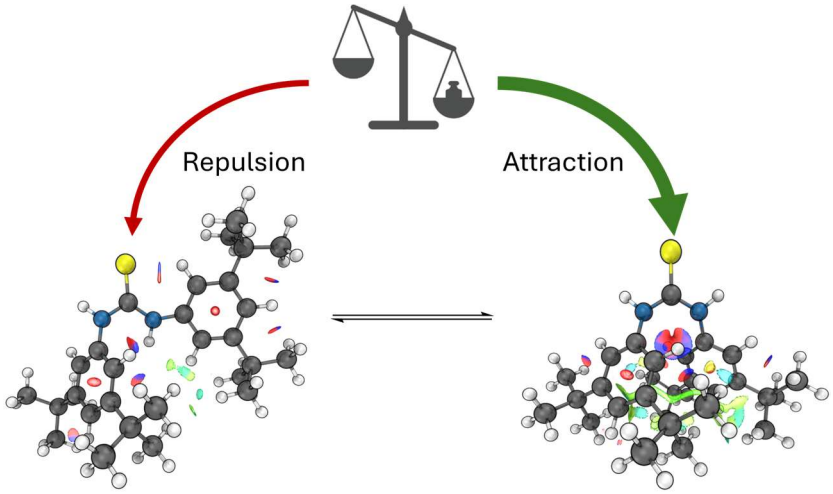
[135] D. R. Edwards, J. Du, C. M. Crudden, Experimental demonstration of base-catalyzed interconversion of isomeric betaine intermediates in the Corey-Chaykovsky epoxidation *Org. Lett.* **2007**, *9*, 2397–400.

[136] V. K. Aggarwal, S. Calamai, J. G. Ford, Additions of benzylsulfonium ylides to aldehydes and ketones: are they under kinetic or thermodynamic control? *J. Chem. Soc. Perkin Trans. 2* **1997**, 593–600.

[137] M. Bursch, J.-M. Mewes, A. Hansen, S. Grimme, Best-Practice DFT Protocols for Basic Molecular Computational Chemistry** *Angew. Chem. Int. Ed.* **2022**, *61*, e202205735.

2. Publications

2.1 London Dispersion Favors Sterically Hindered Diarylthiourea Conformers in Solution



Abstract

We present an experimental and computational study on the conformers of *N,N'*-diphenylthiourea substituted with different dispersion energy donor (DED) groups. While the unfolded anti–anti conformer is the most relevant for thiourea catalysis, intramolecular noncovalent interactions counterintuitively favor the folded *syn–syn* conformer, as evident from a combination of low-temperature nuclear magnetic resonance measurements and computations. In order to quantify the noncovalent interactions, we utilized local energy decomposition analysis and symmetry-adapted perturbation theory at the DLPNO-CCSD(T)/def2-TZVPP and sSAPT0/6-311G(d,p) levels of theory. Additionally, we applied a double-mutant cycle to experimentally study the effects of bulky substituents on the equilibria. We determined London dispersion as the key interaction that shifts the equilibria towards the *syn–syn* conformers. This preference is likely a factor why such thiourea derivatives can be poor catalysts.

***Reference*:**

Lars Rummel, Marvin H. J. Domanski, Heike Hausmann, Jonathan Becker, and Peter R. Schreiner, *Angew. Chem. Int. Ed.* **2022**, *61*, e202204393; *Angew. Chem.* **2022**, *134*, e202204393. **DOI:** 10.1002/anie.202204393

Reproduced with permission from © 2026 Wiley-VCH GmbH.

How to cite: *Angew. Chem. Int. Ed.* **2022**, *61*, e202204393
International Edition: doi.org/10.1002/anie.202204393
German Edition: doi.org/10.1002/ange.202204393

Noncovalent Interactions | Hot Paper

London Dispersion Favors Sterically Hindered Diarylthiourea Conformers in Solution

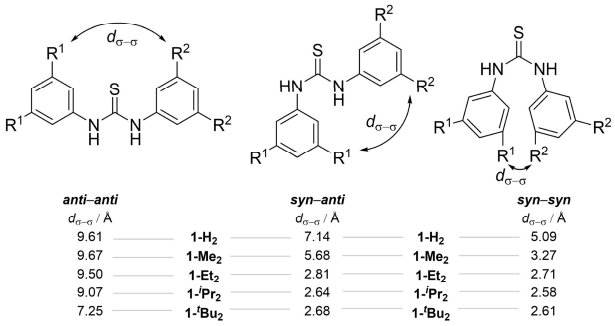
*Lars Rummel[+], Marvin H. J. Domanski[+], Heike Hausmann, Jonathan Becker, and Peter R. Schreiner**

Abstract: We present an experimental and computational study on the conformers of *N*,*N*′-diphenylthiourea substituted with different dispersion energy donor (DED) groups. While the unfolded *anti–anti* conformer is the most relevant for thiourea catalysis, intramolecular noncovalent interactions counterintuitively favor the folded *syn–syn* conformer, as evident from a combination of low-temperature nuclear magnetic resonance measurements and computations. In order to quantify the noncovalent interactions, we utilized local energy decomposition analysis and symmetry-adapted perturbation theory at the DLPNO-CCSD(T)/def2-TZVPP and sSAPT0/6-311G(d,p) levels of theory. Additionally, we applied a double-mutant cycle to experimentally study the effects of bulky substituents on the equilibria. We determined London dispersion as the key interaction that shifts the equilibria towards the *syn–syn* conformers. This preference is likely a factor why such thiourea derivatives can be poor catalysts.

Introduction

In the field of enzyme catalysis, Fischer's "key and lock" hypothesis[1] or the more sophisticated "induced fit" model by Koshland[2] perennially highlight the importance of conformational flexibility and catalytic activity. The structural dynamics of peptides allow enzymes to bind and to recognize substrates effectively and convert them into products. Thus, a specific conformer of the catalyst is needed to exploit transition state stabilization and energetic differentiation among a series of possible transition state geometries. Conformational structure–property relationships can be probed with small molecules as well. The restricted bond rotation within the thioamide functional group offers three differently populated conformers (Scheme 1).[3] While the mechanism for anion recognition or catalytic activation of a substrate due to hydrogen-bonding is most effective via the open *anti–anti* conformer, an analysis of the conformational landscape of thiourea derivatives is an essential part to understand the origin of their catalytic activity and any limitations thereof.[3] Here, we present a study of *all-meta*-disubstituted diphenylthiourea[4] derivatives to elucidate the conformational preferences dependent on noncovalent interactions including London dispersion (LD).[5] Since the compounds discussed in this work both are less catalytically active than commonly exploited thiourea catalysts[4c] and poor anion receptors,[4h,6] we hypothesize this is in part due to the population of a conformer that does not allow double N–H bonding to Lewis-basic atoms or groups in the substrate.[3]

In recent years, a number of studies demonstrated that the catalytically active *anti–anti* diphenyl(thio)urea conformer is not necessarily the predominant conformer in the gas phase and in solution.[3,6a,7] Infrared and temperature-dependent NMR measurements in different solvents demonstrated the presence of multiple conformers for diarylthiourea derivatives.[7] An exception to this conformational flexibility is the well-known *N*,*N*′-bis[3,5-bis(trifluoromethyl)phenyl]thiourea catalyst with the *anti–anti* conformer being predominant in, for example, tetrahydrofuran (THF)



Scheme 1. Lowest energy conformers of diphenylthiourea derivatives with the *anti–anti* (left), *syn–anti* (center), and *syn–syn* (right) conformers. The shown values correspond to the shortest σ–σ distance $d_{\sigma-\sigma}$ contact for each conformer of 1-R^1R^2 computed at B3LYP-D3(BJ)/def2-TZVPP.

[*] L. Rummel,[+] M. H. J. Domanski,[+] H. Hausmann, P. R. Schreiner
Institute of Organic Chemistry, Justus Liebig University
Heinrich-Buff-Ring 17, 35392 Giessen (Germany)
E-mail: prs@uni-giessen.de
J. Becker
Institute of Inorganic and Analytical Chemistry, Justus Liebig University
Heinrich-Buff-Ring 17, 35392 Giessen (Germany)
[+] These authors contributed equally to this work.

© 2022 The Authors. Angewandte Chemie International Edition published by Wiley-VCH GmbH. This is an open access article under the terms of the Creative Commons Attribution Non-Commercial NoDerivs License, which permits use and distribution in any medium, provided the original work is properly cited, the use is non-commercial and no modifications or adaptations are made.

© 2022 The Authors. Angewandte Chemie International Edition published by Wiley-VCH GmbH

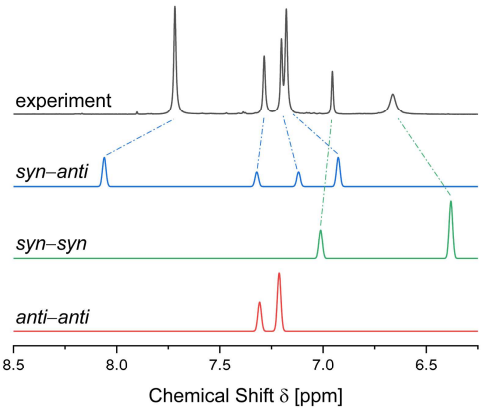


Figure 2. NMR measurements at 193 K of the aromatic signals of **1-^{t}Bu$_2$** (grey) and computed spectra for the *syn–anti* (blue), *syn–syn* (green), and *anti–anti* (red) conformers in THF (SMD solvent model) at the B3LYP-D3(BJ)/def2-TZVPP level of theory. For the full spectral data see the Supporting Information.

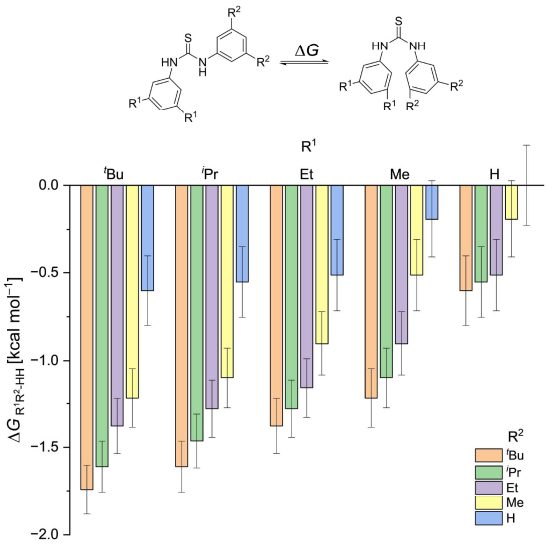


Figure 3. Experimentally determined Gibbs free energy values $\Delta G_{R^1R^2\text{-HH}}$ for the equilibrium between *syn–syn* and *syn–anti* **1-R^{1}R^2** at 193 K' gray lines indicate error bars. $\Delta G < 0$ corresponds to a shift towards the *syn–syn* conformer: The lower and more negative the ΔG expressed, the more favored the *syn–syn* conformer. Note that the supposedly catalytically active *anti–anti* conformation is not populated at all.

(black NMR, Figure 1) shows a distinct symmetric conformer. Nevertheless, **1-^{t}Bu$_2$** favors the *syn–anti* conformer by around $0.5 \pm 0.0(3)$ kcal mol^{-1}. The computed NMR signals (Figure 2) suggest that the new signals belong to the *syn–syn* conformer (green spectrum), which also helped us assign the *syn–anti* (blue spectrum) and disregard the *anti–anti* (red spectrum) conformer. Whereas the N–H proton shift is difficult to determine by NMR computations,[17] the aromatic and aliphatic C–H signals were assigned to the *syn–syn* conformer.

Concentration dependent measurements showed no change in signal ratios with the lowest concentration being 15.5 mM (0.01 mmol). This is in line with NMR measurements investigating the complexation of thiourea catalyst with lactones, where it was found that the *anti–anti* conformer is catalytically most active.[3] Consequently, aggregation in solution was deemed to be unimportant. To ensure that equilibrium had been reached, we equilibrated each NMR sample for one hour at 193 K. Since the barrier height for rotation around the thioamide bond is around 10 kcal mol^{-1}, equilibrium was reached after around 5 min (see Supporting Information for details). After transferring the samples to the NMR spectrometer, they were further equilibrated until the temperature stabilized at 193 K. Figure 1 displays the N–H proton splitting for symmetric **1-R^{1}R^2**. While **1-H$_2$** shows only low concentrations of a second conformer, bulky substituents such as those with *tert*-butyl groups clearly affect the conformer distributions.

Figure 3 displays a summary of the experimentally determined $\Delta G_{R^1R^2\text{-HH}}$ values of the equilibrium between *syn–syn* and *syn–anti* **1-R^{1}R^2** relative to parent *N,N'*-diphenylthiourea **1-H$_2$**. Consequently, **1-H$_2$** is depicted as $\Delta G_{R^1R^2\text{-HH}} = 0.0 \pm 0.2$ kcal mol^{-1} in Figure 3 (rightmost data point). While **1-H$_2$** favors the *syn–anti* conformer by around 2.3 ± 0.1 kcal mol^{-1} (see Supporting Information for absolute energy values), substituents in all-*meta* position shift the equilibrium towards the *syn–syn* conformer ($\Delta G < 0$). In contrast to the often encountered view that large groups repel each other, Figure 3 illustrates that bulky groups favor the conformer that displays close alkyl–alkyl contacts ($d_{\sigma\text{-}\sigma} =$ 2.61 Å for **1-^{t}Bu$_2$**). The *unsymmetric* functionalization in **1-R^{1}H** (blue bars) and **1-HR^2** (rightmost block of columns) only has a small effect on the equilibrium position (up to $\Delta G_{^t\text{BuH-HH}} = -0.6 \pm 0.2$ kcal mol^{-1}). The shift in energy towards the *syn-syn* conformer can be rationalized by attractive σ–π interactions between substituents and opposing phenyl moiety. Thereby, a decrease in distance between substituent and phenyl moiety systematically increases the stabilizing σ–π interactions. A similar effect was already observed and quantified by Shimizu et al. for a *para* substitution pattern utilizing molecular torsion balance.[18] Here, distance dependence of σ–π interactions was documented for a *para* substitution pattern with the largest and bulkiest alkyl groups forming the strongest stabilizing interactions. These observations are consistent with the recent concept of DEDs in which bulky alkyl groups form stabilizing dispersion interactions.[5,13]

By systematically increasing the substituent size on both phenyl moieties, the equilibrium shifts further to the more crowded *syn–syn* structure. The introduction of additional CH_3 groups increases the number of close intramolecular alkyl–alkyl contacts in the *syn–syn* conformer, thereby reducing the distance between substituents (Scheme 1). An increasing number of noncovalent contacts at distances of around 2.5 Å has proven to be effective in stabilizing labile compounds such as hexaphenylethane[19] or rationalizing isomerization energies of linear and branched alkanes.[20] The largest difference in energy due to incorporation of a methyl substituent can be observed from **1-^{t}BuH** (ΔG

© 2022 The Authors. Angewandte Chemie International Edition published by Wiley-VCH GmbH

at elevated temperatures.[3] While the experimental evidence points to the fact that the *anti–anti* conformer of this thiourea catalyst is catalytically most active, other substitution patterns are likely to display a different conformational landscape, which, in turn, is likely to result in reduced catalytic activity.

Most recently, Sandler et al.[6a] highlighted the relationship of conformational effects and the anion binding affinity of receptor molecules such as diphenylthiourea.[4h,6b] Whereas urea and squaramide derivatives prefer the *anti–anti* conformer due to intramolecular CH-carbonyl hydrogen bonding, diphenylthiourea does not benefit as strongly from this stabilization since its phenyl moieties are twisted out of plane.[4c] Consequently, diphenylthiourea populates the *syn–anti* and *syn–syn* conformers, thereby lowering its anion binding affinity.[6a] To explain the enantioselectivity of an asymmetric Henry reaction, Heshmat proposed cinchonathiourea catalyst substrate activation via the *syn–anti* conformer.[8] Experimental data suggest a similar trend. In an extensive study of crystal structures of urea and thiourea derivatives, Luchini et al.[9] showed that around 60% of all thiourea motifs crystallize in a *syn–syn* or *syn–anti* fashion. On the other hand, 98% of urea derivatives are reported to have an *anti–anti* conformation in the solid state.[9] Solid state and gas phase IR[10] and NMR[11] studies in solution support this trend for urea derivatives as well. For diarylthiourea derivatives, IR measurements suggest a significant shift to the *syn–syn* conformer in solution[7] but a systematic NMR study determining the role and the apparent intramolecular stabilization of the *syn–syn* conformer has not been reported.

In order to investigate the equilibria depicted in Scheme 1, we treated the *N,N′*-diphenylthiourea derivatives as molecular balances.[12] By increasing the size of the *all-meta*-substituted aryl dispersion energy donors (DEDs),[5,13] we observed a systematic and counterintuitive shift of the equilibrium toward the folded and more crowded *syn–syn* conformer. The increasing number of close σ–σ contacts is indicative of the prevalence of attractive LD[14] interactions rather than Pauli (exchange) repulsion. This effect was recently emphasized in a study of the equilibria of 1,4- and 1,6-di-*t*butyl cyclooctatetraene in a large series of solvents of very different polarities showing that intramolecular LD interactions do not cancel in solution.[15]

Results and Discussion

To dissect the influence of each DED, we synthesized a logical series of diphenylthiourea derivatives with methyl (Me), ethyl (Et), *iso*-propyl (^{i}Pr), and *tert*-butyl (^{t}Bu) substituents. In brief, the *all-meta*-substituted *N,N′*-diphenylthioureas were synthesized via a two-step addition of aniline precursors to thiophosgene.[3] Prior, the *all-meta*-substituted aniline precursors were generated via bromination and de-diazotization reaction of 2,6-disubstituted aniline derivatives (for details, see Supporting Information).[16] To gather as much information as possible, we generated all R^1 and R^2 combinations of these groups and measured ^{1}H NMR spectra in THF. The choice of solvent was based on its physical properties (i.e., low melting point) and the fact that all diphenylthiourea derivatives remained soluble during the low-temperature NMR measurements.

The restricted bond rotation of all *N,N′*-diphenylthiourea derivatives required low-temperature NMR measurements (performed at 193 K) in order to freeze the C–N bond rotation. The lowest temperature possible to hold up over a longer period of time in the NMR was 193 K. Intrinsic reaction coordinate (IRC) computations suggest activation barriers of 10.3 kcal mol^{-1} (corresponding to a rate constant of 4.0×10^{-3} s^{-1}) and 9.0 kcal mol^{-1} (1.3 s^{-1}) for unsubstituted diphenylthiourea.[3] We first tested our approach with *N,N′*-bis(3,5-di-*tert*-butylphenyl)thiourea **1-^{t}Bu$_2$** (**1-R^{1}R^2**) and the parent *N,N′*-diphenylthiourea **1-H$_2$**. For both derivatives the singlet N–H signal splits into three separate signals upon cooling, two of which belong to the same conformer (blue marking, Figure 1). Additionally, the aromatic signals (Figure 2) split into four, and the aliphatic *tert*-butyl signals into two separate NMR peaks.

Accordingly, these signals were assigned to the *syn–anti* conformer since it is the only structure with inequivalent N–H, aromatic, and *tert*-butyl protons. While the parent **1-H$_2$** (purple NMR, Figure 1) considerably favors the *syn–anti* conformer by around 2.3 ± 0.1 kcal mol^{-1} (all energies were determined via K_{eq} at 193 K), the NMR of **1-^{t}Bu$_2$**

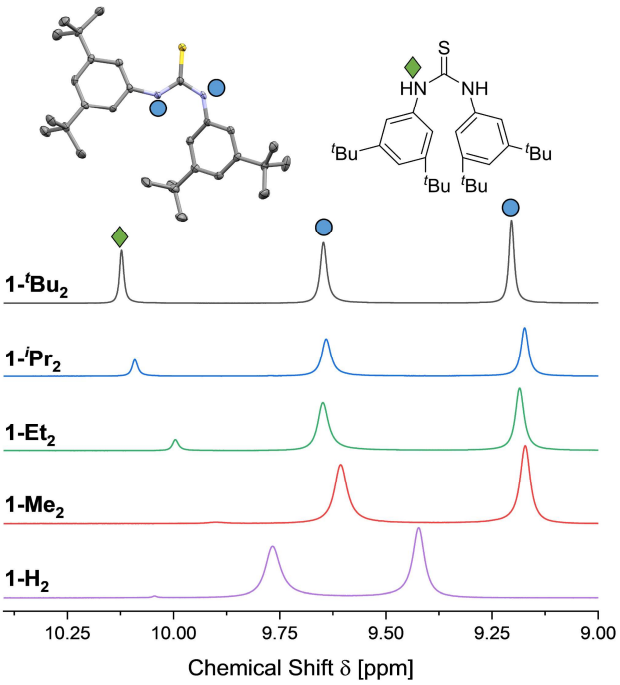


Figure 1. NMR measurements at 193 K of symmetrically substituted *N,N′*-diphenylthiourea derivatives **1-R^{1}R^2** in THF and molecular structure of **1-^{t}Bu$_2$**. For simplicity, the NH signals of symmetric **1**-R^{1}R^2 are depicted only. Thermal ellipsoid plot of the molecular structure obtained by single-crystal X-ray diffraction was drawn at 50% probability level. The blue markings correspond to the NH signals of the *syn–anti* and the green markings to the *syn–syn* conformer. Note that the *anti–anti* conformer is not populated and has therefore been omitted.

© 2022 The Authors. Angewandte Chemie International Edition published by Wiley-VCH GmbH

$_{t}$BuH-HH = −0.6 ± 0.2 kcal mol^{-1}) to **1-^{t}BuMe** ($\Delta G_{^{t}BuMe\text{-}HH}$ = −1.2 ± 0.2 kcal mol^{-1}) with around −0.6 kcal mol^{-1} stabilization due to σ–σ contacts.[21] Additional methyl groups shift the equilibrium further towards the *syn–syn* conformer by around −0.1 kcal mol^{-1}. Consequently, the most prominent effects can be observed for **1-R^{1}/^{t}Bu** derivatives (orange bars), which shift the equilibria significantly towards the *syn–syn* conformer (up to ΔG $_{^{t}Bu/^{t}Bu\text{-}HH}$ = −1.7 ± 0.1 kcal mol^{-1}). Hence, the experimental data suggest that increasingly larger alkyl substituents act as stabilizing DEDs rather than as repulsive steric bulk.[5,19,22] Correlations of our experimental findings with the molecular volume or in the total molecular dipole moment of each conformer are insufficient to rationalize the trends observed (see Supporting Information).

To support these findings, we performed a computational study focusing on the role of intramolecular noncovalent interactions. To be able to switch dispersion corrections on and off, we utilized density functional theory (DFT) to investigate the equilibria depicted in Scheme 1. After an initial conformer analysis using the Conformer–Rotamer Ensemble Sampling Tool[23] (crest) program, the lowest conformers were further optimized with Ahlrich's def2-TZVPP[24] basis set. The B3LYP[25] functional was utilized with and without (Supporting Information) Grimme's D3[26] correction including Becke–Johnson[27] (BJ) damping. All geometry optimizations were performed in the gas phase under standard conditions. The gas phase structures were utilized for single-point energy computations to account for solvation effects and entropy at 193 K. The polarizable continuum model (PCM)[28] was used with THF as solvent and thermal corrections added from DFT (gas phase) frequency computations. Additionally, the B3LYP-D3(BJ) (gas phase) optimized structures were utilized for single-point energy computations at the DLPNO-CCSD(T)/def2-TZVPP level of theory.[29] This analysis follows that of Sandler et al. (Supporting Information)[6a] who demonstrated that the B3LYP functional in conjunction with medium-sized basis sets is an appropriate approach for geometry optimizations of thiourea derivatives and, that DLPNO-CCSD(T)/large basis set is an excellent approximation to its canonical counterpart. Since LD interactions are in a first approximation temperature independent, the results of the thermochemical analysis of the equilibrium fit qualitatively to gas phase computations (see Supporting Information).[14] The thermochemical results (ΔG_{eq}) for the symmetric and unsymmetric *N,N′*-diphenylthiourea molecular balances are depicted in Figure 4. While the *anti–anti* conformer is highest in energy (red markings) for all systems and cannot be observed by NMR, the *syn–syn* (green markings) conformers are generally favored. Computations on B3LYP/def2-TZVPP excluding the LD corrections predict the *syn–anti*/*anti–syn* conformers to be favored by around 3–4 kcal mol^{-1}. Including LD, the unsubstituted balance already slightly favors the *syn–syn* conformer ($\Delta G_{eq} \approx -0.3$ kcal mol^{-1}). Increasing alkyl substitution shifts the global energy minimum further from the *syn–anti* towards the *syn–syn* conformer. The largest effect can be observed for **1-^{t}Bu$_2$** ($\Delta G_{eq} \approx -2.8$ kcal mol^{-1}). These results

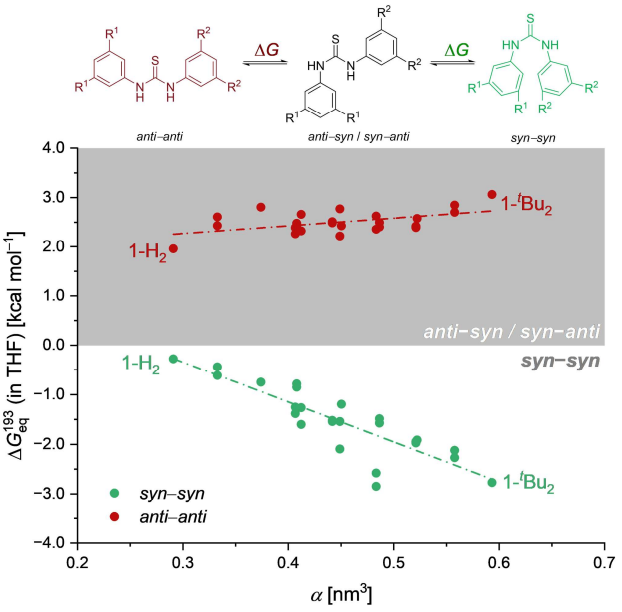


Figure 4. Gibbs free energies at 193 K for the equilibrium of the *syn–syn* (green markings) and *anti–anti* (red markings) conformers relative to the *syn–anti*/*anti–syn* conformers of **1-R^{1}R^{2}** at the DLPNO-CCSD(T)/def2-TZVP//B3LYP-D3(BJ)/def2-TZVPP level of theory including a solvent correction (THF) at the B3LYP-D3(BJ)/def2-TZVPP utilizing the PCM model. Thermal corrections were added from DFT optimizations at 193 K. **1-H$_2$** and **1-^{t}Bu$_2$** are highlighted for clarity.

fit qualitatively well to our experimental data, albeit the attenuation of the attractive interactions due to solvent effects is higher than predicted by the computations.[30]

To assess these counterintuitive results, we visualized the intramolecular noncovalent contacts (Figure 5) utilizing noncovalent interaction (NCI) plots[31] to highlight the main source of thermodynamic stability of **1-^{t}Bu$_2$** by depicting the reduced density gradient in regions of low electron density. While strongly attractive and repulsive interactions are color-coded in blue and red, respectively, green isosurfaces can be assigned to weak NCIs. The *anti–anti* conformer of **1-^{t}Bu$_2$** features a mixture of red and blue isosurfaces due to the substitution pattern and a CH···S contact[4c] a green contact area is not visible. On the other hand, the *syn–anti* conformer already shows small green areas between bulky ^{t}Bu substituents and the opposing phenyl group. Finally, the *syn–syn* conformer shows large green isosurfaces implying significant intramolecular NCIs. An incorporation of bulky alkyl groups increases the number of noncovalent contacts via close σ–σ (i.e., ^{t}Bu–^{t}Bu in Figure 5) and σ–π (^{t}Bu–π) contacts of both substituents. This analysis qualitatively supports experimental and computational findings.

To quantify the amount of LD interactions between each substituent, we dissected the energy values $\Delta\Delta G_{R^1R^2}$ from singly substituted molecular balances.[32] Hereby, two substituents R^{1} and R^{2} are mutated separately to investigate the impact of each substituent on the thiourea molecular backbone. According to the following equation the inter-

© 2022 The Authors. Angewandte Chemie International Edition published by Wiley-VCH GmbH

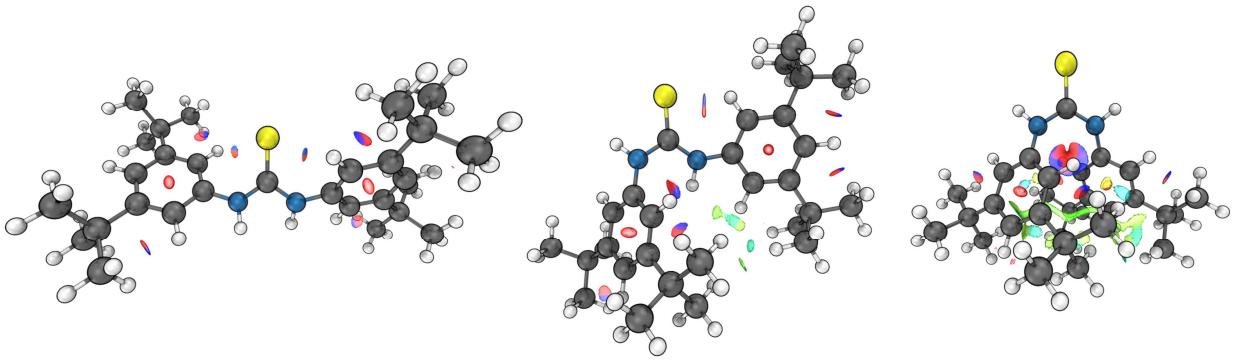


Figure 5. Noncovalent interaction (NCI) plots of the *anti–anti* (left), *syn–anti* (center), and *syn–syn* (right) conformers of **1-^{t}Bu$_2$** at B3LYP-D3(BJ)/def2-TZVPP. Isosurfaces (isovalue s of 0.2, ranging from sign(λ_2)ρ = −0.05 a.u. to +0.05 a.u.) are color-coded red (indicating strong repulsion), blue (strong attractive interactions), and green (corresponding to weak NCI).

action energy $\Delta\Delta G_{R^1R^2}$ between two substituents can be determined as follows:

$$\Delta\Delta G_{R^1R^2} = \Delta G_{R^1R^2} - \Delta G_{R^1H} - \Delta G_{HR^2} + \Delta G_{HH} \quad (1)$$

While this application of Hess's law (also referred to as double mutant cycle) gives an experimental estimate of the role each DED plays, the results have to be treated with caution due to a large error estimate (see Supporting Information for details). Nevertheless, Figure 6 qualitatively supports our findings that sterically hindered diphenylthiourea derivatives favor the *syn–syn* conformer. In general, all calculated energies are negative implying a stabilizing effect between the alkyl groups. Especially for large moieties, a stabilization of the *syn–syn* conformer can be observed ($\Delta\Delta G_{^t\mathrm{Bu}^t\mathrm{Bu}} = -0.5 \pm 0.3$ kcal mol^{-1}). Therefore, around 30% of the observed Gibbs free energy values ($\Delta\Delta G_{^t\mathrm{Bu}^t\mathrm{Bu}\text{-HH}} = -1.7 \pm 0.1$ kcal mol^{-1}) can be assigned to stabilizing alkyl–alkyl contacts. The remaining 70% consists of σ–π interactions between ^{t}Bu and the opposing phenyl moiety.[21] The smallest effect was measured for the **1-Me$_2$** molecular balance ($\Delta\Delta G_{\mathrm{MeMe}} = -0.1 \pm 0.4$ kcal mol^{-1}). In comparison to $\Delta\Delta G_{R^1\mathrm{Me}}$ (yellow bars), $\Delta\Delta G_{R^1\mathrm{Et}}$ (purple bars) does not profit from an additional CH_3 group. This can be rationalized with an entropic penalty[33] due to increasing flexibility of the ethyl substituent.

With the aim to dissect the intramolecular interaction energy into its main contributors, we employed symmetry-adapted-perturbation theory[34] (SAPT) analysis as implemented in PSI4.[35] The scaled version was used according to Sherrill et al.[36] to improve the performance of the decomposition method. We focused solely on the interaction between the two substituted phenyl moieties. As a starting point, we took the B3LYP-D3(BJ)/def2-TZVPP optimized geometries and removed the thiourea moiety. The resulting phenyl radicals were saturated with hydrogen yielding a benzene dimer in geometry of the *syn–syn*, *syn–anti* and *anti–anti* conformer. This approach allows us to transfer the intramolecular into intermolecular interactions between two substituted benzene molecules. While the electronic constitution of benzene varies from the electronic structure

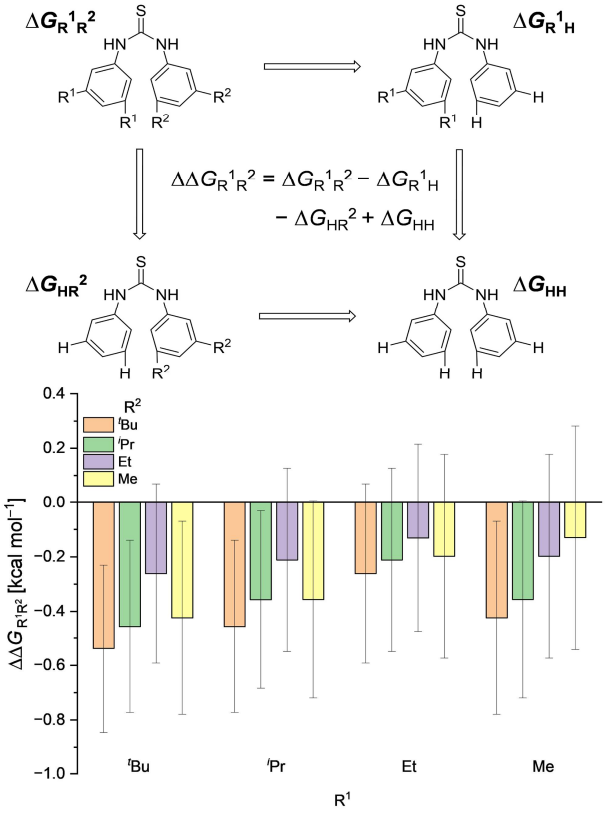


Figure 6. Double mutant cycle (top) to dissect the interaction energy $\Delta\Delta G_{R^1R^2}$ and results of the analysis (bottom); gray lines indicate error bars. $\Delta\Delta G_{R^1R^2}$ describes the relative interaction energies of R^1–R^2 contacts of the *syn–anti* and *syn–syn* equilibrium at 193 K. Negative energies correspond to stabilizing interactions between both groups.

within diphenylthiourea, this method was solely used to identify the main source of thermodynamic stability. Figure 7 displays the energy decomposition of the total interaction energy (E_{tot}) between two di-substituted benzene molecules based on their geometry in the *syn–syn* conformer (for other conformers see Supporting Information). While inductive effects (E_{ind}, blue markings) only play a minor role

© 2022 The Authors. Angewandte Chemie International Edition published by Wiley-VCH GmbH

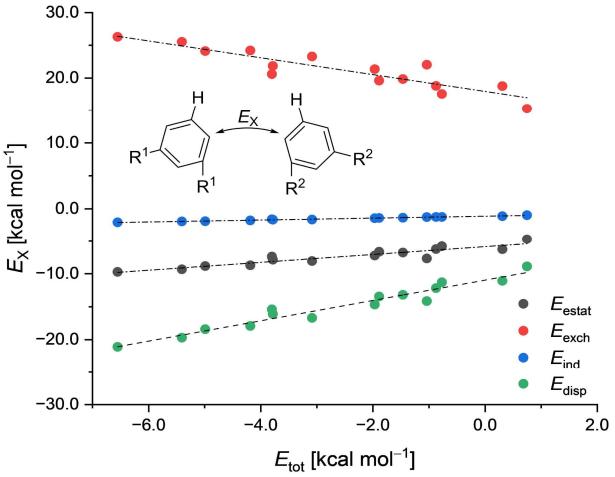


Figure 7. sSAPT analysis of two 1,3-disubstituted benzene molecules in the geometry of the *syn–syn* thiourea conformers at sSAPT0/6-311G(d,p) at 298 K. The dashed lines are used to guide the eye.

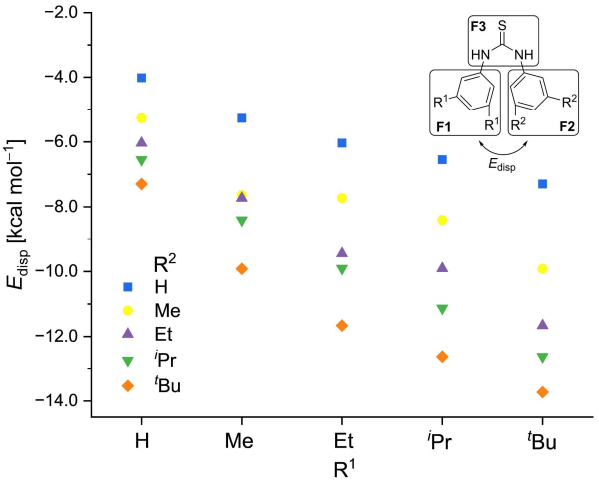


Figure 8. LD interaction energies derived from LED analysis of two **1-R^{1}R^2** substituted phenyl moieties in *syn–syn* conformer at DLPNO-CCSD(T)/def-TZVP//B3LYP-D3(BJ)/def2-TZVPP at 298 K.

in the dimerization of substituted benzene, electrostatic (E_{estat}, grey markings) as well as LD interaction (E_{disp}, green markings) are essential to understand the interaction energy between two benzene molecules. Both energies, E_{estat} and E_{disp}, stabilize the benzene dimer due to alkyl substitution with LD interactions as the major component (up to $E_{disp} = -21.1$ kcal mol^{-1} for **1-^{t}Bu$_2$**). Nevertheless, only a combination of both energies overcompensates the destabilizing contributions of Pauli exchange repulsion (E_{exch}, red markings). Especially for **1-H$_2$**, repulsive interactions ($E_{exch} = +15.3$ kcal mol^{-1}) disfavor the aggregation of benzene and override all stabilizing effects ($E_{tot} = +0.7$ kcal mol^{-1}). While Herbert et al.[37] identified LD as the main attractive component in cofacial π-stacking (via σ–π contacts) of benzene, this effect alone is not strong enough to stabilize **1-H$_2$**. The geometry of close benzene dimers enforced through the thiourea molecular backbone is therefore not ideal to afford the perfect balance between attractive and repulsive contacts. With increasing substituent bulkiness repulsive interactions increase (up to $E_{exch} = +26.3$ kcal mol^{-1} for **1-^{t}Bu$_2$**) but do not overcompensate the attractive interactions.

After establishing that LD interactions are the major factor for the conformational preference of diphenylthiourea derivatives, we set out to quantify the magnitude of LD interactions between the aromatic moieties without changing the electronic structure of *N*,*N*′-diphenylthiourea. While the double mutant cycle (Figure 6) represents the total interaction energy (sum of all attractive and repulsive components) between DED groups attached, the overall energy gain due to LD interactions was dissected using a Local Energy Decomposition (LED) analysis[38] as implemented in ORCA.[39] Therefore, we fragmented every *N*,*N*′-diphenylthiourea molecular balance into three parts (F1, F2, and F3). During this process all bonds are cleaved homolytically resulting in large electrostatic interactions between all fragments. Consequently, we investigated only the gain in energy due to LD interactions between F1 and F2. Figure 8 shows the results of the analysis for the *syn–syn* conformers (see Supporting Information for other conformers).

The LED analysis fits qualitatively to the results of computational and experimental data very well. In comparison to the SAPT analysis, LED suggests lower LD contributions (around 6 kcal mol^{-1}), but this is due to the different models used. Accordingly, **1-H$_2$** and the semi-substituted **1-HR^2** series benefit the least from LD interactions (between −4.0 to −7.3 kcal mol^{-1}). On the other hand, substitution on both phenyl moieties results in higher LD interaction energies up to $E_{disp} = -13.7$ kcal mol^{-1} for **1-^{t}Bu$_2$**. This effect is most prominent in the *syn–syn* conformer. All methods utilized to quantify noncovalent interactions demonstrate the role of LD on the conformational preference of *N*,*N*′-diphenylthiourea derivatives. The experimental and computational data suggest simple additivity of the DED strength due to an increasing preference of the *syn–syn* conformer with growing steric bulk. The double mutant cycle highlights both, σ–σ and σ–π contacts as the origin of stabilization.

Conclusion

We performed a systematic experimental-computational study on the folding equilibria of all-*meta* substituted diphenylthiourea derivatives investigating the impact of steric bulk on the conformer preferences. In stark contrast to the broadly accepted dominance of Pauli repulsion dictating conformations, we identified LD interactions as the main contributor that counterintuitively stabilizes the *syn–syn* conformers. Therefore, LD proves to be a powerful interaction to shift equilibria towards apparently *more crowded* conformers.

A double-mutant cycle allowed us to quantify and differentiate between attractive σ–σ and σ–π contacts as

© 2022 The Authors. Angewandte Chemie International Edition published by Wiley-VCH GmbH

origin of stabilization. The most prominent shift towards the folded *syn–syn* conformer was observed when attaching bulky *tert*-butyl substituents to diphenylthiourea. An SAPT analysis reveals a combination of electrostatic and LD interactions counteracting Pauli repulsion. The LED analysis helped quantify intramolecular LD interactions and confirmed *tert*-butyl substituents to be highly effective DEDs.

Acknowledgements

This work was supported by the priority program "Control of London Dispersion in Molecular Chemistry" (SPP1807) of the Deutsche Forschungsgemeinschaft. We thank Jan M. Schümann for fruitful discussions. Open Access funding enabled and organized by Projekt DEAL.

Conflict of Interest

The authors declare no conflict of interest.

Data Availability Statement

The data that support the findings of this study are available in the Supporting Information of this article.

Keywords: Conformational Analysis · Local Energy Decomposition · Pauli Repulsion · Symmetry-Adapted-Perturbation Theory · σ–σ Interactions

[1] E. Fischer, *Ber. Dtsch. Chem. Ges.* **1894**, *27*, 2985–2993.
[2] D. E. Koshland, *Proc. Natl. Acad. Sci. USA* **1958**, *44*, 98.
[3] K. M. Lippert, K. Hof, D. Gerbig, D. Ley, H. Hausmann, S. Guenther, P. R. Schreiner, *Eur. J. Org. Chem.* **2012**, 5919–5927.
[4] a) P. R. Schreiner, A. Wittkopp, *Org. Lett.* **2002**, *4*, 217–220; b) P. R. Schreiner, *Chem. Soc. Rev.* **2003**, *32*, 289–296; c) A. Wittkopp, P. R. Schreiner, *Chem. Eur. J.* **2003**, *9*, 407–414; d) Y. Takemoto, *Org. Biomol. Chem.* **2005**, *3*, 4299–4306; e) S. J. Connon, *Chem. Eur. J.* **2006**, *12*, 5418–5427; f) M. S. Taylor, E. N. Jacobsen, *Angew. Chem. Int. Ed.* **2006**, *45*, 1520–1543; *Angew. Chem.* **2006**, *118*, 1550–1573; g) A. G. Doyle, E. N. Jacobsen, *Chem. Rev.* **2007**, *107*, 5713–5743; h) Z. Zhang, P. R. Schreiner, *Chem. Soc. Rev.* **2009**, *38*, 1187–1198.
[5] J. P. Wagner, P. R. Schreiner, *Angew. Chem. Int. Ed.* **2015**, *54*, 12274–12296; *Angew. Chem.* **2015**, *127*, 12446–12471.
[6] a) I. Sandler, F. A. Larik, N. Mallo, J. E. Beves, J. Ho, *J. Org. Chem.* **2020**, *85*, 8074–8084; b) F. Dressler, P. R. Schreiner in *Anion–Binding Catalysis* (Ed.: O. G. Mancheño), Wiley-VCH, Weinheim, **2022**, pp. 1–77.
[7] B. Galabov, G. Vassilev, N. Neykova, A. Galabov, *J. Mol. Struct.* **1978**, *44*, 15–21.
[8] M. Heshmat, *J. Phys. Chem. A* **2018**, *122*, 7974–7982.
[9] G. Luchini, D. M. H. Ascough, J. V. Alegre-Requena, V. Gouverneur, R. S. Paton, *Tetrahedron* **2019**, *75*, 697–702.
[10] a) R. Emery, N. A. Macleod, L. C. Snoek, J. P. Simons, *Phys. Chem. Chem. Phys.* **2004**, *6*, 2816–2820; b) H. M. Badawi, W. Förner, *Spectrochim. Acta Part A* **2012**, *95*, 435–441.
[11] L. V. Sudha, D. N. Sathyanarayana, S. N. Bharati, *Magn. Reson. Chem.* **1987**, *25*, 474–479.
[12] a) S. Paliwal, S. Geib, C. S. Wilcox, *J. Am. Chem. Soc.* **1994**, *116*, 4497–4498; b) I. K. Mati, S. L. Cockroft, *Chem. Soc. Rev.* **2010**, *39*, 4195–4205; c) M. A. Strauss, H. A. Wegner, *Eur. J. Org. Chem.* **2019**, 295–302.
[13] S. Grimme, R. Huenerbein, S. Ehrlich, *ChemPhysChem* **2011**, *12*, 1258–1261.
[14] a) F. London, *Z. Phys.* **1930**, *63*, 245–279; b) F. London, *Trans. Faraday Soc.* **1937**, *33*, 8b–26.
[15] J. M. Schümann, J. P. Wagner, A. K. Eckhardt, H. Quanz, P. R. Schreiner, *J. Am. Chem. Soc.* **2021**, *143*, 41–45.
[16] C. Eschmann, L. Song, P. R. Schreiner, *Angew. Chem. Int. Ed.* **2021**, *60*, 4823–4832; *Angew. Chem.* **2021**, *133*, 4873–4882.
[17] H. C. Da Silva, W. B. De Almeida, *Chem. Phys.* **2020**, *528*, 110479.
[18] J. Hwang, P. Li, M. D. Smith, K. D. Shimizu, *Angew. Chem. Int. Ed.* **2016**, *55*, 8086–8089; *Angew. Chem.* **2016**, *128*, 8218–8221.
[19] S. Rösel, C. Balestrieri, P. R. Schreiner, *Chem. Sci.* **2017**, *8*, 405–410.
[20] a) K. S. Pitzer, *J. Chem. Phys.* **1955**, *23*, 1735–1735; b) K. S. Pitzer, E. Catalano, *J. Am. Chem. Soc.* **1956**, *78*, 4844–4846.
[21] a) M. Alonso, T. Woller, F. J. Martín-Martínez, J. Contreras-García, P. Geerlings, F. De Proft, *Chem. Eur. J.* **2014**, *20*, 4931–4941; b) A. A. Fokin, D. Gerbig, P. R. Schreiner, *J. Am. Chem. Soc.* **2011**, *133*, 20036–20039.
[22] a) L. Schweighauser, M. A. Strauss, S. Bellotto, H. A. Wegner, *Angew. Chem. Int. Ed.* **2015**, *54*, 13436–13439; *Angew. Chem.* **2015**, *127*, 13636–13639; b) G. Lu, R. Y. Liu, Y. Yang, C. Fang, D. S. Lambrecht, S. L. Buchwald, P. Liu, *J. Am. Chem. Soc.* **2017**, *139*, 16548–16555.
[23] P. Pracht, F. Bohle, S. Grimme, *Phys. Chem. Chem. Phys.* **2020**, *22*, 7169–7192.
[24] A. Schäfer, C. Huber, R. Ahlrichs, *J. Chem. Phys.* **1994**, *100*, 5829–5835.
[25] a) C. Lee, W. Yang, R. G. Parr, *Phys. Rev. B* **1988**, *37*, 785–789; b) A. D. Becke, *J. Chem. Phys.* **1993**, *98*, 5648–5652.
[26] S. Grimme, J. Antony, S. Ehrlich, H. Krieg, *J. Chem. Phys.* **2010**, *132*, 154104.
[27] S. Grimme, S. Ehrlich, L. Goerigk, *J. Comput. Chem.* **2011**, *32*, 1456–1465.
[28] a) S. Miertuš, E. Scrocco, J. Tomasi, *Chem. Phys.* **1981**, *55*, 117–129; b) J. Tomasi, B. Mennucci, R. Cammi, *Chem. Rev.* **2005**, *105*, 2999–3094.
[29] a) C. Riplinger, F. Neese, *J. Chem. Phys.* **2013**, *138*, 034106; b) D. G. Liakos, M. Sparta, M. K. Kesharwani, J. M. L. Martin, F. Neese, *J. Chem. Theory Comput.* **2015**, *11*, 1525–1539.
[30] a) L. Yang, C. Adam, G. S. Nichol, S. L. Cockroft, *Nat. Chem.* **2013**, *5*, 1006–1010; b) R. Pollice, M. Bot, I. J. Kobylianskii, I. Shenderovich, P. Chen, *J. Am. Chem. Soc.* **2017**, *139*, 13126–13140.
[31] a) E. R. Johnson, S. Keinan, P. Mori-Sánchez, J. Contreras-García, A. J. Cohen, W. Yang, *J. Am. Chem. Soc.* **2010**, *132*, 6498–6506; b) J. Contreras-García, E. R. Johnson, S. Keinan, R. Chaudret, J.-P. Piquemal, D. N. Beratan, W. Yang, *J. Chem. Theory Comput.* **2011**, *7*, 625–632.
[32] a) P. J. Carter, G. Winter, A. J. Wilkinson, A. R. Fersht, *Cell* **1984**, *38*, 835–840; b) H. Adams, F. J. Carver, C. A. Hunter, J. C. Morales, E. M. Seward, *Angew. Chem. Int. Ed. Engl.* **1996**, *35*, 1542–1544; *Angew. Chem.* **1996**, *108*, 1628–1631.
[33] a) D. Van Craen, W. H. Rath, M. Huth, L. Kemp, C. Räuber, J. M. Wollschläger, C. A. Schalley, A. Valkonen, K. Rissanen, M. Albrecht, *J. Am. Chem. Soc.* **2017**, *139*, 16959–16966; b) M. A. Strauss, H. A. Wegner, *Angew. Chem. Int. Ed.* **2019**, *58*, 18552–18556; *Angew. Chem.* **2019**, *131*, 18724–18729.
[34] K. Szalewicz, *WIREs Comput. Mol. Sci.* **2012**, *2*, 254–272.

© 2022 The Authors. Angewandte Chemie International Edition published by Wiley-VCH GmbH

[35] a) J. M. Turney, A. C. Simmonett, R. M. Parrish, E. G. Hohenstein, F. A. Evangelista, J. T. Fermann, B. J. Mintz, L. A. Burns, J. J. Wilke, M. L. Abrams, N. J. Russ, M. L. Leininger, C. L. Janssen, E. T. Seidl, W. D. Allen, H. F. Schaefer, R. A. King, E. F. Valeev, C. D. Sherrill, T. D. Crawford, *WIREs Comput. Mol. Sci.* **2012**, *2*, 556–565; b) R. M. Parrish, L. A. Burns, D. G. A. Smith, A. C. Simmonett, A. E. DePrince, E. G. Hohenstein, U. Bozkaya, A. Y. Sokolov, R. Di Remigio, R. M. Richard, J. F. Gonthier, A. M. James, H. R. McAlexander, A. Kumar, M. Saitow, X. Wang, B. P. Pritchard, P. Verma, H. F. Schaefer, K. Patkowski, R. A. King, E. F. Valeev, F. A. Evangelista, J. M. Turney, T. D. Crawford, C. D. Sherrill, *J. Chem. Theory Comput.* **2017**, *13*, 3185–3197.

[36] T. M. Parker, L. A. Burns, R. M. Parrish, A. G. Ryno, C. D. Sherrill, *J. Chem. Phys.* **2014**, *140*, 094106.

[37] a) K. Carter-Fenk, J. M. Herbert, *Chem. Sci.* **2020**, *11*, 6758–6765; b) K. Carter-Fenk, J. M. Herbert, *Phys. Chem. Chem. Phys.* **2020**, *22*, 24870–24886.

[38] a) W. B. Schneider, G. Bistoni, M. Sparta, M. Saitow, C. Riplinger, A. A. Auer, F. Neese, *J. Chem. Theory Comput.* **2016**, *12*, 4778–4792; b) A. Altun, M. Saitow, F. Neese, G. Bistoni, *J. Chem. Theory Comput.* **2019**, *15*, 1616–1632; c) A. Altun, F. Neese, G. Bistoni, *J. Chem. Theory Comput.* **2019**, *15*, 215–228.

[39] F. Neese, *WIREs Comput. Mol. Sci.* **2018**, *8*, e1327.

Manuscript received: March 24, 2022
Accepted manuscript online: May 11, 2022
Version of record online: June 14, 2022

© 2022 The Authors. Angewandte Chemie International Edition published by Wiley-VCH GmbH

2.2 Assessing Benzene Dimer Interactions in Solution With a Molecular Balance



Abstract

We present a combined experimental and computational study of a 1,4/1,6-dibenzyl substituted cyclooctatetraene (COT)-based molecular balance as a model to assess the benzene dimer interactions in solution. This is accomplished by investigating the equilibrium between the unfolded 1,4- versus folded 1,6-dibenzyl COT in a variety of common organic solvents. NMR measurements demonstrate that the 1,6-COT isomer, in which the phenyl moieties are in proximity, is always favored over the unfolded and sterically less hindered 1,4-COT by ~ 0.3 kcal mol^{-1}, irrespective of solvent. Computations identify London dispersion (LD) interactions between the aromatic moieties in 1,6-COT as the main stabilizing force.

***Reference*:**

Marvin H. J. Domanski, Michael Fuhrmann, Nils F. Hacket, Heike Hausmann, and Peter R. Schreiner, *Chem. Eur. J.* **2026**, *32*, e71126.

DOI: 10.1002/chem.71126

Reproduced with permission from © 2026 Wiley-VCH GmbH.

Chemistry – A European Journal

ChemEurJ Chemistry Europe European Chemical Societies Publishing

RESEARCH ARTICLE OPEN ACCESS

Assessing Benzene Dimer Interactions in Solution With a Molecular Balance

Marvin H. J. Domanski | Michael Fuhrmann | Nils F. Hacket | Heike Hausmann | Peter R. Schreiner

Institute of Organic Chemistry, Justus Liebig University, Giessen, Germany

Correspondence: Peter R. Schreiner (prs@uni-giessen.de)

Received: 19 April 2026 | **Revised:** 19 April 2026 | **Accepted:** 26 April 2026

Keywords: CH-π Interactions | London dispersion | noncovalent interactions | solvent effects | steric effects

ABSTRACT

We present a combined experimental and computational study of a 1,4/1,6-dibenzyl substituted cyclooctatetraene (COT)-based molecular balance as a model to assess the benzene dimer interactions in solution. This is accomplished by investigating the equilibrium between the unfolded 1,4- versus folded 1,6-dibenzyl COT in a variety of common organic solvents. NMR measurements demonstrate that the 1,6-COT isomer, in which the phenyl moieties are in proximity, is always favored over the unfolded and sterically less hindered 1,4-COT by ~0.3 kcal mol^{-1}, irrespective of solvent. Computations identify London dispersion (LD) interactions between the aromatic moieties in 1,6-COT as the main stabilizing force.

1 | Introduction

Noncovalent interactions (NCIs) between aromatic moieties play a key role in biochemistry [1], material science [2], catalysis [3–11], and provide important insights into reaction mechanisms as well as selectivities, as exemplified by the previously investigated Johnson–Corey–Chaykovsky epoxidation [12]. These interactions help rationalize protein folding [13–16], stacking of DNA bases [17], or enantioselectivity in catalytic transformations [5, 10]. Chemists often refer to NCIs between aromatic moieties as "π-π" stacking or "σ-π" interactions (amongst other names) [2, 18, 19]. However, multiple detailed studies on, for example, the benzene dimer conclude that the π-orbitals do not significantly engage in quadrupole overlap-driven bonding and the benzene dimer is best described as a van der Waals complex in which charge transfer, induction, exchange-repulsion, and primarily London dispersion (LD) interactions play a dominant role with an R^{-6} distance dependence of the dimerization energy [18, 20, 21]. These findings have replaced the originally proposed model and rules suggested by Hunter et al. [17, 22, 23], who emphasized the quadrupole-quadrupole electrostatic component of the stacking interaction.

High-level computational studies revealed that the two minima on the potential energy surface (PES) correspond to the tilted T-shaped (**TT**, C_s symmetry) and parallel displaced (**PD**, C_{2h} symmetry) structure (Figure 1) [24]. Early studies suggested the C_{2v}-symmetric **T**-shaped configuration as the global minimum. However, multiple sources now established that the tilted C_s-symmetric **T**-shaped configuration (**TT**) is slightly more stable, with a dissociation energy of $\Delta E = 2.83$ kcal mol^{-1} [24]. The **PD** dimer is the second minimum with a dissociation energy of $\Delta E = 2.68$ kcal mol^{-1} [24, 25]. The computed values align well with gas-phase ionization experiments, which have yielded dissociation energies of $\Delta D_0 = 1.61$ kcal mol^{-1} and 2.40 kcal mol^{-1} for benzene dimer formation [26–28].

However, interactions observed in the gas phase may not directly translate to solution, where entropic and solvent effects often weaken NCIs [7, 10, 29]. Consequently, the dissociation energies

Marvin H. J. Domanski and Michael Fuhrmann contributed equally to this work.

This is an open access article under the terms of the Creative Commons Attribution License, which permits use, distribution and reproduction in any medium, provided the original work is properly cited.
© 2026 The Author(s). *Chemistry – A European Journal* published by Wiley-VCH GmbH

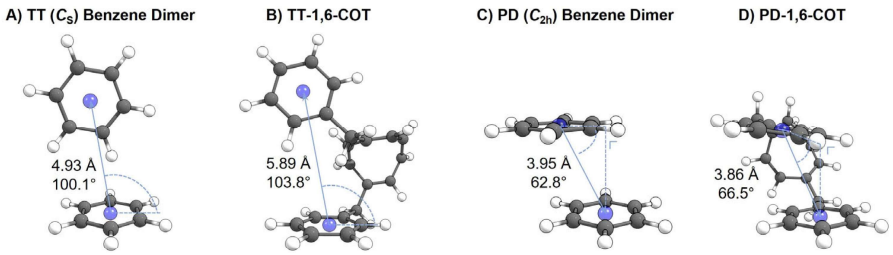


FIGURE 1 | Left: The benzene dimer in the tilted T-shaped (**TT**, C_s symmetry). Right: Parallel displaced (**PD**, C_{2h} symmetry) computed at the CCSD(T)/CBS level of theory [24]. In comparison, our **COT**-model system to mimic the benzene dimer interactions in solution at the ωB97X-D4/def2-TZVPP level of theory. Ph-Ph angles and distances are given for the center of each benzene to highlight the similarities between the reference and model system.

reported for benzene dimers in the gas phase may overestimate interaction strengths in solution.

To address this, the Wilcox group conducted pioneering work on **T**-oriented aromatic interactions using molecular torsion balances [30]. These balances derive relative strengths of NCIs through equilibrium studies involving a "folded" (sterically hindered) state, where two moieties interact intramolecularly, and an "unfolded" (sterically less hindered) state, where the groups are separated and their interactions minimized [31]. ^{1}H-NMR spectroscopy revealed that the **T**-shaped arrangement of the aromatic moieties in the Wilcox balance exhibited a Gibbs free interaction energy of 0.24 kcal mol^{-1} in $CDCl_3$ at 298 K, significantly smaller than the gas-phase values for the benzene dimer [24, 26, 30]. Subsequently, Shimizu and coworkers explored aromatic stacking interactions using *N*-arylimide-based molecular balances, where aromatic moieties interact in a **PD**-like configuration [32, 33]. They reported that increasing the size of the aromatic systems did not lead to significantly stronger interactions, concluding that the LD contribution to stabilization is small in solution [32, 33].

Later, Cockroft extended this research by studying polyaromatic systems with molecular balances, showing that the interaction energy cannot be explained solely by size of interacting groups [34]. Instead, the interaction energy correlates with the solvent-accessible surface area (SASA), which describes the area of solvent-solute interactions, of the folded and unfolded conformers. Additionally, high solvent bulk polarizability such as found for CS_2 exhibit the least favorable stacking interactions due to competing LD interactions between solvent and solute [24, 34].

All molecular balances have in common that the observed interaction energies in solution are significantly weaker than those in the gas phase. Chen and coworkers demonstrated that NCIs can be attenuated by up to 80% in aprotic solvents compared to the corresponding gas-phase structures, based on studies of proton-bound dimers [35, 36]. Subsequently, Shimizu and coworkers revisited this topic using rigid CH–π molecular balances. They observed that enlarging the π-system, thereby enhancing dispersion interactions, indeed increases the interaction strength. This stabilization is again substantially reduced, by as much as 80% in solution [37].

However, owing to the incorporation of polar groups of these model systems the benzene dimer interactions may be affected by local dipole interactions that also alter the local interactions with the solvent. To address these limitations, nonpolar molecular hydrocarbon balances, such as the **1,4/1,6** substituted cyclooctatetraene (**COT**), have been developed [29, 38]. The **1,4**- and **1,6-COT** diastereomers are valence bond isomers that interconvert via a planar π-bond isomerization. In **1,4-COT** the substituents are separated from each other, while **1,6-COT** brings them in close proximity and allows them to interact (Figure 2) [29]. The combination of high symmetry, absence of bond dipoles, temperature-sensitive and well-resolved NMR signals makes them ideally suited for quantifying small differences in intramolecular interaction energies. Previous studies revealed that intramolecular LD interactions do not cancel in solution and are in fact quite constant over a large range of solvent polarities and polarizabilities [29, 38]. These findings were further supported by **COT**-based molecular balances functionalized with highly polarizable alkyl [29, 38, 39–41] and silyl [42, 43] moieties often referred to as dispersion energy donors (DEDs) [7, 8, 44, 45].

2 | Results and Discussion

Here we employ a dibenzyl-substituted **COT** system in which the phenyl groups are connected to the **COT** backbone with a methylene spacer that allows the phenyl groups in the **1,6-COT** isomer to adopt multiple conformations and therefore capture

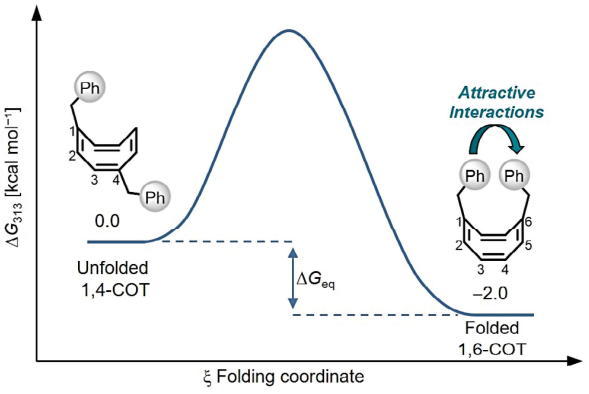


FIGURE 2 | Schematic energy profile of the equilibrium between 1,4/1,6-COT. Gibbs free energies (313 K) are given at the ωB97X-D4/def2-TZVPP [46, 47] level of theory in the gas phase.

all possible interactions of the benzene dimer. We began with investigating the energetic landscape of the **1,4-/1,6-COT** system by computing all possible conformers of each isomer using CREST [48] and further optimized them at the ωB97X-D4/def2-TZVPP level of theory [46, 47]. Unfolded **1,4-COT** shows no interaction between the phenyl moieties as they are separated by ~8 Å, and this represents a model of the dissociated benzene dimer, which is $\Delta G_{313\,K}$ = 2.0 kcal mol^{-1} higher in energy than **1,6-COT**.

The two most stable conformers of **1,6-COT** adopt **TT**- or **PD**-shaped arrangements that are remarkably similar to the gas-phase benzene dimer structures (Figure 1). **TT-1,6-COT** features a central phenyl distance of 5.89 Å and a slip angle of θ_A = 103.8°. In comparison, the **TT** benzene dimer has a shorter central phenyl-phenyl distance of 4.93 Å and a slip angle of 100.1° (Figure 1) [24]. This results in slightly weaker interaction energies. However, the total SAPT energy between the substituents in our system is with 2.2 kcal mol^{-1} (Figure 3) close to the computed **TT**-benzene dimer [49]. In **PD-1,6-COT**, the phenyl moieties have a distance of 3.86 Å and an angle of 66.5°. The phenyl group orientations in **TT-** and **PD-1,6-COT** hence closely resemble the two lowest-lying benzene dimer structures. DFT computations further reveal that **TT-1,6-COT** is slightly lower in energy than **PD-1,6-COT** (Table S14), resulting in a higher equilibrium population of **TT-1,6-COT**. Consequently, **1,4-/1,6-COT** model system can be employed to estimate the benzene dimer interactions in solution.

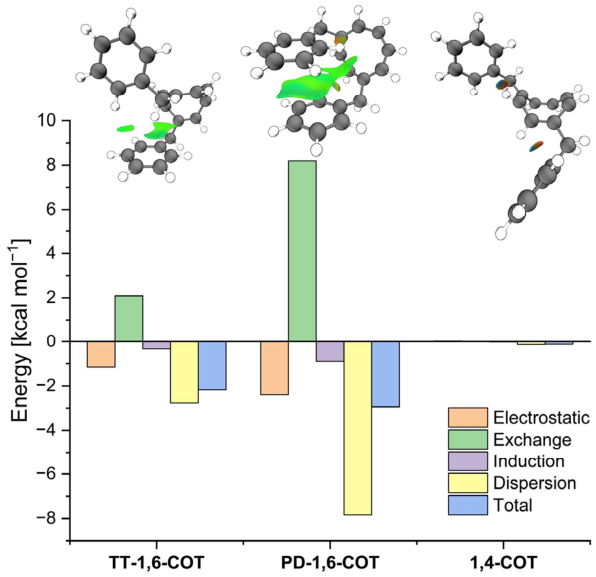


FIGURE 3 | NCI plots [50] of **TT-1,6-COT** (left) and **PD-1,6-COT** (middle) as well as the unfolded **1,4-COT** (right). Isosurfaces (isovalues sign(λ_2)ρ = −0.04 a.u. to +0.04 a.u.) are color-coded red (corresponding to strong repulsion) blue (strong attractive interactions), and green (weak noncovalent interactions). ISAPT [51, 52] computations were carried out using the SIAO1 [53] partition scheme by separating the substituents as well as the **COT**-backbone into one fragment each and computing the interaction energy between the substituents at the fisapt0 jun-cc-pVDZ level of theory.

To examine the stabilizing NCIs in **1,6-COT**, we took the ωB97X-D4/def2-TZVPP [46, 47] optimized structures and performed an NCI plot analysis [50] (Figure 3). In **TT-1,6-COT**, stabilizing NCIs are present both between the two phenyl groups and between the phenyl group and the CH_2 spacer unit. In contrast, in **PD-1,6-COT**, these interactions are primarily driven by the interaction between the two phenyl groups. To quantify and dissect the NCIs into physically meaningful components, we performed ISAPT [51, 52] computations using the SIAO1 [53] partition scheme by separating the substituents and the **COT**-backbone into one fragment each and computing the interaction energies between the substituents (Figure 3). For **TT-1,6-COT** and **PD-1,6-COT** inductive effects only play a minor role, electrostatic and mainly LD stabilize the dimers and compensate Pauli repulsion, resulting in a net negative total energy, in agreement with benzene and toluene dimer computations [54]. These results are also supported by a local energy decomposition (LED) analysis (reported in the SI, including the **1,4-COT**) [55, 56]. The total SAPT-interaction energy in the **TT-1,6-COT** accounts for 2.7 kcal mol^{-1} and is in very good agreement with the computed gas phase benzene dimer energy of 2.8 kcal mol^{-1} in the TT-conformation. We computed the total interaction energy for **PD-1,6-COT** of 3.1 kcal mol^{-1} which also aligns well with the 2.7 kcal mol^{-1} obtained in recent computations for the PD-benzene dimer [24].

For the preparation of the experimental system, we adapted established literature procedures beginning with 1,5-cyclooctadiene **1** to synthesize **1,4-/1,6-COT** (Figure 4) [41, 42, 57–59]. Lithiation of **1** with *n*-BuLi gives the dianion that was trapped with benzyl bromide to provide triene **2**. Notably, we were able to isolate triene **2**, which, unlike its parent that decomposes rapidly, can be stored for several days at low temperatures. We oxidized **2** with iodine in the presence of *n*-BuLi, yielding a mixture of **1,4/1,6-COT**. Reversed-phase HPLC purification gave pure **1,4/1,6-COT**, with a total yield of 22% over two steps. The benzylic protons were assigned according to literature data and by comparing their proton shifts with the computed spectrum (see Supporting Information for details of all spectroscopic assignments and rate determinations in Figures S1–S18 and Tables S1–S12). All COT-protons were assigned using 2D-NMR techniques. The benzylic protons were used for the integration and determination of the isomer ratios. For computed NMR spectra for comparison, see Figure S25, S26.

To establish a suitable equilibration temperature for the isomer mixture, we warmed the samples gradually from 25 °C to 75 °C in 5 °C increments, holding each temperature for one hour in DCE-d_4. The recorded van't Hoff data revealed a linear relationship above 35 °C indicating that the equilibrium was reached within the equilibration time. At lower temperatures, the equilibration between **1,4/1,6-COT** did not occur in a feasible time frame. Additionally, we conducted a series of experiments with varying concentrations of **1,4/1,6-COT**, from 6 to 60 mM, and found no change in the isomer ratios, indicating concentration independence. All further measurements were carried out at 40 °C, with concentrations of 30 mM.

We measured an enthalpic contribution of ΔH = −0.52 ± 0.03 kcal mol^{-1} and an entropy contribution of ΔS = −0.722 ± 0.081 cal mol^{-1} K^{-1} (see Supporting Information for details), resulting in an *exergonic* equilibrium in favor of folded **1,6-COT**;

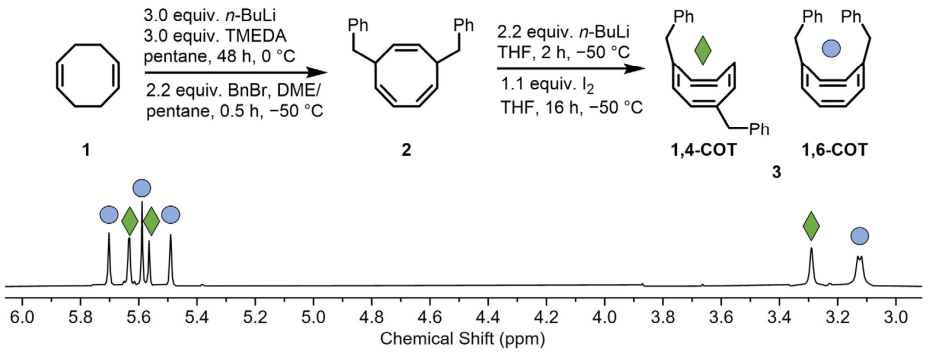


FIGURE 4 | Synthesis of the target compounds starting from 1,5-cyclooctadiene and ^{1}H-NMR assignments of **1,6-COT** and **1,6-COT** in DCE-d_4. Benzylic protons were used for integration and determination of the diastereomer ratios.

our $\Delta G = -0.30 \pm 0.09$ kcal mol^{-1} compares favorably with Wilcox' −0.24 kcal mol^{-1} [30]. These findings are also in line with molecular balances functionalized with DEDs such as ^{t}Bu ($\Delta G = -0.17 \pm 0.01$ kcal mol^{-1}) [29, 38], adamantyl ($\Delta G = -0.15 \pm 0.01$ kcal mol^{-1}) [38], and diamantyl ($\Delta G = -0.25 \pm 0.01$ kcal mol^{-1}) [38] in *n*-octane at 298 K. As observed in these closely related systems, different solvents change the ΔH and ΔS values only slightly but typically in opposite directions (enthalpy-entropy compensation) [29]. An intermediate conclusion is that benzene is one of the strongest mutual DED groups, which underscores its manifold use and recognition as enabling some key interactions highly relevant to chemical and biological systems (*vide supra*).

To investigate solvent effects and their impact on the **1,4/1,6-COT** equilibrium we further optimized the conformers of each isomer at the ωb97X-D4/def2-TZVP[SMD]+GmRRHO(GFN2[alpb]-bhess)//r2scan-3c[SMD], level of theory and applied a Boltzmann weighted distribution using CENSO [60] in twelve common organic solvents to correlate our findings across a range of solvent parameters. The computations predict that **1,6-COT** is favored by 0.2–0.4 kcal mol^{-1} in all solvents (Figure 5, blue line; for details see Table S13–S17). This is in line with the solvent attenuation studies by Chen et al. [35, 36] with respect to the gas phase energies (*vide supra*). The only exception being acetonitrile in which **1,4-COT** is predicted to be more stable; the reasons for this outlier are unclear at this time.

The experimental results confirm our computational predictions and show that the **1,6-COT** is preferred over the **1,4-COT** in all solvents and that the ratio remains remarkably constant (Figure 5, green line). The lowest **1,6/1,4-COT** ratio was observed in benzene-d_6 ($K_{eq(1,6/1,4)} = 1.46$, $\Delta G_{(1,6/1,4)} = -0.23$ kcal mol^{-1}), suggesting competitive interactions between solvent and solute; this has also been found for other balances. The **1,6-COT** preference in hydrocarbon solvents follows the series benzene < toluene < cyclohexane < *n*-hexane with decreasing solvent polarizability (SP) as well as decreasing cohesive energy density (ced) [61]. The highest ratio in favor of folded **1,6-COT** was observed for the least polarizable solvent methanol-d_4 ($K_{eq(1,6/1,4)} = 1.83$, $\Delta G_{(1,6/1,4)} = -0.37$ kcal mol^{-1}).

The reduced solvent accessible surface area of **1,6-COT** (482.5 Å^2) compared to **1,4-COT** (573.6 Å^2) reduces unfavorable solvent-solute interactions in less polarizable solvents. The minimized

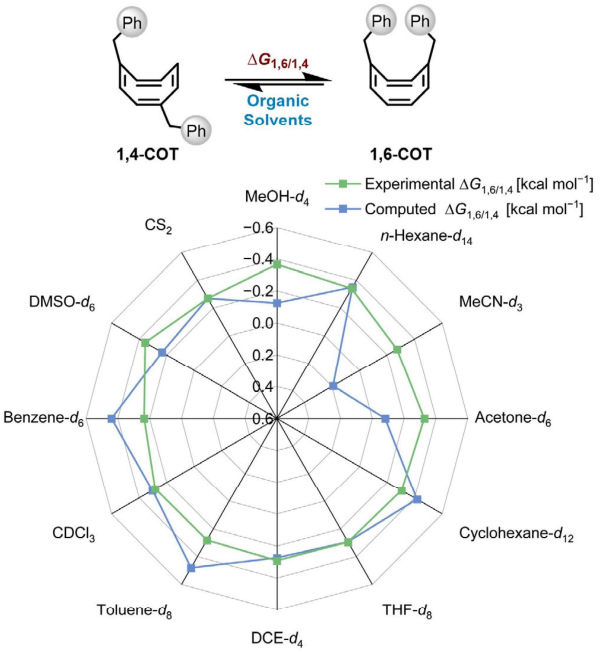


FIGURE 5 | Experimentally (green) and computed (blue) ΔG values at 313 K for the **1,6/1,4-COT** equilibrium ordered clockwise with respect to increasing solvent polarizabilities [61]. The substrate concentration for all measurements was 30 mM. Negative values correspond to an equilibrium favoring **1,6-COT**. Computations were performed at ωb97X-d4/def2-TZVP[SMD]+GmRRHO(GFN2[alpb]-bhess)//r2scan-3c[SMD], taking all conformers for each isomer into account with a Boltzmann weighted distribution using CENSO [60].

molecular volume leads to a smaller cavity within the solvent cage, which additionally entropically favors **1,6-COT**. Overall, there seems to be little to no correlation between the observed ratios and commonly employed solvent parameter scales such as SP, solvent polarity–polarizability (SPP) [61], or bulk SP [34] possibly owning to the absence of polar functional groups in our system. This finding highlights that intramolecular LD interactions between aromatic moieties do not change much over a large range of rather different solvents.

3 | Conclusions

Here we present a **1,4-/1,6**-dibenzyl-substituted **COT**-based molecular balance as a model system to quantify benzene dimer interactions using ^{1}H-NMR studies in various solvents. A comparison of the computationally most stable **1,6-COT** conformers reveals that the **TT** and **PD** conformations (optimized at ωB97X-D4/def2-TZVPP [46, 47]) closely resemble the computed key experimental geometries of the gas-phase benzene dimer [24]. Both the Ph-Ph angles and distances also align well with those observed in computational gas-phase studies of the benzene dimer [24, 25]. Additionally, the SAPT computations of the **TT** and **PD** conformations (Figure 3) are in very good agreement with the computed energies for the benzene dimer [24]. Therefore, the **1,4-/1,6-COT** balance is a suitable model to evaluate benzene dimer interaction energies in solution, which are otherwise challenging to quantify. The measured and computed **1,4/1,6**-dibenzyl **COT** equilibrium shows a clear preference for folded ("more crowded") **1,6-COT**, irrespective of solvent. NCI plot and SAPT analyses (see Figures S19–S24 and Tables S18–S20) of the **TT** and **PD** structures support the conclusion that LD interactions are the primary stabilizing force governing the intramolecular interactions in **1,6-COT** in solution. The derived experimental interaction energy in solution ranges from $\Delta G_{(1,6/1,4)} = -0.23$ kcal mol^{-1} (in benzene) up to $\Delta G_{(1,6/1,4)} = -0.37$ kcal mol^{-1} (in methanol) and is thereby considerably weaker than the computed gas phase energy of $\Delta E_{\text{int}} = -2.7$ kcal mol^{-1}.

Acknowledgments

We thank Jan M. Schümann, Lars Rummel, and Henrik F. König for fruitful discussions.

Open access funding enabled and organized by Projekt DEAL.

Conflicts of Interest

The authors declare no conflicts of interest.

References

1. E. A. Meyer, R. K. Castellano, and F. Diederich, "Interactions With Aromatic Rings in Chemical and Biological Recognition," *Angewandte Chemie International Edition* 42 (2003): 1210–1250, https://doi.org/10.1002/anie.200390319.

2. A. A. Fokin, D. Gerbig, and P. R. Schreiner, "σ/σ- and π/π-Interactions Are Equally Important: Multilayered Graphanes," *Journal of the American Chemical Society* 133 (2011): 20036–20039, https://doi.org/10.1021/ja206992j.

3. S. E. Wheeler, T. J. Seguin, Y. Guan, and A. C. Doney, "Noncovalent Interactions in Organocatalysis and the Prospect of Computational Catalyst Design," *Accounts of Chemical Research* 49 (2016): 1061–1069, https://doi.org/10.1021/acs.accounts.6b00096.

4. T. J. Seguin and S. E. Wheeler, "Stacking and Electrostatic Interactions Drive the Stereoselectivity of Silylium-Ion Asymmetric Counteranion-Directed Catalysis," *Angewandte Chemie International Edition* 55 (2016): 15889–15893, https://doi.org/10.1002/anie.201609095.

5. C. Eschmann, L. Song, and P. R. Schreiner, "London Dispersion Interactions Rather Than Steric Hindrance Determine the Enantioselectivity of the Corey–Bakshi–Shibata Reduction," *Angewandte Chemie International Edition* 60 (2021): 4823–4832, https://doi.org/10.1002/anie.202012760.

6. R. Maji, S. C. Mallojjala, and S. E. Wheeler, "Electrostatic Interactions in Asymmetric Organocatalysis," *Accounts of Chemical Research* 56 (2023): 1990–2000, https://doi.org/10.1021/acs.accounts.3c00198.

7. J. P. Wagner and P. R. Schreiner, "London Dispersion in Molecular Chemistry—Reconsidering Steric Effects," *Angewandte Chemie International Edition* 54 (2015): 12274–12296, https://doi.org/10.1002/anie.201503476.

8. L. Rummel and P. R. Schreiner, "Advances and Prospects in Understanding London Dispersion Interactions in Molecular Chemistry," *Angewandte Chemie International Edition* 63 (2024): e202316364, https://doi.org/10.1002/anie.202316364.

9. M. Petroselli and P. Ballester, "Molecular Balances as Physical Organic Chemistry Tools to Quantify Non-Covalent Interactions," *Chemistry—A European Journal* 31 (2025): e202404351, https://doi.org/10.1002/chem.202404351.

10. M. H. J. Domanski, M. Fuhrmann, and P. R. Schreiner, "London Dispersion as a Design Element in Molecular Catalysis," *Journal of the American Chemical Society* 147 (2025): 29611–29623, https://doi.org/10.1021/jacs.5c09212.

11. C. M. Carter, J. Brossette, and H. Zipse, "Size and Polarizability as Design Principles for Stereoselective Catalysis," *Chemistry—A European Journal* 31 (2025): e02741, https://doi.org/10.1002/chem.202502741.

12. M. H. J. Domanski, L. Rummel, S. N. Krug, H. Hausmann, E. Solel, and P. R. Schreiner, "London Dispersion Favors Cis Selectivity in the Johnson–Corey–Chaykovsky Epoxidation," *The Journal of Organic Chemistry* 91 (2026): 4829–4841, https://doi.org/10.1021/acs.joc.6c00154.

13. N. Kannan and S. Vishveshwara, "Aromatic Clusters: A Determinant of Thermal Stability of Thermophilic Proteins," *Protein Engineering, Design and Selection* 13 (2000): 753–761, https://doi.org/10.1093/protein/13.11.753.

14. S. K. Burley and G. A. Petsko, "Aromatic-Aromatic Interaction: A Mechanism of Protein Structure Stabilization," *Science* 229 (1985): 23–28, https://doi.org/10.1126/science.3892686.

15. S. K. Burley and G. A. Petsko, "Weekly Polar Interactions in Proteins," *Advances in Protein Chemistry* 39 (1988): 125–189, https://doi.org/10.1016/S0065-3233(08)60376-9.

16. A. N. Bootsma, A. C. Doney, and S. E. Wheeler, "Predicting the Strength of Stacking Interactions Between Heterocycles and Aromatic Amino Acid Side Chains," *Journal of the Chemical Society* 141 (2019): 11027–11035, https://doi.org/10.1021/jacs.9b00936.

17. C. A. Hunter, K. R. Lawson, J. Perkins, and C. J. Urch, "Aromatic Interactions," *Journal of the Chemical Society, Perkin Transactions* 2 (2001): 651–669, https://doi.org/10.1039/B008495F.

18. S. Grimme, "Do Special Noncovalent π–π Stacking Interactions Really Exist?," *Angewandte Chemie International Edition* 47 (2008): 3430–3434, https://doi.org/10.1002/anie.200705157.

19. E. M. Cabaleiro-Lago and J. Rodríguez-Otero, "On the Nature of σ–σ, σ–π, and π–π Stacking in Extended Systems," *ACS Omega* 3 (2018): 9348–9359, https://doi.org/10.1021/acsomega.8b01339.

20. C. D. Sherrill, "Energy Component Analysis of π Interactions," *Accounts of Chemical Research* 46 (2013): 1020–1028, https://doi.org/10.1021/ar3001124.

21. J. Henrichsmeyer, M. Thelen, M. Bröckel, et al., "Rationalizing Aggregate Structures With Orbital Contributions to the Exchange-Repulsion Energy," *Chemphyschem* 24 (2023): e202300097, https://doi.org/10.1002/cphc.202300097.

22. C. A. Hunter and J. K. M. Sanders, "The Nature of .pi.-.pi. interactions," *Journal of the American Chemical Society* 112 (1990): 5525–5534, https://doi.org/10.1021/ja00170a016.

23. C. A. Hunter, "Arene—Arene Interactions: Electrostatic or Charge Transfer?," *Angewandte Chemie International Edition in English* 32 (1993): 1584–1586, https://doi.org/10.1002/anie.199315841.

24. J. Czernek and J. Brus, "Revisiting the Most Stable Structures of the Benzene Dimer," *International Journal of Molecular Sciences* 25 (2024): 8272, https://doi.org/10.3390/ijms25158272.

25. K. Carter-Fenk and J. M. Herbert, "Reinterpreting π-stacking," *Physical Chemistry Chemical Physics* 22 (2020): 24870–24886, https://doi.org/10.1039/D0CP05039C.

26. J. R. Grover, E. A. Walters, and E. T. Hui, "Dissociation Energies of the Benzene Dimer and Dimer Cation," *The Journal of Physical Chemistry* 91 (1987): 3233–3237, https://doi.org/10.1021/j100296a026.

27. B. Ernstberger, H. Krause, A. Kiermeier, and H. J. Neusser, "Multiphoton Ionization and Dissociation of Mixed van der Waals Clusters in a Linear Reflectron Time-of-flight Mass Spectrometer," *The Journal of Chemical Physics* 92 (1990): 5285–5296, https://doi.org/10.1063/1.458603.

28. H. Krause, B. Ernstberger, and H. J. Neusser, "Binding Energies of Small Benzene Clusters," *Chemical Physics Letters* 184 (1991): 411–417, https://doi.org/10.1016/0009-2614(91)80010-U.

29. J. M. Schümann, J. P. Wagner, A. K. Eckhardt, H. Quanz, and P. R. Schreiner, "Intramolecular London Dispersion Interactions Do Not Cancel in Solution," *Journal of the American Chemical Society* 143 (2021): 41–45, https://doi.org/10.1021/jacs.0c09597.

30. S. Paliwal, S. Geib, and C. S. Wilcox, "Molecular Torsion Balance for Weak Molecular Recognition Forces. Effects of "Tilted-T" Edge-to-Face Aromatic Interactions on Conformational Selection and Solid-State Structure," *Journal of the American Chemical Society* 116 (1994): 4497–4498, https://doi.org/10.1021/ja00089a057.

31. I. K. Mati and S. L. Cockroft, "Molecular Balances for Quantifying Non-covalent Interactions," *Chemical Society Reviews* 39 (2010): 4195, https://doi.org/10.1039/b822665m.

32. J. Hwang, B. E. Dial, P. Li, M. E. Kozik, M. D. Smith, and K. D. Shimizu, "How Important Are Dispersion Interactions to the Strength of Aromatic Stacking Interactions in Solution?," *Chemical Science* 6 (2015): 4358–4364, https://doi.org/10.1039/C5SC01370D.

33. J. Hwang, P. Li, M. D. Smith, and K. D. Shimizu, "Distance-Dependent Attractive and Repulsive Interactions of Bulky Alkyl Groups," *Angewandte Chemie International Edition* 55 (2016): 8086–8089, https://doi.org/10.1002/anie.201602752.

34. A. Elmi, K. M. Bąk, and S. L. Cockroft, "Solvent Attenuation of London Dispersion in Polycyclic Aromatic Stacking," *Angewandte Chemie* 136 (2024): e202412056, https://doi.org/10.1002/ange.202412056.

35. R. Pollice, M. Bot, I. J. Kobylianskii, I. Shenderovich, and P. Chen, "Attenuation of London Dispersion in Dichloromethane Solutions," *Journal of the American Chemical Society* 139 (2017): 13126–13140, https://doi.org/10.1021/jacs.7b06997.

36. R. Pollice, F. Fleckenstein, I. Shenderovich, and P. Chen, "Compensation of London Dispersion in the Gas Phase and in Aprotic Solvents," *Angewandte Chemie International Edition* 58 (2019): 14281–14288, https://doi.org/10.1002/anie.201905436.

37. H. Liu, H. M. Scott, B. Lin, X. Huang, M. D. Smith, and K. D. Shimizu, "Solvent Attenuation of Dispersion Interactions Quantified in Polar and Nonpolar media Using Rigid CH–π Balances," *Chemical Science* 16 (2025): 17772–17778, https://doi.org/10.1039/D5SC02852C.

38. J. M. Schümann, L. Ochmann, J. Becker, et al., "Exploring the Limits of Intramolecular London Dispersion Stabilization with Bulky Dispersion Energy Donors in Alkane Solution," *Journal of the American Chemical Society* 145 (2023): 2093–2097, https://doi.org/10.1021/jacs.2c13301.

39. M. H. Lyttle, A. Streitwieser Jr., and R. Q. Kluttz, "Unusual Equilibrium Between 1,4- and 1,6-di-tert-butylcyclooctatetraenes," *Journal of the American Chemical Society* 103 (1981): 3232–3233, https://doi.org/10.1021/ja00401a061.

40. L. A. Paquette, G. J. Hefferon, R. Samodral, and Y. Hanzawa, "Bond Fixation in Annulenes. 14. Synthesis of and Bond Shifting Equilibrium Between 1,4- and 1,6-di-tert-butylcyclooctatetraenes," *The Journal of Organic Chemistry* 48 (1983): 1262–1266, https://doi.org/10.1021/jo00156a023.

41. J. E. Anderson and P. A. Kirsch, "Structural Equilibria Determined by Attractive Steric Interactions. 1,6-Dialkylcyclooctatetraenes and Their Bond-shift and Ring Inversion Investigated by Dynamic NMR Spectroscopy and Molecular Mechanics Calculations," *Journal of the Chemical Society, Perkin Transactions 2* 11 (1992): 1951, https://doi.org/10.1039/p29920001951.

42. H. F. König, L. Rummel, H. Hausmann, J. Becker, J. M. Schümann, and P. R. Schreiner, "Gauging the Steric Effect of Silyl Groups with a Molecular Balance," *Journal of Organic Chemistry* 87 (2022): 4670–4679, https://doi.org/10.1021/acs.joc.1c03103.

43. L. Rummel, H. F. König, H. Hausmann, and P. R. Schreiner, "Silyl Groups Are Strong Dispersion Energy Donors," *The Journal of Organic Chemistry* 87 (2022): 13168–13177, https://doi.org/10.1021/acs.joc.2c01633.

44. S. Grimme, R. Huenerbein, and S. Ehrlich, "On the Importance of the Dispersion Energy for the Thermodynamic Stability of Molecules," *Chemphyschem* 12 (2011): 1258–1261, https://doi.org/10.1002/cphc.201100127.

45. L. Rummel, M. H. J. Domanski, H. Hausmann, J. Becker, and P. R. Schreiner, "London Dispersion Favors Sterically Hindered Diarylthiourea Conformers in Solution," *Angewandte Chemie International Edition* 61 (2022): e202204393, https://doi.org/10.1002/anie.202204393.

46. J.-D. Chai and M. Head-Gordon, "Systematic Optimization of Long-range Corrected Hybrid Density Functionals," *The Journal of Chemical Physics* 128 (2008): 084106, https://doi.org/10.1063/1.2834918.

47. E. Caldeweyher, C. Bannwarth, and S. Grimme, "Extension of the D3 Dispersion Coefficient Model," *The Journal of Chemical Physics* 147 (2017): 034112, https://doi.org/10.1063/1.4993215.

48. P. Pracht, S. Grimme, C. Bannwarth, et al., "CREST - A Program for the Exploration of Low-Energy Molecular Chemical Space," *Journal of Chemical Physics* 160 (2024): 114110, https://doi.org/10.1063/5.0197592.

49. R. Podeszwa, R. Bukowski, and K. Szalewicz, "Potential Energy Surface for the Benzene Dimer and Perturbational Analysis of π–π Interactions," *The Journal of Physical Chemistry A* 110 (2006): 10345–10354, https://doi.org/10.1021/jp064095o.

50. J. Contreras-García, E. R. Johnson, S. Keinan, et al., "NCIPLOT: A Program for Plotting Noncovalent Interaction Regions," *Journal of Chemical Theory and Computation* 7 (2011): 625–632, https://doi.org/10.1021/ct100641a.

51. R. M. Parrish, J. F. Gonthier, C. Corminboeuf, and C. D. Sherrill, "Communication: Practical Intramolecular Symmetry Adapted Perturbation Theory via Hartree-Fock Embedding," *The Journal of Chemical Physics* 143 (2015): 051103, https://doi.org/10.1063/1.4927575.

52. E. Pastorczak, A. Prlj, J. F. Gonthier, and C. Corminboeuf, "Intramolecular Symmetry-adapted Perturbation Theory With a Single-determinant Wavefunction," *The Journal of Chemical Physics* 143 (2015): 224107, https://doi.org/10.1063/1.4936830.

53. D. Luu and K. Patkowski, "Overcoming Artificial Multipoles in Intramolecular Symmetry-Adapted Perturbation Theory," *The Journal of Physical Chemistry A* 127 (2023): 356–377, https://doi.org/10.1021/acs.jpca.2c06465.

54. M. O. Sinnokrot and C. D. Sherrill, "Substituent Effects in π–π Interactions: Sandwich and T-Shaped Configurations," *Journal of the American Chemical Society* 126 (2004): 7690–7697, https://doi.org/10.1021/ja049434a.

55. W. B. Schneider, G. Bistoni, M. Sparta, et al., "Decomposition of Intermolecular Interaction Energies Within the Local Pair Natural Orbital Coupled Cluster Framework," *Journal of Chemical Theory and Computation* 12 (2016): 4778–4792, https://doi.org/10.1021/acs.jctc.6b00523.

56. A. Altun, M. Saitow, F. Neese, and G. Bistoni, "Local Energy Decomposition of Open-Shell Molecular Systems in the Domain-Based Local Pair Natural Orbital Coupled Cluster Framework," *Journal of Chemical*

Theory and Computation 15 (2019): 1616–1632, https://doi.org/10.1021/acs.jctc.8b01145.

57. N. C. Burton, F. G. N. Cloke, S. C. P. Joseph, H. Karamallakis, and A. A. Sameh, "Trimethylsilyl Derivatives of Cyclooctatetraene," *Journal of Organometallic Chemistry* 462 (1993): 39–43, https://doi.org/10.1016/0022-328X(93)83339-W.

58. J. S. Parry, Cloke, S. J. Coles, and M. B. Hursthouse, "Synthesis and Characterization of the First Sandwich Complex of Trivalent Thorium: a Structural Comparison With the Uranium Analogue," *Journal of the American Chemical Society* 121 (1999): 6867–6871, https://doi.org/10.1021/ja9903633.

59. O. T. Summerscales, F. G. N. Cloke, P. B. Hitchcock, J. C. Green, and N. Hazari, "Reductive Cyclotetramerization of CO to Squarate by a U(III) Complex: the X-ray Crystal Structure of $[(U(\eta\text{-}C_8H_6\{Si^iPr_3\text{-}1,4\}_2)(\eta\text{-}C_5Me_4H)]_2(\mu\text{-}\eta_2\text{:}\eta^2\text{-}C_4O_4)$," *Journal of the American Chemical Society* 128 (2006): 9602–9603, https://doi.org/10.1021/ja063222r.

60. S. Grimme, F. Bohle, A. Hansen, P. Pracht, S. Spicher, and M. Stahn, "Efficient Quantum Chemical Calculation of Structure Ensembles and Free Energies for Nonrigid Molecules," *The Journal of Physical Chemistry A* 125 (2021): 4039–4054, https://doi.org/10.1021/acs.jpca.1c00971.

61. J. Catalán and H. Hopf, "Empirical Treatment of the Inductive and Dispersive Components of Solute–Solvent Interactions: The Solvent Polarizability (SP) Scale," *European Journal of Organic Chemistry* (2004): 4694–4702, https://doi.org/10.1002/ejoc.200400311.

62. P. Pracht, F. Bohle, and S. Grimme, "Automated Exploration of the Low-energy Chemical Space With Fast Quantum Chemical Methods," *Physical Chemistry Chemical Physics* 22 (2020): 7169–7192, https://doi.org/10.1039/C9CP06869D.

63. F. Neese, "The ORCA Program System," *WIREs Computational Molecular Science* 2 (2012): 73–78, https://doi.org/10.1002/wcms.81.

64. F. Neese, "Software Update: The ORCA Program System—Version 5.0," *WIREs Computational Molecular Science* 12 (2022): e1606, https://doi.org/10.1002/wcms.1606.

65. F. Weigend and R. Ahlrichs, "Balanced Basis Sets of Split Valence, Triple Zeta Valence and Quadruple Zeta Valence Quality for H to Rn: Design and Assessment of Accuracy," *Physical Chemistry Chemical Physics* 7 (2005): 3297, https://doi.org/10.1039/b508541a.

66. E. R. Johnson, S. Keinan, P. Mori-Sánchez, J. Contreras-García, A. J. Cohen, and W. Yang, "Revealing Noncovalent Interactions," *Journal of the American Chemical Society* 132 (2010): 6498–6506, https://doi.org/10.1021/ja100936w.

67. W. Humphrey, A. Dalke, and K. Schulten, "VMD: Visual Molecular Dynamics," *Journal of Molecular Graphics* 14 (1996): 33–38, https://doi.org/10.1016/0263-7855(96)00018-5.

68. T. Lu and F. Chen, "Multiwfn: A Multifunctional Wavefunction Analyzer," *Journal of Computational Chemistry* 33 (2012): 580–592, https://doi.org/10.1002/jcc.22885.

69. K. Szalewicz, "Symmetry-Adapted Perturbation Theory of Intermolecular Forces," *WIREs Computational Molecular Science* 2 (2012): 254–272, https://doi.org/10.1002/wcms.86.

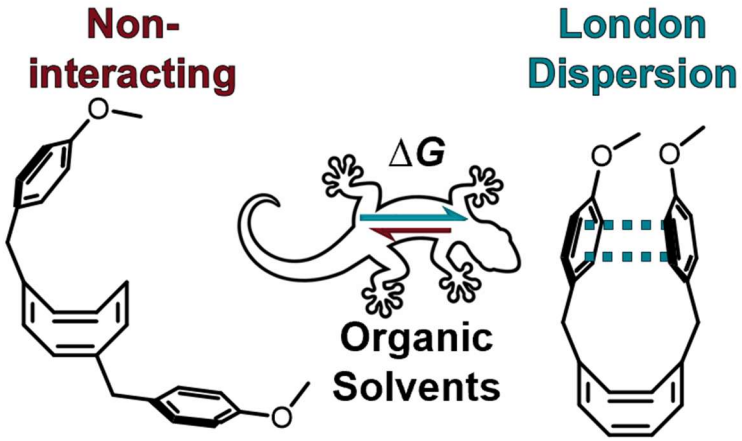
70. J. M. Turney, A. C. Simmonett, R. M. Parrish, et al., *WIREs Computational Molecular Science* 2 (2012): 556–565, https://doi.org/10.1002/wcms.93.

Supporting Information

Additional supporting information can be found online in the Supporting Information section.

References from the Supporting Information are provided in the following listing as well: [62–70].

2.3 Quantifying Anisole Dimer Interactions in Solution with a Molecular Balance



Abstract

We report a combined experimental and computational study that quantifies the interaction strength of anisole–anisole stacking in solution using a 1,4/1,6-dianisole-substituted cyclooctatetraene (COT) molecular balance. 1H NMR spectroscopy revealed that the folded (sterically more crowded) 1,6-COT isomer is consistently favored over the unfolded (sterically less crowded) 1,4-COT isomer by up to −0.9 kcal mol^{-1} across a broad range of solvents. Solvents with low polarizability preferentially stabilize the folded isomer. Complementary quantum chemical computations reproduce the experimental trends and identify London dispersion as the dominant stabilizing contribution to the folded 1,6-COT.

***Reference*:**

Marvin H. J. Domanski, Saskia N. Krug, Heike Hausmann, and Peter R. Schreiner, Eur. *J. Org. Chem.*, **2026**, *29*, e70649.

DOI: 10.1002/ejoc.70649

Reproduced with permission from © 2026 Wiley-VCH GmbH.

European Journal of Organic Chemistry

EurJOC
European Journal of Organic Chemistry

Chemistry Europe
European Chemical Societies Publishing

RESEARCH ARTICLE OPEN ACCESS

Quantifying Anisole Dimer Interactions in Solution With a Molecular Balance

Marvin H. J. Domanski | Saskia N. Krug | Heike Hausmann | Peter R. Schreiner

Institute of Organic Chemistry, Justus Liebig University, Giessen, Germany

Correspondence: Peter R. Schreiner (prs@uni-giessen.de)

Received: 2 April 2026 | **Revised:** 2 June 2026 | **Accepted:** 13 June 2026

Keywords: computational chemistry | equilibrium | London dispersion | NMR spectroscopy | noncovalent interactions

ABSTRACT

We report a combined experimental and computational study that quantifies the interaction strength of anisole–anisole stacking in solution using a 1,4/1,6-dianisole-substituted cyclooctatetraene (COT) molecular balance. ^{1}H NMR spectroscopy revealed that the folded (sterically more crowded) 1,6-COT isomer is consistently favored over the unfolded (sterically less crowded) 1,4-COT isomer by up to 0.9 kcal mol^{-1} across a broad range of solvents. Solvents with low polarizability preferentially stabilize the folded isomer. Complementary quantum chemical computations reproduce the experimental trends and identify London dispersion as the dominant stabilizing contribution to the folded 1,6-COT.

1 | Introduction

Aromatic interactions are a ubiquitous structural element in chemistry, biology, and material science [1, 2]. They govern protein folding [3–6], stabilize nucleic acid base stacking [7], and, most relevant for synthetic chemists, influence the reactivity and selectivity of homogeneous catalysts bearing aryl ligands or substrates [8–10]. In catalytic systems, noncovalent interactions, often London dispersion (LD) [9, 11], between an aryl-containing ligand and an incoming aryl substrate can help preorganize reactive complexes [12, 13], lower activation barriers of elementary steps [14], and exert control over regio- and enantioselectivity [15–17]. A quantitative understanding of how aromatic interactions respond to substituent effects, solvent polarity, and solvent polarizability is therefore essential for the design of catalysts and functional molecules [10].

The benzene dimer has long served as the canonical model for aromatic interactions [7, 18]. High-level gas-phase computations and spectroscopic data established that the binding arises from a balance between LD, exchange repulsion, charge–transfer, and inductive interactions, with the tilted T-shaped and parallel-displaced (PD) dimer geometries representing the two most stable dimer structures [19]. While the parent benzene dimer defines the base line of aromatic interactions, many catalytic systems incorporate substituted aryl groups [20, 21]. Electron-donating and electron-withdrawing substituents affect electrostatic interactions, introduce dipoles, alter polarizabilities, and therefore influence LD, and enable additional induction and dipole–induced dipole interactions [22, 23]. These substituent effects manifest directly in the free energy of dimer formation. Whereas the PD benzene dimer exhibits a stabilization energy of $\Delta E = -2.7$ kcal mol^{-1} computed at the CCSD(T)/CBS level of theory in the gas phase [19], methoxy substitution substantially enhances this interaction, with computed anisole dimer stabilization energy of $\Delta E = -7.0$ kcal mol^{-1} in the head-to-tail arrangement at the same level [24]. The computed total dissociation energy (including zero-point vibrational energies ZPVE) amounts to $D_0 = -5.0$ kcal mol^{-1} and was confirmed in gas phase by molecular beam–laser spectroscopy measurements ($D_0 = -5.2$ kcal mol^{-1}) [24].

Marvin H. J. Domanski and Saskia N. Krug contributed equally to this work.

In Memory of Henning Hopf.

This is an open access article under the terms of the Creative Commons Attribution License, which permits use, distribution and reproduction in any medium, provided the original work is properly cited.

© 2026 The Author(s). *European Journal of Organic Chemistry* published by Wiley-VCH GmbH.

Experimental investigations of noncovalent aromatic interactions in solution have frequently relied on molecular balances [25–29]. These systems interconvert between two spectroscopically distinguishable states: an unfolded, sterically less congested state in which the interacting groups remain spatially separated, and a folded, sterically more crowded state in which the same groups are forced into proximity [30]. The equilibrium between these two states provides a direct measure of the intramolecular interactions. Studies employing molecular balances to probe aromatic–aromatic and alkyl–alkyl interactions consistently show that solution-phase interaction energies are reduced by approximately 80% relative to their gas-phase counterparts, but they do not vanish [31–34]. Despite the relevance of anisole motifs in catalysis [20, 21, 35], systematic experimental and theoretical data quantifying anisole–anisole interactions in solution are essentially absent [36].

To enable a more precise assessment of noncovalent intramolecular interactions, we opted for nonpolar hydrocarbon-based molecular balances, mostly derived from 1,4- and 1,6-substituted cyclooctatetraene (**COT**) scaffolds [32, 37]. The **1,4-COT** and **1,6-COT** isomers are valence-bond isomers that interconvert via a planar valence-bond isomerism. In the **1,4-COT** isomer, the substituents occupy distal positions and are essentially noninteracting, whereas the **1,6-COT** geometry enforces spatial proximity and enables intramolecular contacts (Figure 1) [32, 37]. The high symmetry of the parent **COT** framework, the absence of permanent bond dipoles, and the presence of temperature-dependent, well-resolved NMR signals render these systems ideally suited for quantifying small free-energy differences arising from noncovalent interactions. Early models using the **COT** system directly attached substituents on the backbone, which, however, restricts conformational flexibility of the substituent of interest [32, 37]. Modified approaches connect the backbone and the substituents of interest with a methylene spacer [38–41]. This allows the system to adopt multiple conformations and results in a more realistic picture of the dynamic interactions observed in solution.

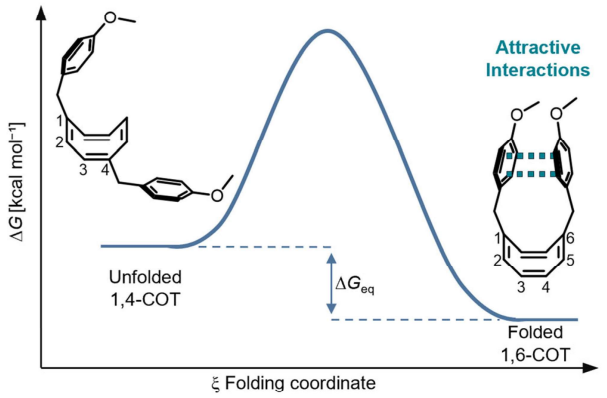


FIGURE 1 | Schematic energy profile of the equilibrium between **1,4/1,6-COT** to investigate attractive noncovalent interactions for the head-to-head anisole dimer in solution.

2 | Results and Discussion

We synthesized the target dianisole-substituted **1,4/1,6-COT** derivatives by adapting established literature procedures, starting from 1,5-cyclooctadiene **1** [38, 41–45]. Treatment with *n*-BuLi generated the corresponding dianion, which we subsequently trapped with 4-methoxybenzyl chloride to afford the corresponding triene. Oxidation with iodine in the presence of *n*-BuLi resulted in a mixture of the **1,4-COT** and **1,6-COT** valence-bond isomers (Figure 2). Following purification by reversed-phase HPLC separated products from residual starting material and resulted in a pure mixture of **1,4/1,6-COT**. We assigned the benzylic proton signals by comparison with reported literature data [38–41] and assigned the **COT** backbone protons using two-dimensional NMR spectroscopic techniques (Figure S6). Full experimental details and characterization data are provided in the supporting information (see Section S3.2).

To establish suitable equilibration conditions for the isomeric mixture, we gradually heated the samples from 25 to 55 °C in 5 °C increments, holding each temperature for 30 min in DCE-d_4. Van't Hoff analysis revealed a linear relationship above 35 °C, indicating that the system reached thermodynamic equilibrium within the equilibration time. From these measurements, we extracted an enthalpic contribution of $\Delta H = -0.37 \pm 0.05$ kcal mol^{-1} and an entropic contribution of $\Delta S = -0.35 \pm 0.15$ cal mol^{-1} K^{-1} at 40 °C, resulting in an exergonic equilibrium that favors the folded **1,6-COT** isomer (Figure S2).

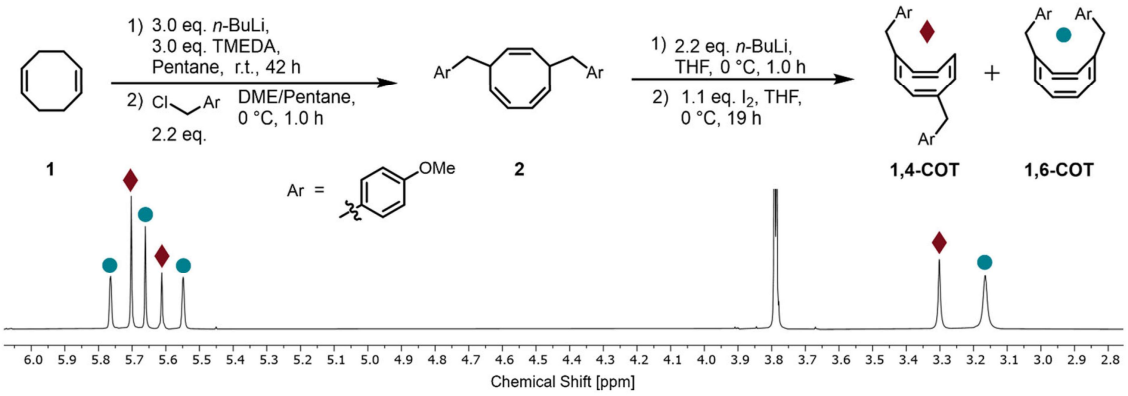


FIGURE 2 | Synthesis and ^{1}H-NMR assignments of **1,4-COT** and **1,6-COT** in DCE-d_4, synthesized from 1,5-cyclooctadiene. Benzylic protons (3.2 and 3.3 ppm) were used for integration and determination of the isomer ratios.

We next expanded the solvent scope to include 11 solvents spanning a wide range of polarities and polarizabilities [46]. Each sample was preequilibrated for at least 16 h and measured in the NMR at 40 °C. The highest equilibrium constant ($K_{eq\ (1,6/1,4)} = 1.69$, $\Delta G = -0.33 \pm 0.03$ kcal mol^{-1}) was observed in MeOH-d_4, whereas the lowest equilibrium constant ($K_{eq\ (1,6/1,4)} = 1.32$, $\Delta G = -0.17 \pm 0.03$ kcal mol^{-1}) was measured in benzene-d_6. The resulting Gibbs free energies correlate strongly with solvent polarizability (Figure 3) and solvent bulk polarizability, whereas other solvent scales, such as the solvent polarity/polarizability, cohesive energy density, and dielectric constant, showed no significant correlation (Figure S18) [46–48]. Solvents with low polarizability stabilize the folded **1,6-COT** isomer most strongly, whereas highly polarizable solvents such dimethylsulfoxide attenuate the intramolecular interaction. Similar trends have been reported for other heteroatom-containing molecular balances [31–33]. In contrast, studies with **COT**-based scaffolds substituted only with hydrocarbon moieties, revealed lower solvent sensitivity despite comparable interaction strengths [32, 41]. This comparison indicates that solvent effects predominantly originate from interactions of the heteroatoms rather than from the hydrocarbons, and the reliable quantification of hydrocarbon–hydrocarbon interactions requires molecular balances that minimize or avoid heteroatoms.

Despite this clear solvent dependence, the experimentally determined interaction energies remain substantially smaller than their gas-phase counterparts, which reach values of up to $D_0 = -5.2$ kcal mol^{-1} [24], and exceed the ~80% reduce interaction strength commonly observed for noncovalent interactions in solution [31–34]. This discrepancy prompted us to re-examine and further investigate the system computationally.

We quantified the equilibrium between the **1,4/1,6-COT** valence-bond isomers in solution using quantum chemical methods. First, we generated a conformational ensemble of each isomer using CREST [49, 50], followed by refinement with CENSO [51] at the ωB97X-D4 [52, 53]/def2-TZVP(SMD [54])//r^{2}SCAN-3c [55]/def2-mTZVPP(SMD) level of theory for all solvents investigated experimentally. Across all solvents, the computations consistently indicate that the **1,6-COT** isomer is more stable than the **1,4-COT** isomer (Figure S19), in agreement with experiment (Figure S20). Inspection of the different conformations in **1,6-COT** reveals that the anisole substituents approach each other in a head-to-head orientation (Figure 4, top left). In comparison to the free anisole dimer, its lowest-energy configuration corresponds to a head-to-tail arrangement in which the methoxy groups are pointing in opposite directions, reducing the overall dipole moment and maximizing the quadrupolar interactions. Computational studies at the CCSD(T)/CBS level of theory showed that the head-to-tail arrangement of the anisole dimer is the global minimum on the potential energy surface and 1 kcal mol^{-1} lower in energy then its head-to-head arrangement [65]. Additionally, the head-to-head arrangement in **1,6-COT** requires a slight distortion of the CH_2 units attached to the **COT** backbone, introducing an energetic penalty associated with ring strain as observed in earlier studies [39].

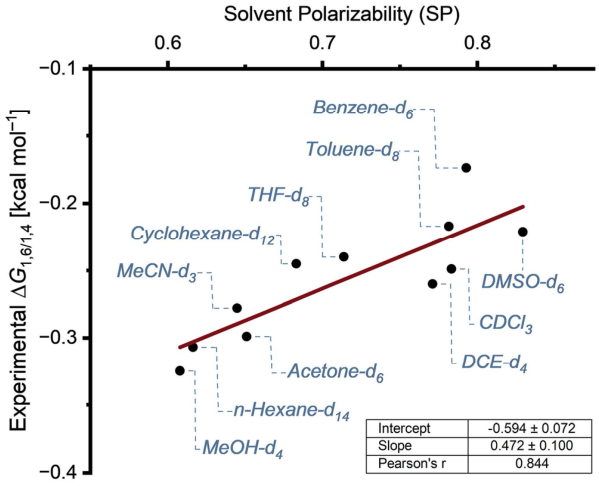


FIGURE 3 | Measured Gibbs free energies at 40 °C for the interaction of the anisole dimer in solution phase using the **1,4/1,6-COT** equilibrium.

To quantify the energetic cost associated with backbone distortion in the folded isomer, we evaluated the ring strain for each **1,6-COT** conformer, by removing the anisole substituents from the optimized minimum-energy structures and saturated the resulting radicals with hydrogen atoms. After initial optimization of the newly formed C–H bonds to obtain the strained geometry, we performed a full geometry optimization to obtain the corresponding relaxed structure. Single-point calculations at the DLPNO-CCSD(T) [66]/cc-pVTZ [67]//ωB97X-D4/def2-TZVP level on both geometries yielded strain energies of up to $\Delta E_{strain} = 0.6$ kcal mol^{-1}. Because the experimentally observed equilibrium reflects the net free-energy difference between the folded and unfolded isomers, it inherently includes this strain penalty. Correcting for the backbone distortion therefore increases the intrinsic anisole–anisole interaction strength to approximately 0.8–0.9 kcal mol^{-1} in solution, which aligns well with the expected ~80% reduction in interaction energy in solution [31–34].

To visualize and characterize the stabilizing noncovalent interactions in **1,6-COT** (Figure 4, left), we generated noncovalent interaction (NCI) plots [56–59] for the r^{2}SCAN-3c/def2-mTZVPP (SMD) optimized structures and compared them to the parent parallel-displaced benzylic **1,6-COT** system (Figure 4, middle) [41], as well as the spatially separated **1,4-COT** isomer (Figure 4, right). In addition, we performed intramolecular symmetry-adapted perturbation theory (ISAPT) [60–63] calculations using the SIAO1 [64] partitioning scheme to dissect these interactions into physically meaningful components. For this purpose, the substituents and the COT backbone were defined as separate fragments, and the interaction energies between the substituents were computed.

The reference parallel-displaced dibenzylic COT system exhibits a Ph–Ph distance of 3.85 Å (Figure 4, middle) and displays noncovalent interactions between the phenyl moieties [41], visualized by the green NCI isosurface. ISAPT analysis reveals that the interaction is dominated by a balance between Pauli exchange repulsion (8.2 kcal mol^{-1}) and LD (−7.8 kcal mol^{-1}), whereas induction (−0.9 kcal mol^{-1}) and electrostatic contributions (−2.3 kcal mol^{-1}) play comparatively minor roles [41]. Overall, the interaction remains weakly attractive. In the anisole **1,6-COT** system, the anisole moieties adopt a constrained head-to-head arrangement. The larger Ph–Ph distance (4.01 Å) reduces Pauli

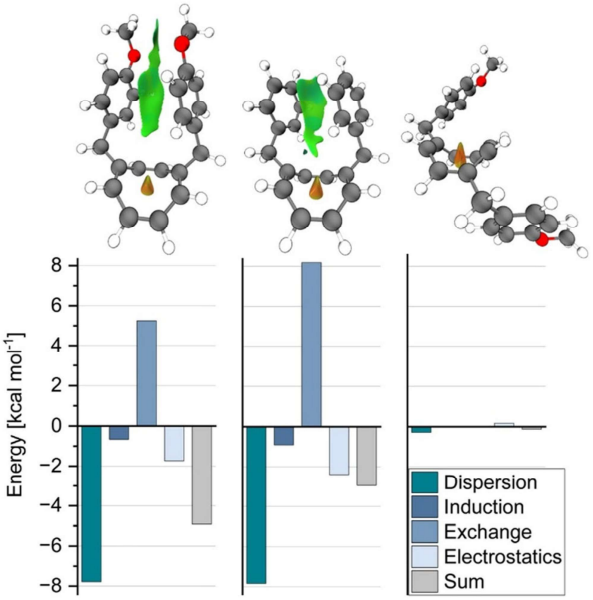


FIGURE 4 | NCI plots [56–59] of **1,6-COT** (left), the reference parallel-displaced 1,6-dibenzylic cyclooctatetraene (middle) and **1,4-COT** (right). Isosurfaces (isovalues sign(λ_2)ρ = −0.04 a.u. to +0.04 a.u.) green isosurfaces correspond to weak noncovalent interactions. ISAPT [60–63] calculations were carried out using the SIAO1 [64] partition scheme by separating the substituents as well as the COT-backbone into one fragment each and computing the interaction energy between the *anisole moieties* at the fisapt0 jun-cc-pVDZ level of theory.

exchange repulsion to 5.3 kcal mol^{-1}, while the additional methoxy substituents maintain attractive interactions. LD contributes −7.8 kcal mol^{-1} and accounts for roughly 70% of the total stabilization, whereas electrostatic (−1.7 kcal mol^{-1}) and induction (−0.6 kcal mol^{-1}) interactions remain comparatively small. The resulting total interaction energy amounts to −4.9 kcal mol^{-1}, demonstrating that LD remains the dominant stabilizing interaction even in the presence of electron-donating substituents. Consistent with a dissociated anisole dimer, the unfolded **1,4-COT** isomer contains spatially separated anisole moieties and therefore shows no significant interaction between them (Figure 4, right).

3 | Conclusion

We quantified anisole–anisole interactions in solution using a **1,4/1,6-COT** molecular balance that enables intramolecular aromatic contacts. ^{1}H-NMR spectroscopic measurements show that folded **1,6-COT** is consistently favored over the unfolded **1,4-COT** across a broad range of solvents, with stronger stabilization in solvents of low polarizability. After correcting for intrinsic **COT** strain, the interaction strength for the head-to-head anisole dimer ranges from 0.8 kcal mol^{-1} in benzene to 0.9 kcal mol^{-1} in methanol. These values are significantly reduced compared to the gas-phase anisole dimer, consistent with the ∼80% attenuation of noncovalent interaction strengths typically observed upon solvation. Still, the incorporation of polarizable substituents such as methoxy groups as dispersion energy donors (DEDs) [14, 68, 69], offer a viable strategy to utilized these attractive interactions in molecular design.

Acknowledgments

We thank Michael Fuhrmann, Charlotte E. Lauter, Jan M. Metzler, Tom L. R. Kirschstein, Judith K. Metz, and Madison J. Sowden for fruitful discussions.

Open Access funding enabled and organized by Projekt DEAL.

Conflicts of Interest

The authors declare no conflicts of interest.

Data Availability Statement

The data that support the findings of this study are available in the supplementary material of this article.

References

1. E. A. Meyer, R. K. Castellano, and F. Diederich, "Interactions with Aromatic Rings in Chemical and Biological Recognition," *Angewandte Chemie International Edition* 42 (2003): 1210–1250.

2. A. A. Fokin, D. Gerbig, and P. R. Schreiner, "σ/σ- and π/π-Interactions Are Equally Important: Multilayered Graphanes," *Journal of the American Chemical Society* 133 (2011): 20036–20039.

3. S. K. Burley and G. A. Petsko, "Aromatic-Aromatic Interaction: A Mechanism of Protein Structure Stabilization," *Science* 229 (1985): 23–28.

4. S. K. Burley and G. A. Petsko, "Advances in Protein Chemistry," *Advances in Protein Chemistry* 39 (1988): 125–189.

5. N. Kannan and S. Vishveshwara, "Aromatic Clusters: A Determinant of Thermal Stability of Thermophilic Proteins," *Protein Engineering, Design and Selection* 13 (2000): 753–761.

6. A. N. Bootsma, A. C. Doney, and S. E. Wheeler, "Predicting the Strength of Stacking Interactions between Heterocycles and Aromatic Amino Acid Side Chains," *Journal of the American Chemical Society* 141 (2019): 11027–11035.

7. C. A. Hunter, K. R. Lawson, J. Perkins, and C. J. Urch, "Aromatic Interactions," *Journal of the Chemical Society, Perkin Transactions 2* (2001): 651–669.

8. J. P. Wagner and P. R. Schreiner, "London Dispersion in Molecular Chemistry—Reconsidering Steric Effects," *Angewandte Chemie International Edition* 54 (2015): 12274–12296.

9. L. Rummel and P. R. Schreiner, "Advances and Prospects in Understanding London Dispersion Interactions in Molecular Chemistry," *Angewandte Chemie International Edition* 63 (2024): e202316364.

10. M. H. J. Domanski, M. Fuhrmann, and P. R. Schreiner, "London Dispersion as a Design Element in Molecular Catalysis," *Journal of the American Chemical Society* 147 (2025): 29611–29623.

11. F. London, "Zur Theorie und Systematik der Molekularkräfte," *Zeitschrift für Physik* 63 (1930): 245–279.

12. C. Eschmann, L. Song, and P. R. Schreiner, "London Dispersion Interactions Rather than Steric Hindrance Determine the Enantioselectivity of the Corey–Bakshi–Shibata Reduction," *Angewandte Chemie International Edition* 60 (2021): 4823–4832.

13. Z. Huan, Z.-C. Han, L. Dong, et al., "London Dispersion-Induced Contraction of the Cu—O Bond in Copper(I) Phenolates," *Angewandte Chemie International Edition* 64 (2025): e202513210.

14. M. H. J. Domanski, L. Rummel, S. N. Krug, H. Hausmann, E. Solel, and P. R. Schreiner, "London Dispersion Favors *Cis* Selectivity in the Johnson–Corey–Chaykovsky Epoxidation," *The Journal of Organic Chemistry* 91 (2026): 4829–4841.

15. D. Yepes, F. Neese, B. List, and G. Bistoni, "Unveiling the Delicate Balance of Steric and Dispersion Interactions in Organocatalysis Using High-Level Computational Methods," *Journal of the American Chemical Society* 142 (2020): 3613–3625.

16. I. Harden, F. Neese, and G. Bistoni, "An Induced-Fit Model for Asymmetric Organocatalytic Reactions: A Case Study of the Activation of Olefins *via* Chiral Brønsted Acid Catalysts," *Chemical Science* 13 (2022): 8848–8859.

17. J. Gramüller, M. Franta, and R. M. Gschwind, "Tilting the Balance: London Dispersion Systematically Enhances Enantioselectivities in Brønsted Acid Catalyzed Transfer Hydrogenation of Imines," *Journal of the American Chemical Society* 144 (2022): 19861–19871.

18. C. A. Hunter, "Arene—Arene Interactions: Electrostatic or Charge Transfer?," *Angewandte Chemie International Edition* 32 (1993): 1584–1586.

19. J. Czernek and J. Brus, "Revisiting the Most Stable Structures of the Benzene Dimer," *International Journal of Molecular Sciences* 25 (2024): 8272.

20. M. C. Holland, J. B. Metternich, C. Daniliuc, W. B. Schweizer, and R. Gilmour, "Aromatic Interactions in Organocatalyst Design: Augmenting Selectivity Reversal in Iminium Ion Activation," *Chemistry – A European Journal* 21 (2015): 10031–10038.

21. B. K. Werley, X. Hou, E. P. Bertonazzi, A. Chianese, and T. W. Funk, "Substituent Effects and Mechanistic Insights on the Catalytic Activities of (Tetraarylcyclopentadienone)iron Carbonyl Compounds in Transfer Hydrogenations and Dehydrogenations," *Organometallics* 42 (2023): 3053–3065.

22. E. G. Hohenstein and C. D. Sherrill, "Effects of Heteroatoms on Aromatic π–π Interactions: Benzene–Pyridine and Pyridine Dimer," *The Journal of Physical Chemistry A* 113 (2009): 878–886.

23. C. D. Sherrill, "Energy Component Analysis of π Interactions," *Accounts of Chemical Research* 46 (2013): 1020–1028.

24. J. Řezáč, D. Nachtigallová, F. Mazzoni, et al., "Binding Energies of the π-Stacked Anisole Dimer: New Molecular Beam—Laser Spectroscopy Experiments and CCSD(T) Calculations," *Chemistry – A European Journal* 21 (2015): 6740–6746.

25. S. Paliwal, S. Geib, and C. S. Wilcox, "Molecular Torsion Balance for Weak Molecular Recognition Forces. Effects of "Tilted-T" Edge-to-Face Aromatic Interactions on Conformational Selection and Solid-State Structure," *Journal of the American Chemical Society* 116 (1994): 4497–4498.

26. S. L. Cockroft and C. A. Hunter, "Chemical Double-Mutant Cycles: Dissecting Non-Covalent Interactions," *Chemical Society Reviews* 36 (2007): 172–188.

27. I. K. Mati and S. L. Cockroft, "Molecular Balances for Quantifying Non-Covalent Interactions," *Chemical Society Reviews* 39 (2010): 4195–4205.

28. A. E. Aliev and W. B. Motherwell, "Some Recent Advances in the Design and Use of Molecular Balances for the Experimental Quantification of Intramolecular Noncovalent Interactions of π Systems," *Chemistry – A European Journal* 25 (2019): 10516–10530.

29. M. A. Strauss and H. A. Wegner, "Molecular Systems for the Quantification of London Dispersion Interactions," *European Journal of Organic Chemistry* (2019): 295–302.

30. L. Rummel, M. H. J. Domanski, H. Hausmann, J. Becker, and P. R. Schreiner, "London Dispersion Favors Sterically Hindered Diarylthiourea Conformers in Solution," *Angewandte Chemie International Edition* 61 (2022): e202204393.

31. R. Pollice, M. Bot, I. J. Kobylianskii, I. Shenderovich, and P. Chen, "Attenuation of London Dispersion in Dichloromethane Solutions," *Journal of the American Chemical Society* 139 (2017): 13126–13140.

32. J. M. Schümann, J. P. Wagner, A. K. Eckhardt, H. Quanz, and P. R. Schreiner, "Intramolecular London Dispersion Interactions Do Not Cancel in Solution," *Journal of the American Chemical Society* 143 (2021): 41–45.

33. A. Elmi, K. M. Bąk, and S. L. Cockroft, "Solvent Attenuation of London Dispersion in Polycyclic Aromatic Stacking," *Angewandte Chemie International Edition* 63 (2024): e202412056.

34. H. Liu, H. M. Scott, B. Lin, X. Huang, M. D. Smith, and K. D. Shimizu, "Solvent Attenuation of Dispersion Interactions Quantified in Polar and Nonpolar Media Using Rigid CH–π Balances," *Chemical Science* 16 (2025): 17772–17778.

35. E. Peris and R. H. Crabtree, "Key Factors in Pincer Ligand Design," *Chemical Society Reviews* 47 (2018): 1959–1968.

36. J. K. Malongwe, D. Nachtigallová, P. Corrochano, and P. Klán, "Spectroscopic Properties of Anisole at the Air–Ice Interface: A Combined Experimental–Computational Approach," *Langmuir* 32 (2016): 5755–5764.

37. J. M. Schümann, L. Ochmann, J. Becker, et al., "Exploring the Limits of Intramolecular London Dispersion Stabilization with Bulky Dispersion Energy Donors in Alkane Solution," *Journal of the American Chemical Society* 145 (2023): 2093–2097.

38. H. F. König, L. Rummel, H. Hausmann, J. Becker, J. M. Schümann, and P. R. Schreiner, "Gauging the Steric Effects of Silyl Groups with a Molecular Balance," *The Journal of Organic Chemistry* 87 (2022): 4670–4679.

39. H. F. König, H. Hausmann, and P. R. Schreiner, "Assessing the Experimental Hydrogen Bonding Energy of the Cyclic Water Dimer Transition State with a Cyclooctatetraene-Based Molecular Balance," *Journal of the American Chemical Society* 144 (2022): 16965–16973.

40. L. Rummel, H. F. König, H. Hausmann, and P. R. Schreiner, "Silyl Groups Are Strong Dispersion Energy Donors," *The Journal of Organic Chemistry* 87 (2022): 13168–13177.

41. M. H. J. Domanski, M. Fuhrmann, N. F. Hacket, H. Hausmann, and P. R. Schreiner, "Assessing Benzene Dimer Interactions in Solution With a Molecular Balance," *Chemistry – A European Journal* 32 (2026): e711126.

42. J. E. Anderson and P. A. Kirsch, "Structural Equilibria Determined by Attractive Steric Interactions. 1,6-Dialkylcyclooctatetraenes and Their Bond-Shift and ring Inversion Investigated by Dynamic NMR Spectroscopy and Molecular Mechanics Calculations," *Journal of the Chemical Society, Perkin Transactions 2* (1992): 1951–1957.

43. N. C. Burton, F. G. N. Cloke, S. C. P. Joseph, H. Karamallakis, and A. A. Sameh, "Trimethylsilyl Derivatives of Cyclooctatetraene," *Journal of Organometallic Chemistry* 462 (1993): 39–43.

44. J. S. Parry, F. G. N. Cloke, S. J. Coles, and M. B. Hursthouse, "Synthesis and Characterization of the First Sandwich Complex of Trivalent Thorium: A Structural Comparison with the Uranium Analogue," *Journal of the American Chemical Society* 121 (1999): 6867–6871.

45. O. T. Summerscales, F. G. N. Cloke, P. B. Hitchcock, J. C. Green, and N. Hazari, "Reductive Cyclotetramerization of CO to Squarate by a U(III) Complex: the X-Ray Crystal Structure of $[(U(\eta\text{-}C_8H_6\{Si^iPr_3\text{-}1,4\}_2)(\eta\text{-}C_5Me_4H)]_2(\mu\text{-}\eta^2\text{:}\eta^2\text{-}C_4O_4)$," *Journal of the American Chemical Society* 128 (2006): 9602–9603.

46. J. Catalán and H. Hopf, "Empirical Treatment of the Inductive and Dispersive Components of Solute–Solvent Interactions: The Solvent Polarizability (SP) Scalc," *European Journal of Organic Chemistry* (2004): 4694–4702.

47. R. Bosque and J. Sales, "Polarizabilities of Solvents from the Chemical Composition," *Journal of Chemical Information and Computer Sciences* 42 (2002): 1154–1163.

48. C. Adam, L. Yang, and S. L. Cockroft, "Partitioning Solvophobic and Dispersion Forces in Alkyl and Perfluoroalkyl Cohesion," *Angewandte Chemie International Edition* 54 (2015): 1164–1167.

49. P. Pracht, F. Bohle, and S. Grimme, "Automated Exploration of the Low-Energy Chemical Space with Fast Quantum Chemical Methods," *Physical Chemistry Chemical Physics* 22 (2020): 7169–7192.

50. P. Pracht, S. Grimme, C. Bannwarth, et al., "CREST—A Program for the Exploration of Low-Energy Molecular Chemical Space," *The Journal of Chemical Physics* 160 (2024): 114110.

51. S. Grimme, F. Bohle, A. Hansen, P. Pracht, S. Spicher, and M. Stahn, "Efficient Quantum Chemical Calculation of Structure Ensembles and Free Energies for Nonrigid Molecules," *The Journal of Physical Chemistry A* 125 (2021): 4039–4054.

52. E. Caldeweyher, J.-M. Mewes, S. Ehlert, and S. Grimme, "Extension and Evaluation of the D4 London-Dispersion Model for Periodic Systems," *Physical Chemistry Chemical Physics* 22 (2020): 8499–8512.

53. A. Najibi and L. Goerigk, "DFT -D4 Counterparts of Leading Meta-Generalized-gradient Approximation and Hybrid Density Functionals for Energetics and Geometries," *Journal of Computational Chemistry* 41 (2020): 2562–2572.

54. A. V. Marenich, C. J. Cramer, and D. G. Truhlar, "Universal Solvation Model Based on Solute Electron Density and on a Continuum Model of the Solvent Defined by the Bulk Dielectric Constant and Atomic Surface Tensions," *The Journal of Physical Chemistry B* 113 (2009): 6378–6396.

55. S. Grimme, A. Hansen, S. Ehlert, and J.-M. Mewes, "R2SCAN-3c: A "Swiss Army Knife" Composite Electronic-Structure Method," *The Journal of Chemical Physics* 154 (2021): 064103.

56. W. Humphrey, A. Dalke, and K. Schulten, "VMD: Visual Molecular Dynamics," *Journal of Molecular Graphics* 14 (1996): 33–38.

57. J. Contreras-García, E. R. Johnson, S. Keinan, et al., "NCIPLOT: A Program for Plotting Noncovalent Interaction Regions," *Journal of Chemical Theory and Computation* 7 (2011): 625–632.

58. T. Lu and F. Chen, "Multiwfn: A Multifunctional Wavefunction Analyzer," *Journal of Computational Chemistry* 33 (2012): 580–592.

59. R. Laplaza, F. Peccati, R. A. Boto, et al., "NCIPLOT and the Analysis of Noncovalent Interactions Using the Reduced Density Gradient," *WIREs Computational Molecular Science* 11 (2021): e1497.

60. R. M. Parrish, T. M. Parker, and C. D. Sherrill, "Chemical Assignment of Symmetry-Adapted Perturbation Theory Interaction Energy Components: The Functional-Group SAPT Partition," *Journal of Chemical Theory and Computation* 10 (2014): 4417–4431.

61. R. M. Parrish, J. F. Gonthier, C. Corminbœuf, and C. D. Sherrill, "Communication: Practical Intramolecular Symmetry Adapted Perturbation Theory via Hartree-Fock Embedding," *The Journal of Chemical Physics* 143 (2015): 051103.

62. T. M. Parker, L. A. Burns, R. M. Parrish, A. G. Ryno, and C. D. Sherrill, "Levels of Symmetry Adapted Perturbation Theory (SAPT). I. Efficiency and Performance for Interaction Energies," *The Journal of Chemical Physics* 140 (2014): 094106.

63. J. M. Turney, A. C. Simmonett, R. M. Parrish, et al., "Psi4: an Open-source *Ab Initio* Electronic Structure Program," *WIREs Computational Molecular Science* 2 (2012): 556–565.

64. D. Luu and K. Patkowski, "Overcoming Artificial Multipoles in Intramolecular Symmetry-Adapted Perturbation Theory," *The Journal of Physical Chemistry A* 127 (2023): 356–377.

65. G. Pietraperzia, M. Pasquini, N. Schiccheri, et al., "The Gas Phase Anisole Dimer: A Combined High-Resolution Spectroscopy and Computational Study of a Stacked Molecular System," *The Journal of Physical Chemistry A* 113 (2009): 14343–14351.

66. C. Riplinger, B. Sandhoefer, A. Hansen, and F. Neese, "Natural Triple Excitations in Local Coupled Cluster Calculations with Pair Natural Orbitals," *The Journal of Chemical Physics* 139 (2013): 134101.

67. T. H. Dunning, "Gaussian Basis Sets for use in Correlated Molecular Calculations. I. The Atoms Boron through Neon and Hydrogen," *The Journal of Chemical Physics* 90 (1989): 1007–1023.

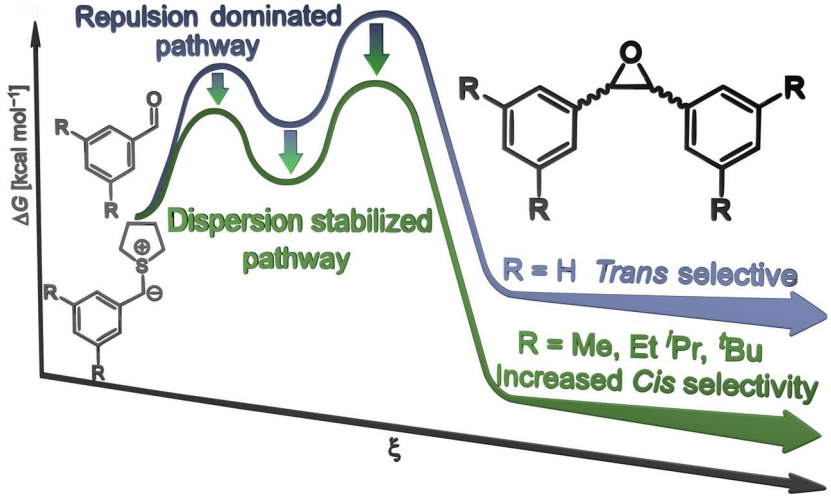
68. C. Eschmann, L. Song, and P. R. Schreiner, "London Dispersion Interactions Rather than Steric Hindrance Determine the Enantioselectivity of the Corey–Bakshi–Shibata Reduction," *Angewandte Chemie* 133 (2021): 4873–4882.

69. M. Fuhrmann, N. F. Hacket, and P. R. Schreiner, "Streamlined Synthesis of Bulky (Dispersion Energy Donor) Iodobenzenes," *Synthesis* 58 (2026): 421–424.

Supporting Information

Additional supporting information can be found online in the Supporting Information section.

2.4 London Dispersion Favors *Cis* Selectivity in the Johnson−Corey−Chaykovsky Epoxidation



Abstract

We elucidate the role of dispersion energy donors on the *cis/trans* selectivity of the Johnson–Corey–Chaykovsky epoxidation, focusing on bulky alkyl groups as well as halides as dispersion energy donors. Whereas the generally accepted explanation of the observed diastereoselectivity solely invokes steric repulsion, we determined that London dispersion interactions are an important source of stabilization of the preferred transition structures. This was brought forth experimentally by utilizing a series of NMR measurements, double mutant cycles, and crossover experiments. Additionally, density functional theory computations and symmetry-adapted perturbation theory computations were used to determine and quantify the role of noncovalent interactions.

***Reference*:**

Marvin H. J. Domanski, Lars Rummel, Saskia N. Krug, Heike Hausmann, Ephrath Solel, and Peter R. Schreiner, *J. Org. Chem.* **2026**, *91*, 4829–4841.

DOI: 10.1021/acs.joc.6c00154

Reproduced (or adapted) with permission from © 2026 American Chemical Society.

JOC The Journal of Organic Chemistry

Open Access
This article is licensed under CC-BY 4.0

pubs.acs.org/joc
Featured Article

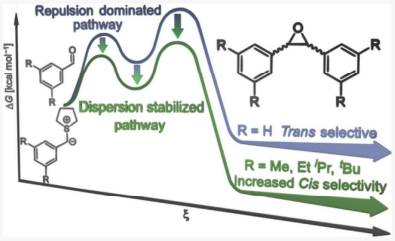
London Dispersion Favors *Cis* Selectivity in the Johnson–Corey–Chaykovsky Epoxidation

Marvin H. J. Domanski, Lars Rummel, Saskia N. Krug, Heike Hausmann, Ephrath Solel,* and Peter R. Schreiner*

Cite This: *J. Org. Chem.* 2026, 91, 4829–4841
Read Online

ACCESS | Metrics & More | Article Recommendations | Supporting Information

ABSTRACT: We elucidate the role of dispersion energy donors on the *cis*/*trans* selectivity of the Johnson–Corey–Chaykovsky epoxidation, focusing on bulky alkyl groups as well as halides as dispersion energy donors. Whereas the generally accepted explanation of the observed diastereoselectivity solely invokes steric repulsion, we determined that London dispersion interactions are an important source of stabilization of the preferred transition structures. This was brought forth experimentally by utilizing a series of NMR measurements, double mutant cycles, and crossover experiments. Additionally, density functional theory computations and symmetry-adapted perturbation theory computations were used to determine and quantify the role of noncovalent interactions.

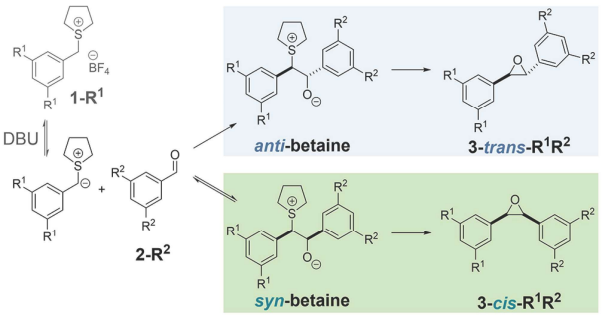


INTRODUCTION

In chemistry, insights into reaction mechanisms are essential to maximize yields and stereoselectivities, especially the latter, which requires extensive knowledge of how molecules interact and connect via elementary reaction steps. The applicability of a detailed understanding of reaction pathways ranges from basic S_N2 reactions[1] proceeding via stereospecific backside attacks, to highly complex catalytic processes.[2] In the past the origin of stereoselectivity was most often rationalized by repulsive steric interactions either between substrates or catalyst and substrate.[3] While the concept of steric hindrance can typically explain the stereochemical outcome of reactions between *small* molecules and groups, bulky substituents counterintuitively can have the opposite effect through steric attraction.[4−6] This has been recently demonstrated, for example, in the copper-catalyzed hydroamination of unactivated olefins,[7] in paddlewheel catalysts,[8,9] in the Brønsted acid-catalyzed transfer hydrogenation of imines,[10] and for the Corey–Bakshi–Shibata reduction utilizing sterically highly encumbered oxazaborolidine catalysts.[11] Here, the rate-determining step of the reduction proceeds through the more *crowded* transition state that profits from *attractive* noncovalent interactions. For hydroamination reactions it was demonstrated that increasing steric bulk promotes catalyst-substrate interactions, thereby accelerating the reaction.[7,12,13] Both studies highlight the importance of London dispersion[14,15] (LD) interactions as the key driving force for aggregation and as the essential interaction to rationalize the experimental results.[16] To maximize LD, highly polarizable groups called dispersion energy donors (DEDs) were introduced as a concept and in practice.[4,17]

In comparison to ground-state stabilization via attractive $\sigma-\sigma$ contacts, for example, in molecular balances,[18,19] the preferential LD stabilization of transition states has not been thoroughly investigated. Here, we chose the Johnson–Corey–Chaykovsky (JCC) reaction[5,20−23] to study the effects of DEDs on the stereodifferentiating transition states of this reaction. The JCC reaction takes place between an ylide and an aldehyde (Scheme 1); numerous procedures exist that give a variety of products, for example aziridines,[24] cyclopropanes,[24,25] and epoxides.[26−30] Additionally, there are theoreti-

Scheme 1. Currently Accepted Reaction Sequence of the Johnson–Corey–Chaykovsky Epoxidation



Received: January 22, 2026
Revised: February 27, 2026
Accepted: March 13, 2026
Published: March 26, 2026



ACS Publications
© 2026 The Authors. Published by American Chemical Society

https://doi.org/10.1021/acs.joc.6c00154
J. Org. Chem. 2026, 91, 4829–4841

cal[31−34] and experimental studies[35,36] on the mechanism of the JCC reaction.

The current consensus is that after a pre-equilibrium deprotonation with base to generate the ylide from sulfonium salt **1-R^1**, the ylide adds nucleophilically to the aldehyde **2-R^2** in the rate-determining step. Subsequent bond rotation around the central C−C bond gives the *syn*- or *anti*-betaine, followed by stereospecific elimination of sulfide to yield the *cis*- or *trans*-epoxide (**3-*cis*/*trans*-R^{1}R^2**), respectively.

Experimentally, the Gibbs free energy of activation was determined as $\Delta G^{\ddagger}$ = 22.2 kcal mol^{-1} (with R^1 = H and R^2 = H) at 298 K for the nucleophilic addition of the ylide to form the *trans*-epoxide.[35] In contrast, previous computations suggested that the rotation around the central betaine C−C bond is rate-determining for the formation of the *cis*-epoxide.[34] The origin of the diastereoselectivity lies in the reversibility of the *syn*-betaine formation on the one hand and the irreversibility of the *anti*-betaine formation (from crossover experiments) on the other. Accordingly, Aggarwal et al.[3] outlined four main principles to rationalize stereoselectivity in the Johnson−Corey−Chaykovsky reaction: (1) steric repulsion between the phenyl moieties in the *syn*-betaine structure, (2) the inherent stability of the ylide, (3) the stability of the aldehyde, and (4) the role of solvation in promoting reversible *syn*-betaine formation. Herein, we investigate the role of DEDs in the JCC reaction, demonstrating the importance of LD in this reaction in particular and in stereoselective reactions in general.[16]

RESULTS

Alkyl Substituents

To study the impact of DEDs on the JCC epoxidation, we systematically varied the substituent at **1-R^1** and **2-R^2** in the logical series from methyl (Me) through ethyl (Et) and isopropyl (^{i}Pr) to *tert*-butyl (^{t}Bu). We utilized 1-bromo-3,5-dialkyl-substituted benzene as starting material to generate all precursors. **2-R^2** was prepared *via* a formylation reaction with DMF.[37] The aldehyde was reduced utilizing $LiAlH_4$, and the resulting alcohol was brominated *via* PBr_3.[38,39] A Finkelstein-type reaction with tetrahydrothiophene and $NaBF_4$ yielded **1-R^1**.[40] In addition, we utilized halides as DEDs in the all-*meta* position. Starting from 3,5-dihalo-substituted benzaldehyde, we generated the logical series from fluorine (F) to chlorine (Cl) and bromine (Br) at **1-R^1** and **2-R^2**. The iodine(I)-substituted starting material was synthesized from benzocaine according to Lindsey et al.[41]

To probe the effects of DEDs on the JCC reaction, the reaction conditions were chosen in analogy to Crudden et al.[35] who experimentally investigated the mechanism of the JCC reaction. The epoxidation was performed in DCM under pseudo-first order kinetic conditions. Accordingly, the aldehyde was utilized in excess (0.5 M, 10 equiv) with limiting sulfonium salt (1.0 equiv) present. A buffer (1.0 equiv) of 1,8-diazabicyclo(5.4.0)undec-7-ene (DBU) and *p*-toluenesulfonic acid (*p*-TSA) was utilized for a steady pH. Additionally, DBU (1.0 equiv) was added as a base to generate the ylide and to start the reaction. The reaction progress was monitored by ^{1}H NMR spectroscopy at room temperature. The ratio of **3-*cis*-R^{1}R^2** and **3-*trans*-R^{1}R^2** was determined by integration of the *cis* and *trans* proton signals at the epoxide. Crudden et al.[35] already demonstrated irreversibility of the parent system. To determine whether bulky substituents influence the reaction mechanism, we followed the reaction progress for **1-Me** and **2-Me** as well as **1-^{t}Bu** and **2-^{t}Bu** (see the Supporting Information (SI)). In both cases the product concentration steadily increased while the ratio between both epoxides remained constant. Additionally, we exposed a 1:1 mixture of **3-*trans*-HH** and **3-*cis*-HH** to the reaction conditions without observing a change in ratio (see the SI). Figure 1 shows the ^{1}H NMR signals of the symmetric epoxides (R = R^1 = R^2) utilizing the alkyl substitution pattern with a chemical shift between 3.75 and 4.40 ppm.

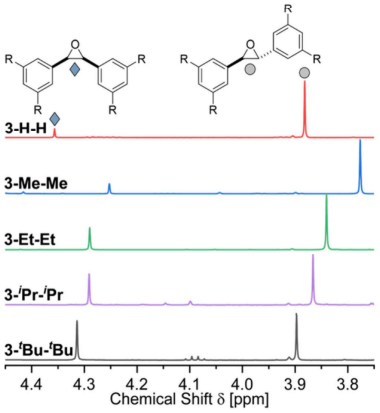


Figure 1. ^{1}H NMR measurements of symmetric **3-*cis*-R^{1}R^2** (blue marking) and **3-*trans*-R^{1}R^2** (gray marking) as a result of the reaction of **1-R^1**and **2-R^2** with alkyl substituents in DCM at 298 K. For simplicity, only the CH signals of the symmetric epoxides are depicted. It is already apparent from the relative intensities that the amount of *cis*-epoxide increases with steric bulk.

The parent unsubstituted starting material resulted in a product ratio of 0.17:1.00 (*cis*:*trans*) (Figure 1, red NMR). In accordance with the literature,[35] the larger signal (gray marking) was assigned to **3-*trans*-HH** and the smaller signal (blue marking) to **3-*cis*-HH**. The generation of **3-*trans*-HH** and **3-*cis*-HH** from stilbene with *m*-chloroperoxybenzoic acid (*m*CPBA) confirmed our assignment (see the SI). To gather as much information as possible on the influence of DEDs on the reaction we followed our procedure for all possible **1-R^1** and **2-R^2** combinations. The results for the symmetric alkyl-substituted products are depicted in Figure 1. Counter-intuitively, the epoxide ratio (*cis*:*trans*) shifts to the more crowded **3-*cis*-R^{1}R^2** with increasing DED size. Accordingly, the ratio of **3-*trans*-^{t}Bu^{t}Bu** and **3-*cis*-^{t}Bu^{t}Bu** (Figure 1, black) is almost 1:1 (see the SI for all exact ratios).

Figure 2 displays the experimentally determined $\Delta G^{\ddagger}_{R^1R^2\text{-HH}}$ values for the reaction between differently alkyl-substituted tetrahydrothiophene salts **1-R^1** and aldehydes **2-R^2** to generate mixtures of **3-*cis*-R^{1}R^2** and **3-*trans*-R^{1}R^2**. The energy values are derived from integration of the *cis* and *trans* proton signals of the epoxide. The unsubstituted system was utilized as reference reaction. $\Delta G^{\ddagger}_{R^1R^2\text{-HH}}$ refers to the free energy of the rate-determining transition state relative to that of the parent unsubstituted reaction of **1-H** and **2-H**. Therefore, $\Delta G^{\ddagger}_{R^1R^2\text{-HH}}$ for the reaction of **1-H** and **2-H** is denoted as $\Delta G^{\ddagger}_{HH\text{-HH}}$ = 0.0 ± 0.1 kcal mol^{-1} (leftmost data point). With an absolute free energy value of $\Delta G^{\ddagger}_{HH}$ = 1.0 ± 0.0 kcal mol^{-1} (see the SI for absolute values) the reaction of **1-H** and **2-H** favors the less crowded **3-*trans*-HH** over **3-*cis*-HH** ($K^{\ddagger}_{HH}$ = 0.17). In line with

https://doi.org/10.1021/acs.joc.6c00154
J. Org. Chem. 2026, 91, 4829−4841

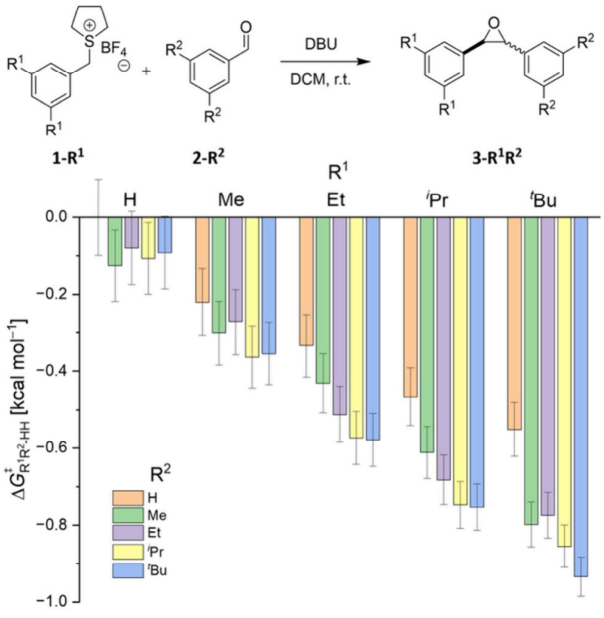


Figure 2. Experimentally determined relative Gibbs free energy values $\Delta G^{\ddagger}_{R^1R^2\text{-HH}}$ for the reaction of alkyl-substituted **1-R^1** and **2-R^2** at room temperature relative to the parent case with $R^1 = R^2 = H$ (leftmost data point, *cis*:*trans* ratio of 0.17:1.00). The depicted energy values correspond to the energy differences of the transition states in the rate-determining step. $\Delta G^{\ddagger} < 0$ indicates favoring of **3-*cis*-R^{1}R^2** formation relative to the parent system. $R^1 = R^2 = {}^t$Bu results almost in a *cis*:*trans* ratio of 1:1. The gray lines indicate error bars.

the argument that large groups such as phenyl moieties interact repulsively, the transition state leading to **3-*trans*-HH** is lower in energy by around 1.0 kcal mol^{-1} than its more crowded counterpart. With this result and classic "steric repulsion thinking" in mind, bulkier groups, *e.g.*, with an all-*meta* substitution pattern, should shift the ratio even further to **3-*trans*-R^{1}R^2** ($\Delta G^{\ddagger} > 0$).[3] In stark contrast, Figure 2 shows the *opposite* trend. The attached substituents shift the ratio to the more crowded **3-*cis*-RR** ($\Delta G^{\ddagger} < 0$) contradicting the well-established rationale that increasing steric bulk predominantly favors **3-*trans*-R^{1}R^2**. However, our results are well in line with investigations focusing on attractive $\sigma-\sigma$ and $\sigma-\pi$ interactions.[4,42−47] Similar effects were observed in numerous catalytic processes highlighted earlier.[7−11] In those cases, bulky substituents were utilized to lower the energy of the more crowded transition state by enforcing close $\sigma-\sigma$ and $\sigma-\pi$ contacts between catalyst and substrate. A similar effect appears to govern the JCC reaction as well.

To study the effect of LD on the transition state of the reaction, all combinations of **1-R^1** and **2-R^2** were measured. The unsubstituted **1-H** always favors the reaction forming **3-*trans*-HR^2** (leftmost block of columns). The energy difference of the transition states does not change with increasing substituent size at **2-R^2** ($\Delta G^{\ddagger}_{HR^2\text{-HH}} \approx -0.1 \pm 0.1$ kcal mol^{-1}). On the other hand, in a reaction with unsubstituted benzaldehyde **2-H** (orange bars) increasing substituent size at **1-R^1** decreases the energy gap between the two transition states. Stabilizing $\sigma-\pi$ interactions appear to decrease the energy of the *more crowded* transition state. While the transition state to **3-*cis*-MeH** benefits by around $\Delta G^{\ddagger}_{MeH\text{-HH}} \approx -0.2 \pm 0.1$ kcal mol^{-1} from stabilizing $\sigma-\pi$ contacts, the incorporation of additional CH_3 substituents increases this effect by around −0.1 kcal mol^{-1}. In the series of singly substituted starting materials (orange bars and leftmost block of columns), the largest effect can be observed for the reaction of **1-^{t}Bu** and **2-H** ($\Delta G^{\ddagger}_{^t\text{BuH-HH}} \approx -0.6 \pm 0.1$ kcal mol^{-1}). In stark contrast to the well-established rule-of-thumb that steric hindrance governs the transition state of the JCC reaction, an increase in substituent size at **1-R^1** and **2-R^2** shifts the *dr* toward the more crowded **3-*cis*-R^{1}R^2**. The systematic increase of **2-R^2** within each series of **1-R^1** identifies the *tert*-butyl substituent (blue bars) as the best DED. The strongest interaction can be observed for the reaction of **1-^{t}Bu** and **2-^{t}Bu** almost resulting in a 1:1 mixture ($K^{\ddagger}_{^t\text{Bu}^t\text{Bu}} = 0.93$). Since we are under kinetic conditions, the transition state along the reaction to the more crowded **3-*cis*-^{t}Bu^{t}Bu** is favored by around $\Delta G^{\ddagger}_{^t\text{Bu}^t\text{Bu-HH}} \approx -0.9 \pm 0.1$ kcal mol^{-1} relative to its parent counterpart.

Halogen Substituents

Having studied the alkyl substitution pattern, we shifted our focus to halogen substitution. While recent studies[46,48−56] demonstrated that halogens can act as DEDs, polar effects could potentially override LD interactions. The same procedure as for the alkyl-substituted starting material was applied for reactions between differently halo-substituted tetrahydrothiophene salts **1-R^1** and aldehydes **2-R^2**. In addition, we expanded our scope and included all possible alkyl-halogen combinations by varying **1-R^1** and **2-R^2** systematically. Since **1-F** was insoluble in DCM, it had to be excluded.

Moreover, all possible combinations of aldehydes with all-*meta* halogen-substituted tetrahydrothiophene salts **1-R^1** resulted only in **3-*trans*-R^{1}R^2**. This implies that secondary effects, such as electronegativity, significantly influence the behavior of **1-R^1**. Interestingly, this is not the case for the halo-substituted **2-R^2**. Figure 3 displays the experimentally determined $\Delta G^{\ddagger}_{R^1R^2\text{-HH}}$ values for the reaction of alkyl-substituted **1-R^1** and halo-substituted **2-R^2**. For the reaction of **1-H** and **2-H**, $\Delta G^{\ddagger}_{HH\text{-HH}} = 0.0 \pm 0.1$ kcal mol^{-1} (leftmost data point). In contrast to alkyl−alkyl interactions (Figure 2), the reactions of **1-H** or **1-Me** (leftmost and second leftmost block of columns, Figure 3) with halo-substituted **2-R^2** result in the formation of more **3-*trans*-HR^2** in comparison to the parent system. Consequently, the electronic effects due to halogen incorporation increase the energy difference of the transition states. This effect is most obvious for the reaction of **1-H** and **2-F**. Here, the energy difference of the transition states increases to $\Delta G^{\ddagger}_{HF\text{-HH}} \approx 0.5 \pm 0.1$ kcal mol^{-1}. Nevertheless, bulkier halogens, such as iodine, shift the *dr* again toward the more crowded **3-*cis*-R^{1}R^2**. While the energy difference of the transition states for the reaction of **1-^{i}Pr** and **2-F** is about the same as of **1-H** and **2-H** (and essentially thermoneutral), combinations of bulky alkyl groups and halogens clearly favor the more crowded transition states. By utilizing **1-^{t}Bu** and **2-I** (the biggest and bulkiest substituents incorporated), the transition state to the more crowded **3-*cis*-^{t}BuI** is favored by around $\Delta G^{\ddagger}_{^t\text{BuI-HH}} \approx -0.6 \pm 0.1$ kcal mol^{-1}.

■ DISCUSSION

As described in the introduction, four main factors were made responsible for diastereoselectivity of the reaction between sulfur ylide and aldehyde. On the basis of our experimental data, three of these can be re-evaluated and refined (differential solvation is not part of our study).

https://doi.org/10.1021/acs.joc.6c00154
J. Org. Chem. 2026, 91, 4829−4841

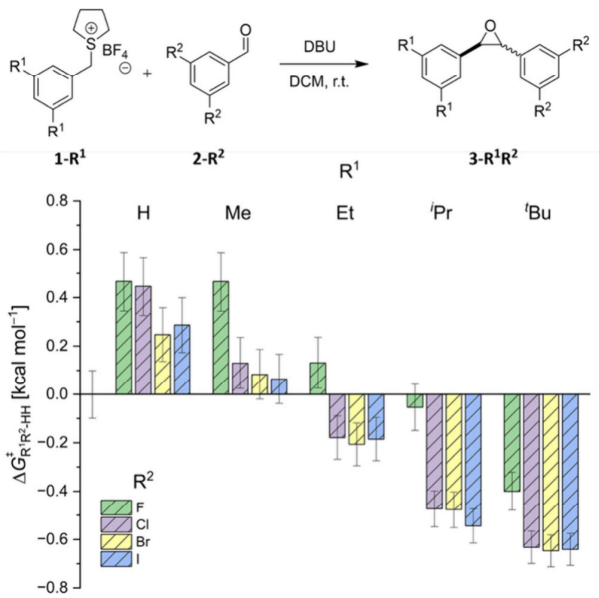


Figure 3. Experimentally determined relative Gibbs free energy values $\Delta G^{\ddagger}_{R^1R^2\text{-HH}}$ for the reaction of alkyl-substituted **1-R^1** and halo-substituted **2-R^2** relative to the parent case with $R^1 = R^2 = H$ (leftmost data point). The depicted energy values correspond to the energy differences of the transition states in the rate-determining step. $\Delta G^{\ddagger} < 0$ indicates favoring of **3-*cis*-R^{1}R^2** formation with regards to the parent system. The gray lines indicate error bars.

Stability of the Carbonyl Group

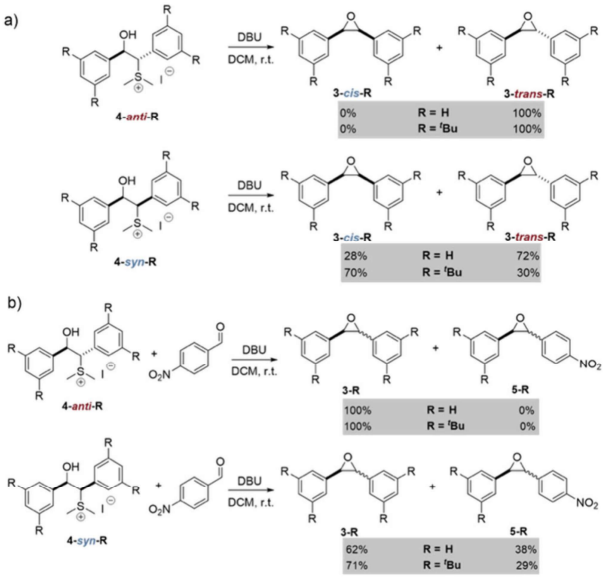
Aggarwal et al.[3] observed a significant increase in *trans* diastereoselectivity when utilizing aromatic instead of aliphatic aldehydes. While the formation of the *syn*-betaine structure is reversible (Scheme 1), stabilization of the starting material allows for an increase in *trans*-betaine formation. Aryl moieties stabilize the carbonyl form over the betaine structure. Accordingly, high *dr* is expected for benzaldehyde derivatives. Additionally, this effect should be amplified by electron-donor substituents due to an increase in electron density (for alkyl substituents) at the carbonyl carbon resulting in lower electrophilicity.[3] However, our experimental data show the opposite selectivity. While unsubstituted phenyl moieties favor **3-*trans*-R^{1}R**,[2] the attachment of DEDs clearly shifts the ratio toward **3-*cis*-R^{1}R^2** (for example, $K^{\ddagger}_{^t\text{Bu}^t\text{Bu}} = 0.93$). The same is true for halogen substituents at **2-R^2**, although the relative Gibbs free energy values $\Delta G^{\ddagger}_{R^1R^2\text{-HH}}$ are shifted toward **3-*trans*-R^{1}R^2**. Accordingly, we deduce that the stability of the carbonyl group is less important and conclude that the action of increasingly larger alkyl groups at the aryl ring mainly act through stabilizing LD interactions.

Stability of the Ylide

In line with the argument above, Aggarwal et al.[3] found that the more stable the ylide, the higher the *trans* selectivity. Accordingly, electron-deficient functional groups increase diastereocontrol, whereas electron-rich groups yield lower *dr*. This statement is in line with our experimental findings. The attached alkyl groups decrease stereocontrol. The energy gap between both rate determining transition states is equal in height to result in 1:1 mixture of *cis* and *trans* epoxide with bulky *tert*-butyl groups attached. At the same time, the *dr* increases to high *trans* selectivity with electron-deficient functional groups, such as halogens. The halogen-substituted **1-R^1** resulted in **3-*trans*-R^{1}R^2**. Nevertheless, our experimental findings let us conclude that the stability of the ylide is not the only factor for stereocontrol but that this also depends on the fine balance between attractive and repulsive interactions. A combination of an increasing number of close LD contacts and a higher electron density maximize LD interactions in the more crowded transition state.

Since the first two principles are based on reversible betaine formation, we performed ring closure and crossover experiments to investigate the reversibility for the unsubstituted and heavily substituted alkyl systems. Hence, we synthesized the protonated diastereomers of betaine intermediates **4-*anti*-R** and **4-*syn*-R** (Scheme 2) to probe the epoxide formation

Scheme 2. Ring Closure Experiments (top) and Crossover Experiments (bottom) of 4-*anti*-R and 4-*syn*-R in DCM at Room Temperature with DBU as the Base



starting with a single diastereomer. The starting materials were generated from *cis*- and *trans*-stilbene after epoxidation and stereoselective ring opening with thiomethoxide, methylation with methyliodide yields **4-*syn*-H** and **4-*anti*-H** selectively.[57] The *tert*-butyl derivative was synthesized accordingly. Hereby, the *cis*- and *trans*-stilbene derivatives were prepared from hydrogenation of bis(3,5-di-*tert*-butylphenyl)acetylene, which was the product of a coupling reaction with 2-butynedioic acid.[58]

The ring closure experiments (Scheme 2, top) of **4-*anti*-R** and **4-*syn*-R** were performed at room temperature in DCM by adding 1.0 equiv of base (DBU). With **4-*anti*-R** with R = H or ^{t}Bu, the less crowded **3-*trans*-R^{1}R^2** forms exclusively. This implies that the rate-determining step for the JCC reaction has to occur *prior* to the final epoxidation step (thus betaine formation). In line with earlier reports,[29,30,36,57,59,60] the epoxidation of **4-*syn*-H** results in a 28:72 *cis*:*trans* product ratio. Thus, the rate-determining step of **3-*cis*-HH** formation lies *after* betaine formation. Upon deprotonating **4-*syn*-H** the *syn*-betaine can either be directly converted to **3-*cis*-HH** or equilibrate to form the starting material (Figure 4). Recombination of **1*-R** (the asterisk indicates minor changes

https://doi.org/10.1021/acs.joc.6c00154
J. Org. Chem. 2026, 91, 4829−4841

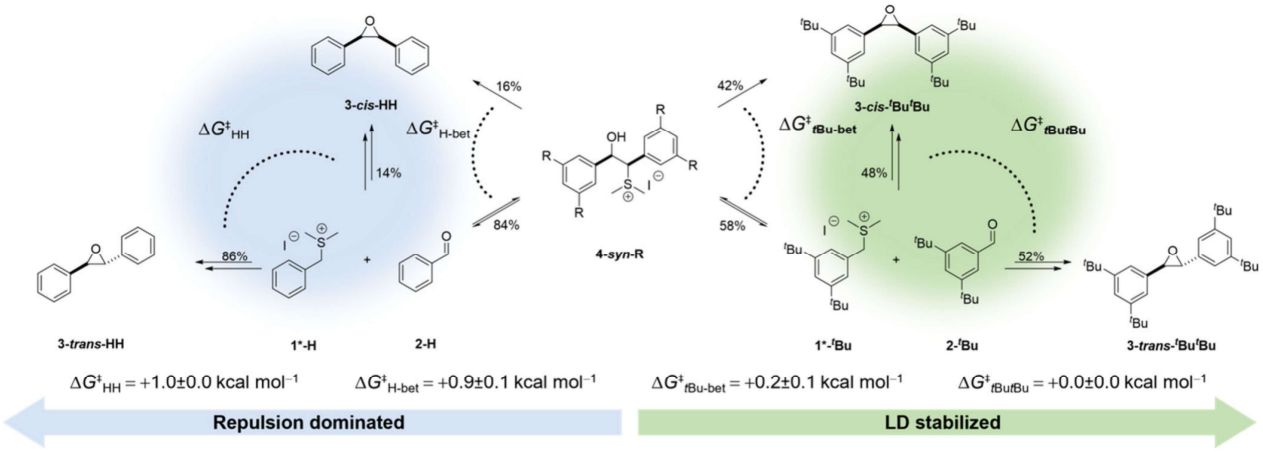


Figure 4. Reaction path shown in its protonated form for ring closure experiments of **4-*syn*-R** with R = H (left, blue) and R = ^{t}Bu (right, green). The percentage give the probability of conversion of **4-*syn*-R** and recombination of **1*-R** and **2-R**. The Gibbs free energy values correspond to the difference in transition state of the conversion of **4-*syn*-R** ($\Delta G^{\ddagger}_{\text{R-bet}}$) and for rate-determining transition states of recombination of **1*-R** and **2-R** ($\Delta G^{\ddagger}_{R^1R^2}$).

of the molecule to **1-R**) and **2-R** also results in a *cis* and *trans* product mixture.

Under the assumption that molecular changes in **1*-R** are minor and that, in a second approximation, the ratio of the pseudo-first order kinetic experiments is transferable to a reaction of **1-R** and **2-R** under thermodynamic conditions (control experiments confirm this assumption; see the SI), $\Delta G^{\ddagger}_{R^1R^2\text{-HH}}$ (Figure 2) can be utilized to calculate the probability for the conversion of **4-*syn*-R**. The ratio for the reaction of **4-*syn*-H** in combination with results of the JCC epoxidation to form **3-*cis*/*trans*-HH** (Figure 2) corresponds to a theoretical difference of $\Delta G^{\ddagger}_{\text{H bet}} \approx +0.9 \pm 0.1$ kcal mol^{-1} for the transition states of the conversion (ring closure reaction or equilibration) according to probability calculations. This suggests that the majority of **4-*syn*-H** (~84%) equilibrates while the remaining 16% are directly converted to **3-*cis*-HH** (Figure 4). The same effect can be observed for **4-*syn*-^{t}Bu**. Remarkably, now the final ratio for the consumption of **4-*syn*-^{t}Bu** is 70:30 (*cis*:*trans*) in favor of the more crowded product **3-*cis*- ^{t}Bu^{t}Bu**, suggesting a significant change in transition structures for the conversion of **4-*syn*-^{t}Bu**. The ratio corresponds to a theoretical energy difference of $\Delta G^{\ddagger}_{\text{Bu-bet}} \approx +0.2 \pm 0.1$ kcal mol^{-1}, thereby, slightly favoring conversion to **1-^{t}Bu** and **2-^{t}Bu**. Accordingly, 42% of **4-*syn*-^{t}Bu** are directly converted to **3-*cis*-^{t}Bu^{t}Bu** while the remaining 58% equilibrate to **1-R** and **2-R** (Figure 4). The direct formation of **3-*cis*-^{t}Bu^{t}Bu** from **4-*syn*-^{t}Bu** significantly increases in comparison to parent **4-*syn*-H**. This can be related to additional LD interactions favoring the folded conformation **4-*syn*-^{t}Bu** with the hydroxyl function in the *anti* position to the thioether functional group.

A similar DED-effect was already observed for hexaphenylethane.[61−66] While the unsubstituted hexaphenylethane is not thermodynamically stable due to steric hindrance,[65] the *tert*-butyl-substituted derivative offers multiple LD contacts to stabilize the molecule.[63] Likewise, the unsubstituted reaction pathway of **4-*syn*-H** is governed by repulsive interactions. On the other hand, LD interactions stabilize the folded *syn*-betaine structure, thereby increasing the probability of direct conversion to **3-*cis*-^{t}Bu^{t}Bu**.

To demonstrate that an equilibration must occur by reopening the betaine structure, we performed crossover experiments (Scheme 2, bottom).[29,30,36,57,59,60] Activated *p*-nitrobenzaldehyde was utilized as trapping agent for the ylide due to its higher reactivity (reactions proceed around 62 times faster than with benzaldehyde).[36] Whereas **4-*anti*-R** with R = H or ^{t}Bu solely results in the formation of **3-*trans*-R^{1}R^2** without incorporating nitrobenzaldehyde, **4-*syn*-R** gives a mixture of **3-*trans*-R^{1}R^2** and the corresponding nitro-product **5-R** (Scheme 2b). This demonstrates that the equilibration of the *syn*-betaine has to occur by breaking the central carbon bond to give ylide and aldehyde.

Steric Hindrance of the Ylide/Aldehyde

Finally, steric hindrance is widely believed to affect the stereochemical outcome of the JCC reaction.[3] While this may be true for special cases, it is unlikely the sole contributor to selectivity because all bulky substituents used here (and elsewhere) show the opposite (Figure 2): The parent reaction of **1-H** with **2-H** yields the highest *trans* selectivity with a transition state energy difference of $\Delta G^{\ddagger}_{\text{HH}} = 1.0 \pm 0.0$ kcal mol^{-1}). On the contrary, the reaction of **1-^{t}Bu** with **2-^{t}Bu** results in an approximately 1:1 mixture of **3-*cis*-^{t}Bu^{t}Bu** and **3-*trans*-^{t}Bu^{t}Bu** (i.e., $\Delta G^{\ddagger}_{\text{Bu}^t\text{Bu}} \approx 0.0$ kcal mol^{-1}). Consequently, the energy gap of around 1.0 ± 0.0 kcal mol^{-1} between the two diastereomeric transition states of the parent case vanishes due to the attachment of bulky *tert*-butyl groups.

To shed more light on the origin of the transition state stabilization, we dissected the $\Delta\Delta G^{\ddagger}_{R^1R^2}$ energy values by mutating all substituents separately. By comparing and applying this against energies of singly substituted reactions the interaction energy $\Delta\Delta G^{\ddagger}_{R^1R^2}$ can be dissected (Figure 5, top). $\Delta\Delta G^{\ddagger}_{R^1R^2}$ solely resembles the interaction energy between both alkyl groups R^1 and R^2, thereby disregarding the energy gain due to close $\sigma-\pi$ contacts. For this procedure[67,68] (termed a double mutant cycle, a practical application of Hess' law) we applied the following equation:

$$\Delta\Delta G^{\ddagger}_{R^1R^2} = \Delta G^{\ddagger}_{R^1R^2} - \Delta G^{\ddagger}_{R^1H} - \Delta G^{\ddagger}_{HR^2} + \Delta G^{\ddagger}_{HH} \quad (1)$$

The result provides an experimental estimate of the role DEDs play in the reaction of ylide and aldehyde. While all

https://doi.org/10.1021/acs.joc.6c00154
J. Org. Chem. 2026, 91, 4829−4841

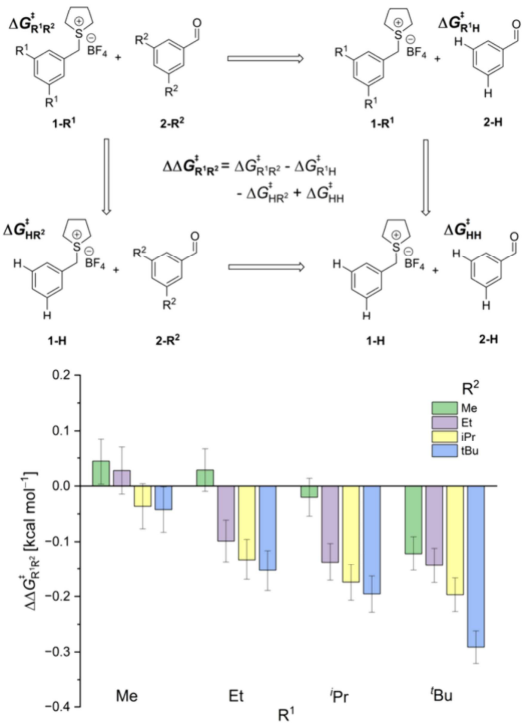


Figure 5. Double mutant cycle (top) and experimental results of the analysis (bottom). $\Delta\Delta G^{\ddagger}_{R^1R^2}$ illustrates the interaction energy between R^1 and R^2 in the reaction of **1-R¹** with **2-R²**. Negative energy values correspond to stabilizing interactions between R^1 and R^2. Gray lines indicate error bars.

combinations were measured for alkyl−alkyl interactions, the double mutant cycle could not be determined for halogen substituents since all-*meta* halogen-substituted tetrahydrothiophene salt **1-R¹** resulted only in **3-*trans*-R¹R²**. In contrast to the concept of steric repulsion, Figure 5 (bottom) qualitatively highlights the stabilizing effect (negative energy values) of each DED in the transition state of the reaction.

Apart from Me-Et combinations, all energy values are negative corresponding to stabilizing interactions between the alkyl substituents. While this effect is small for **1-Me** (leftmost block of columns), the stabilization increases with DED size, i.e., polarizability. Consequently, the largest effect can be observed for ^{t}Bu−^{t}Bu contacts ($\Delta\Delta G^{\ddagger}_{^t\mathrm{Bu}^t\mathrm{Bu}} = -0.3 \pm 0.1$ kcal mol^{-1}). By comparing the relative Gibbs free energy values $\Delta G^{\ddagger}_{R^1R^2\text{-HH}}$ (Figure 2) to the results of the double mutant cycle (Figure 5), the interaction energy between each DED can be dissected into $\sigma-\sigma$ interactions (between DEDs) and $\sigma-\pi$ interactions (between DED and phenyl system). Accordingly, the energy difference $\Delta G^{\ddagger}_{^t\mathrm{Bu}^t\mathrm{Bu-HH}} \approx -0.9 \pm 0.1$ kcal mol^{-1} for the reaction of **1-^{t}Bu** with **2-^{t}Bu** (Figure 2) contains stabilizing $\sigma-\sigma$ interactions of $\Delta\Delta G^{\ddagger}_{^t\mathrm{Bu}^t\mathrm{Bu}} = -0.3 \pm 0.1$ kcal mol^{-1} (Figure 5). Around 30% of the experimentally determined relative Gibbs free energies can be accounted for with LD attractive alkyl−alkyl contacts. The remaining 70% correspond to LD attractive $\sigma-\pi$ interactions. These results qualitatively fit to measurements performed for molecular balances in the ground state.[47]

Most recently, *N*,*N*-diphenylthiourea was shown to experience the same distribution of $\sigma-\sigma$ and $\sigma-\pi$ interactions to stabilize the most crowded *syn*,*syn* conformer.[47] Accordingly, the observations and values concerning the role of LD in molecular balances can be directly transferred to transition state stabilizations, but might we weaker due to the loosely bound nature of transition states.[18]

■ COMPUTATIONS

There have been previous computational studies on the Corey−Chaykovsky mechanism,[31−34] but to the best of our knowledge, none considered the effect of LD interactions on the rates and selectivity. The mechanism of the Corey−Chaykovsky reaction can, generally, be divided into three stages, according to Figure 6:

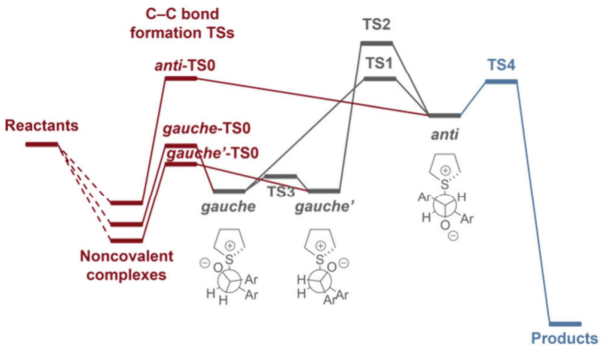


Figure 6. Schematic representation of the complete reaction profile for one of the possible anti configurations (leading to a *trans*-epoxide product).

1. **C−C bond formation:** This stage is shown in red in Figure 6. Formation of noncovalently bound complexes of the reactants, which then react to form the bond between the two carbon atoms (the SC−CO bond) leading to the betaines. The relative orientation of the oxygen and sulfur groups around the new C−C bond can be either *gauche* or *anti*. If irreversible, this step determines the stereochemistry of the epoxide product.
2. **Rotation around the C−C bond:** This stage is shown in black in Figure 6. Once one of the above-mentioned betaine rotamers is formed, rotation around the SC−CO bond can interconvert them. The *gauche* and *gauche′* rotamers are lower in energy than the *anti* rotamers, and interchange between the two possible *gauche* rotamers (via **TS3**) has a low barrier, so that they are in equilibrium with one another. The barriers to form the *anti* betaine (**TS1** and **TS2**) are higher in energy.
3. **Ring closing to form the epoxide:** This stage is shown in blue in Figure 6. Once the *anti*-betaine has formed via either of the two former stages, it can react further in an S_N2-type reaction to form the epoxide product.

A suggested route through a [2 + 2] cycloaddition to form a four-membered oxathietane, resembling the Wittig oxaphosphetane intermediate, that then directly forms the epoxide, was previously shown to be significantly higher in energy.[33] In our computations the oxathietanes were identified as nonstationary structures.

From the above, there are two possible routes for the formation of the *anti* betaine: (1) direct formation from the reactants (through *anti*-**TS0**) or (2) formation of either of the *gauche*/*gauche′* rotamers (through *gauche*-**TS0**/*gauche′*-**TS0**) and then conversion to the *anti* rotamer through **TS1** or **TS2**.

https://doi.org/10.1021/acs.joc.6c00154
J. Org. Chem. 2026, 91, 4829−4841

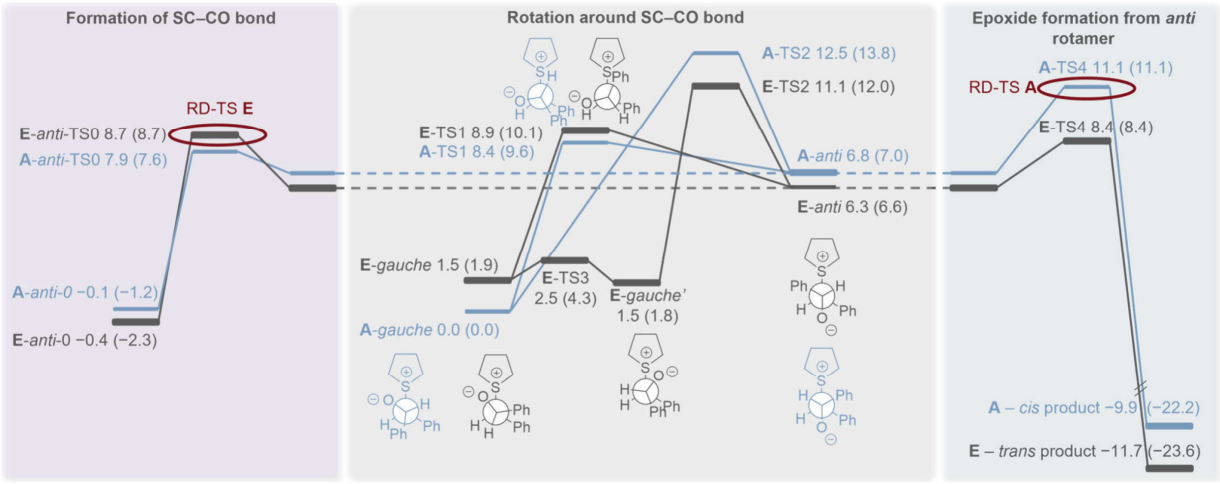


Figure 7. Energy diagram at the B3LYP-D3(BJ)/def2-TZVPP level of theory for the most stable pathways leading to each of the two products (**A** and **E**) for $R^1 = R^2 = H$, showing the ZPVE-corrected energies in kcal mol^{-1} (and free energies in parentheses).

Practically, this means that formation of the *anti* rotamer can happen through at least one of five possible pathways, represented by the TSs along the path: (a) *anti*-**TS0**; (b) *gauche*-**TS0**, **TS1**; (c) *gauche'*-**TS0**, **TS2**; (d) *gauche*-**TS0**, **TS3**, **TS2**; (e) *gauche'*-**TS0**, **TS3**, **TS1**.

In order to determine which of these five routes is preferred, we computed all intermediates and TSs using the B3LYP[69,70]/def2-TZVPP[71] level of theory, with Grimme's D3(BJ) dispersion correction[72,73] for unsubstituted Ph ($R^1 = R^2 = H$, Figure 7) and for the ^{t}Bu-substituted reactants ($R^1 = R^2 = {}^t$Bu, Figure 9). To match the experimental conditions, our computations included dichloromethane (DCM) as an implicit solvent, using the solvation model based on density (SMD).[74] All reported energies are ZPVE-corrected, unless stated otherwise. The highest TS for each of the five routes was found, and this was defined as the barrier value for this route. The pathway with the lowest barrier value will be the preferred one. This process was done for four possible conformers of each of the *anti*-betaines leading to the *cis*- and *trans*-epoxides (**A**–**H**, Figure 8)

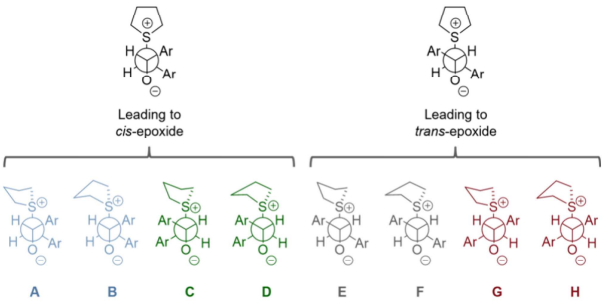


Figure 8. Newman projections of the computed *anti* rotamers at the B3LYP-D3(BJ)/def2-TZVPP level of theory.

After formation of the *anti* rotamer, the products can form via **TS4** (Figures 6 and 7). If **TS4** is higher in energy than the barrier value for formation of the *anti*-betaine, then the TS for epoxide formation will be the rate-determining TS (RD-TS), and all steps leading to it could be considered in quasi-equilibrium. If the barrier value for the *anti* rotamer formation is higher than **TS4**, then the TS associated with this barrier would be considered the RD-TS, and the formation of the *anti*-betaine could be considered irreversible.

After computing the pathways for **A**-**H** (for the full pathways see the SI), we found that for both derivatives ($R^1 = R^2 = H$ and $R^1 = R^2 = {}^t$Bu) the path with the lowest RD-TS leading to the *trans* product is **E**, while for the *cis* product the lowest RD-TS is in path **A**. The energy diagrams of pathways **A** and **E** are shown in Figures 7 and 9. Interestingly, for both derivatives, the RD-TS of path **E** is one of the TSs leading to the *anti*-betaine (**E-*anti*-TS0 for** $R^1 = R^2 = H$). However, for path **A** the epoxide formation (**TS4**) involves the RD-TS.

For $R^1 = R^2 = H$, the difference in ZPVE-corrected energy between the RD-TSs for paths **A** and **E** is 2.4 kcal mol^{-1} (and the difference in free energy is 2.4 kcal mol^{-1}), predicting a preference for the *trans* product, in agreement with the experiment.

For the ^{t}Bu-substituted reactants ($R^1 = R^2 = {}^t$Bu), for **A** the RD-TS is **TS4**, while **TS1** and ***anti*-TS0** are lower in energy and close to each other (Figure 9). For **E** the RD-TS is **TS1** (according to ZPVE-corrected energies, 0.8 kcal mol^{-1} below the **A** RD-TS) or ***anti*-TS0** (according to free energies, 0.5 kcal mol^{-1} below the **A** RD-TS), while **TS4** is lower in energy. These computations identify the ^{t}Bu-substituted reaction to show preference for the formation of the *trans* product, but this preference is much smaller than for the unsubstituted reaction, matching the experimental results.

Regarding the reversibility of the formation of the two epoxide products, for the *trans*-epoxide (pathway **E**), **E-*anti*-TS0** and **E-TS1** are somewhat higher in energy than **E-TS4**, meaning that the formation of the *anti*-betaine should be irreversible. For the *cis*-epoxide (pathway **A**), **TS4** is the highest TS (for $R^1 = R^2 = H$ and for $R^1 = R^2 = {}^t$Bu), and so only the epoxidation step is expected to be irreversible, while the steps leading to the *anti* rotamer are expected to be reversible. This matches the experimental results from previous studies and from the ring closure and crossover experiments shown above. A closer inspection of the RD-TSs can provide insight into the effects that influence their energies. To explore the effects of noncovalent interactions, we performed intramolecular symmetry-adapted perturbation theory (I-SAPT) analysis[75,76] using the SIAO1 partitioning algorithm.[77] I-SAPT

https://doi.org/10.1021/acs.joc.6c00154
J. Org. Chem. 2026, 91, 4829−4841

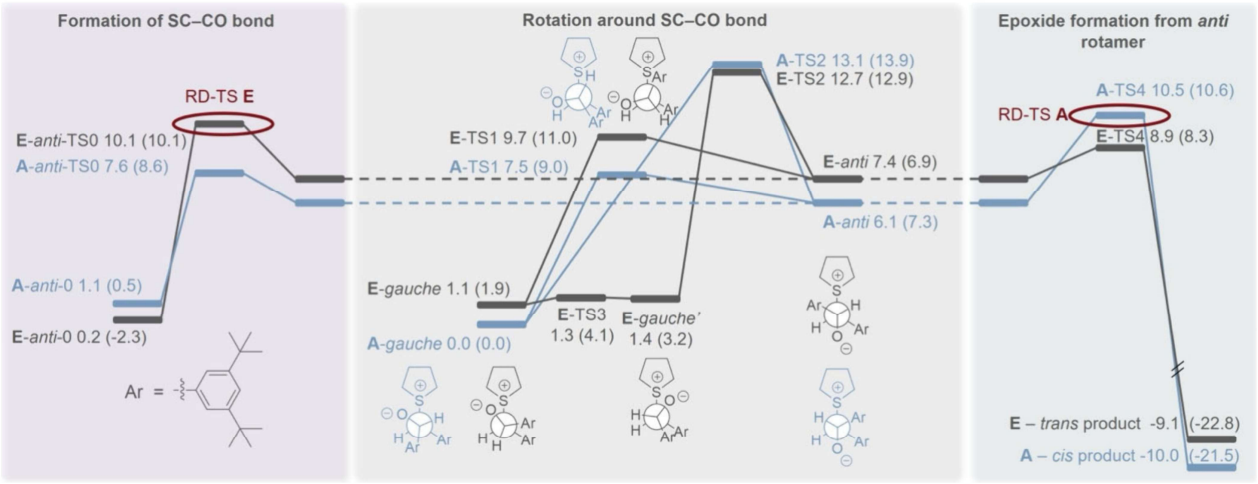


Figure 9. Energy diagram at the B3LYP-D3(BJ)/def2-TZVPP level of theory for the most stable pathways leading to each of the two products (**A** and **E**) for $R^1 = R^2 = {}^t$Bu, showing the ZPVE-corrected energies in kcal mol^{-1} (and free energies in parentheses). Two RD-TSs are shown here for pathway **E**: **E-*anti*-TS0** (RD-TS according to free energies) and **E-TS1** (according to free energies).

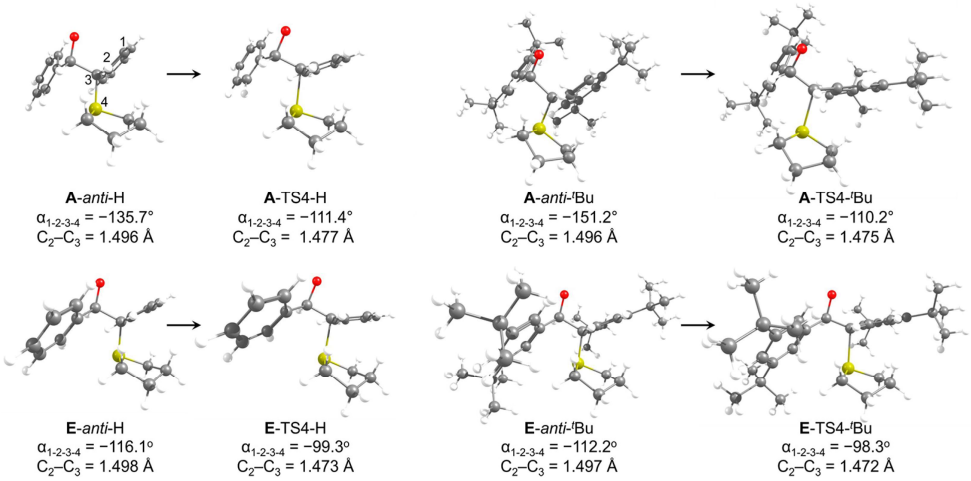


Figure 10. Changes in orientation of the aromatic rings going from the *anti* rotamer to **TS4**. See the diagram at the top left for atom numbering.

is a method for decomposition of the intramolecular interaction energies between two parts of the same molecule that are connected by a linker. The interaction can be decomposed into basic contributions: electrostatic, exchange (repulsion), induction, and dispersion. We chose the SIAO1 partitioning method, as it can mitigate the effects of artificial dipole moments (such as an unphysically large electrostatic repulsion), produced by previous partitioning algorithms. The analysis was performed on the interaction between the two aromatic rings (including R groups), while the two sp^3 carbons, the oxygen and sulfur groups, where defined as the linker. The changes in the orientation of the aromatic rings are shown in Figure 10, and the energies are presented in Figure 11.

First, looking at the epoxidation TS (Figures 7 and 9), we observe that for both $R^1 = R^2 = t$Bu and for $R^1 = R^2 =$ H, **TS4** is lower for pathway **E** than for pathway **A**. The structures of **TS4** in Figure 10 show that the aromatic ring on the sulfur-bound carbon rotates during the reaction (the ring becomes more perpendicular to the C–S bond, such that $\alpha_{1-2-3-4}$ becomes closer to −90° upon formation of **TS4**; for more structural data, see the SI). This rotation allows for a better conjugation between the π system and the orbitals that participate in the S_N2-type reaction (as evidenced by the shortening of the C_2–C_3 bond in **TS4**, and from the LUMO and HOMO−4 orbitals in Figure S8). However, this geometric change is expected to weaken LD interactions, as the two aromatic rings are no longer oriented parallel to one another. Comparing all the **E** species in Figure 10 to the analogous **A** species, we can see that $\alpha_{1-2-3-4}$ is closer to −90 ° in all **E** species, which is expected to result in better orbital overlap (and a shorter C_2–C_3 bond) and explains the increased stabilization of **TS4** in the **E** pathway. In addition, the change in angle going from **E-*anti*** to **E-TS4** is smaller than the change from **A-*anti*** to **A-TS4**, contributing also to the smaller barrier along the **E** pathway. Another interesting point we can learn from the structures shown in Figure 10 is that in **A-TS4-^{t}Bu** the R^1 groups are directed toward the aldehyde aromatic ring in a geometry that facilitates σ–π interactions, while the R^2 groups point outward relative to the sulfide aromatic ring and are expected to have mainly σ–σ interactions with the R^1

https://doi.org/10.1021/acs.joc.6c00154
J. Org. Chem. 2026, 91, 4829−4841

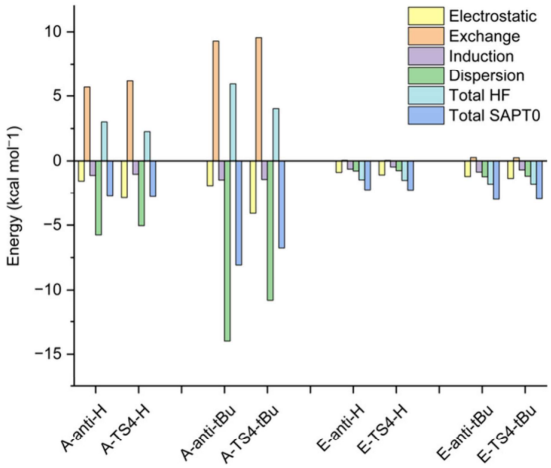


Figure 11. Results of the I-SAPT analysis at the DF-SAPT0 aug-cc-pVTZ level of theory between the two aromatic rings in the *anti*-betaine and in **TS4** of pathways **A** and **E**.

groups (for the larger R^1 groups) and no $\sigma-\pi$ interactions with the sulfide aromatic ring. As a result, we would expect the R^1 groups to have a more significant LD-based effect (relative to R^2) of stabilizing **A-TS4** and increasing the amounts of the *cis*-epoxide product. Further, when R^1 = H we would expect relatively weak LD interactions between the aromatic groups, even with large R^2 substituents, close to the interactions for $R^1 = R^2$ = H.

This matches and explains the experimental results in Figure 2, which show indeed that the effect of R^2 on increasing the amount of *cis* product is smaller than the effect of R^1, and is negligible when R^1 = H. In addition, the geometry of **A-TS4** suggests that if there were halogens at the R^2 position, they would not interact significantly with the smaller R^1 groups (H and Me) in this TS, and the main interactions in this case would be C−H(R^1)···π interactions. Such interactions would be less stabilizing for π-systems with more electron-withdrawing halogens, explaining their higher preference for the *trans* product in Figure 3.

Figure 11 shows the I-SAPT analyses for the *anti*-betaine and **TS4** for pathways **A** and **E**. The total interaction energies between the two aromatic rings in **E-*anti*** and **E-TS4** are very small (up to only 3 kcal mol^{-1}) both for $R^1 = R^2 = {}^t$Bu and for $R^1 = R^2$ = H, and there is no significant difference between the interaction energies in **E-*anti*** and **E-TS4**. This is to be expected, as the aromatic groups are far away from one another in these **E** species.

However, going from **E** to **A**, the individual parts of the interaction become much larger, and the most significant contributions are from exchange and dispersion. Again, this is to be expected, as the aromatic groups are close to one another and have no significant electron donating/withdrawing groups. For all **A** species shown on the graph, except for **A-TS4**-H, the dispersion stabilization is larger than the exchange destabilization, and this difference is especially large for **A-*anti*-^{t}Bu** (more than 4 kcal mol^{-1}). Comparing **A-*anti*** with **A-TS4**, for both R groups the dispersion contribution is more stabilizing in **A-*anti*** than in **TS4**. The exchange repulsion increases somewhat when going from **A-*anti*** to **A-TS4**.

All of these observations regarding **A**, support the suggestion presented above, that the rotation of one aromatic ring in **A-TS4** disrupts some of the dispersion attraction between the rings. This results in a decrease in total interaction energy between the rings when going from **A-*anti*-^{t}Bu** to **A-TS4-^{t}Bu**. For **A-*anti*-H** and **A-TS4-H** the total interaction energy is almost the same, because of the increase in electrostatic interaction in **TS4**, possibly from Ar−H···π interactions. As a result of the decrease in total interaction energy for **A-TS4-^{t}Bu** but not for **A-TS4-H**, we would expect the energy barrier for the epoxidation step to be larger for $R^1 = R^2 = {}^t$Bu than for $R^1 = R^2$ = H. This is indeed the case, but the difference is very small (4.40 for ^{t}Bu, 4.29 for H).

In general, the total interaction energies in **A-*anti*-H**, **A-TS4-H**, **E-*anti*-H**, **E-TS4-H**, **E-*anti*-^{t}Bu**, and **E-TS4-^{t}Bu** are very similar and small (all between 2 and 3 kcal mol^{-1}). For **A-*anti*-^{t}Bu** and **A-TS4-^{t}Bu**, the total interaction energies become larger (more stabilizing), because of LD from the bulky groups. So, when comparing the epoxidation-step PESs of pathways **A** and **E**, even though **E-TS4** is lower in energy than **A-TS4**, we expect the energy difference between **A-TS4-^{t}Bu** and **E-TS4-^{t}Bu** to be smaller than that between **A-TS4-H** and **E-TS4-H**. This can be observed in Figures 7 and 9, along with the fact that **A-*anti*-H** is higher in energy than **E-*anti*-H** while **A-*anti*-^{t}Bu** is more stable than **E-*anti*-^{t}Bu** due to these interactions. Note, however, that there are additional interactions that can affect the energies, such as LD interactions between the aromatic rings (especially the aldehyde aromatic ring) and the sulfonium five-membered ring (see Figure S9).

Regarding the two mechanisms for formation of the *anti* betaine, either directly from the complex via **TS0** or from the gauche rotamer via **TS1**, both of these TSs, **TS0** and **TS1**, are lower in energy for pathway **A** relative to **E** (for both $R^1 = R^2$ = H and $R^1 = R^2 = {}^t$Bu), even though the aromatic rings are closer to one another for both TSs on **A**. But the difference in energy between the pathways is significantly larger for $R^1 = R^2 = {}^t$Bu, indicating that also here the **A** PES is lowered in energy relative to the **E** PES when going to the bulkier R groups. This is again a result of LD interactions, as evidenced by I-SAPT analysis (Figures 12 and 13).

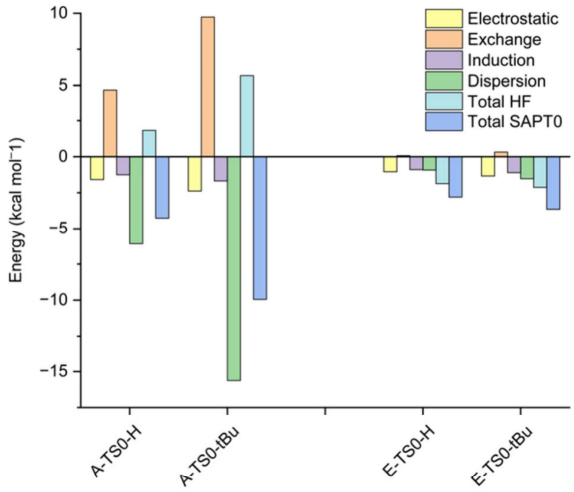


Figure 12. Results of the I-SAPT analysis at the DF-SAPT0 aug-cc-pVTZ level of theory between the two aromatic rings in **TS0** of pathways **A** and **E**.

https://doi.org/10.1021/acs.joc.6c00154
J. Org. Chem. 2026, 91, 4829−4841

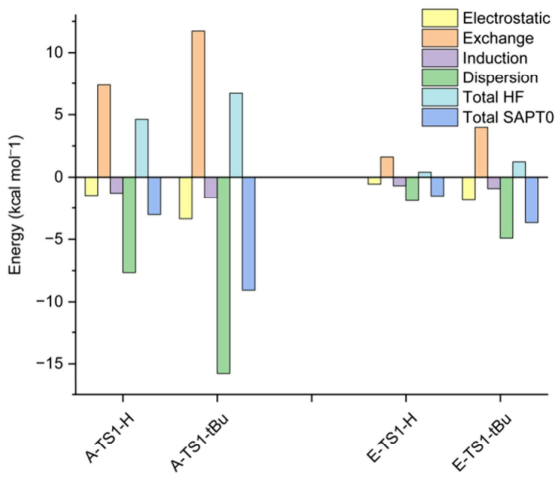


Figure 13. Results of the I-SAPT analysis at the DF-SAPT0 aug-cc-pVTZ level of theory between the two aromatic rings in **TS1** of pathways **A** and **E**.

It can be seen that for **E-TS0** (Figure 12) and **E-TS1** (Figure 13), the interactions between the two rings are weak for both R groups. The total interactions in **A-TS0-H** and **A-TS1-H** are also weak and close in magnitude to those in the **E** species. The total interaction in **A-TS0-H** and **A-TS1-H** is small even though the LD stabilization is larger than in **E**, because the repulsion is also larger. However, in **A-TS0-^{t}Bu** and **A-TS1-^{t}Bu** LD is more significant, and the exchange part is smaller than the LD part, causing the total interaction energy to be more stabilizing, and thus lowering the energies of **A-TS0-^{t}Bu** and **A-TS1-^{t}Bu** relative to the energies of **E-TS0-^{t}Bu** and **E-TS1-^{t}Bu**, more than for $R^1 = R^2 = H$. This matches the energy profiles in Figures 7 and 9. Note that in all the species shown in Figure 12 and 13, the LD stabilization outweighs the exchange destabilization, indicating that we are at the attractive region of the van der Waals potential. In this region, larger groups are expected to be mainly a source of stabilization via LD and not primarily a source of steric repulsion.

CONCLUSIONS

This study underscores the pivotal role of London dispersion (LD) interactions in influencing the *cis*/*trans* diastereoselectivity of the Johnson−Corey−Chaykovsky (JCC) epoxidation. While traditional views attribute diastereoselectivity to steric repulsion, our findings reveal that LD interactions preferentially stabilize transition states, favoring the *cis* product in the presence of bulky (highy polarizable) dispersion energy donors (DEDs).

Through NMR spectroscopy, we demonstrate that larger DEDs stabilize crowded transition states with little steric penalties, with *tert*-butyl substituents showing the strongest shift toward the *cis*-products with $\Delta G^{\ddagger}_{^t\mathrm{Bu}/^t\mathrm{Bu}\text{-HH}} \approx -0.9 \pm 0.1$ kcal mol^{-1} for the reaction of **1-^{t}Bu** with **2-^{t}Bu**. In addition, we confirmed the potential of halogens to act as DEDs when interacting with alkyl groups. Crossover and ring-closure experiments confirm the reversible formation of *syn*-betaine intermediates, further highlighting the contribution of noncovalent interactions to the reaction pathway.

Computational studies using dispersion-corrected DFT provided deeper insights into the molecular interactions driving these trends. The reaction pathway was mapped for various substituents, revealing that LD interactions stabilize crowded betaine and epoxide-forming transition states. I-SAPT analyses demonstrate that with bulky DEDs like *tert*-butyl groups, dispersion outweighs repulsion, resulting in preferential net stabilization.

By demonstrating that LD interactions, rather than steric repulsion, govern transition state stabilizations in the JCC reaction, this work challenges conventional steric models and provides a deeper understanding of the role of noncovalent interactions in stereoselective organic synthesis. Additionally, our study demonstrates, for the first time, that halogen substituents can serve as dispersion energy donors in this reaction context. In contrast to alkyl substituents, halogenation provides a synthetically practical means to modulate stereoselectivity while retaining the potential for further functionalization. This represents a new and potentially useful strategy for reaction design.

ASSOCIATED CONTENT

Data Availability Statement

The data underlying this study are available in the published article and its Supporting Information.

Supporting Information

The Supporting Information is available free of charge at https://pubs.acs.org/doi/10.1021/acs.joc.6c00154.

Experimental details, compound characterization, analytical data, and computational details (PDF)

AUTHOR INFORMATION

Corresponding Authors

Peter R. Schreiner − *Institute of Organic Chemistry, Justus Liebig University, 35392 Giessen, Germany;* orcid.org/0000-0002-3608-5515; Email: prs@uni-giessen.de

Ephrath Solel − *EaStCHEM School of Chemistry, University of Edinburgh, Edinburgh EH9 3FJ, United Kingdom;* orcid.org/0000-0002-0513-8995; Email: Ephrath.Solel@ed.ac.uk

Authors

Marvin H. J. Domanski − *Institute of Organic Chemistry, Justus Liebig University, 35392 Giessen, Germany;* orcid.org/0000-0002-1934-5223

Lars Rummel − *Institute of Organic Chemistry, Justus Liebig University, 35392 Giessen, Germany;* orcid.org/0000-0002-3772-2109

Saskia N. Krug − *Institute of Organic Chemistry, Justus Liebig University, 35392 Giessen, Germany*

Heike Hausmann − *Institute of Organic Chemistry, Justus Liebig University, 35392 Giessen, Germany;* orcid.org/0000-0003-0347-9064

Complete contact information is available at: https://pubs.acs.org/10.1021/acs.joc.6c00154

Notes

The authors declare no competing financial interest.

ACKNOWLEDGMENTS

We thank Salome Wagner, Valeria Malynych, and Anna Shurando for synthetic support and Bastian Bernhardt, Finn M. Wilming, Jan M. Schümann, Henrik F. König, and Madison

J. Sowden for fruitful discussions. This work was supported by the Deutsche Forschungsgemeinschaft.

REFERENCES

(1) Cowdrey, W. A.; Hughes, E. D.; Ingold, C. K.; Masterman, S.; Scott, A. D., 257 Reaction kinetics and the Walden inversion. Part VI. Relation of steric orientation to mechanism in substitutions involving halogen atoms and simple or substituted hydroxyl groups. *J. Chem. Soc.* **1937**, 1252−1271.
(2) Kozuch, S.; Shaik, S. How to Conceptualize Catalytic Cycles? The Energetic Span Model. *Acc. Chem. Res.* **2011**, *44* (2), 101−110.
(3) Illa, O.; Namutebi, M.; Saha, C.; Ostovar, M.; Chen, C. C.; Haddow, M. F.; Nocquet-Thibault, S.; Lusi, M.; McGarrigle, E. M.; Aggarwal, V. K. Practical and Highly Selective Sulfur Ylide-Mediated Asymmetric Epoxidations and Aziridinations Using a Cheap and Readily Available Chiral Sulfide: Extensive Studies To Map Out Scope, Limitations, and Rationalization of Diastereo- and Enantioselectivities. *J. Am. Chem. Soc.* **2013**, *135* (32), 11951−11966.
(4) Wagner, J. P.; Schreiner, P. R. London Dispersion in Molecular Chemistry—Reconsidering Steric Effects. *Angew. Chem. Int. Ed.* **2015**, *54* (42), 12274−12296.
(5) Rummel, L. *Following London's Footsteps - Implications for Structure and Reactivity*. Doctoral Thesis, Justus-Liebig-University, Gießen, Germany, 2023.
(6) Rummel, L.; Schreiner, P. R. Advances and Prospects in Understanding London Dispersion Interactions in Molecular Chemistry. *Angew. Chem. Int. Ed.* **2024**, *63* (12), e202316364.
(7) Lu, G.; Liu, R. Y.; Yang, Y.; Fang, C.; Lambrecht, D. S.; Buchwald, S. L.; Liu, P. Ligand−Substrate Dispersion Facilitates the Copper-Catalyzed Hydroamination of Unactivated Olefins. *J. Am. Chem. Soc.* **2017**, *139* (46), 16548−16555.
(8) Singha, S.; Buchsteiner, M.; Bistoni, G.; Goddard, R.; Fürstner, A. A New Ligand Design Based on London Dispersion Empowers Chiral Bismuth−Rhodium Paddlewheel Catalysts. *J. Am. Chem. Soc.* **2021**, *143* (15), 5666−5673.
(9) Buchsteiner, M.; Singha, S.; Decaens, J.; Fürstner, A. Chiral Bismuth-Rhodium Paddlewheel Complexes Empowered by London Dispersion: The C−H Functionalization Nexus. *Angew. Chem. Int. Ed.* **2022**, *61* (45), e202212546.
(10) Gramüller, J.; Franta, M.; Gschwind, R. M. Tilting the Balance: London Dispersion Systematically Enhances Enantioselectivities in Brønsted Acid Catalyzed Transfer Hydrogenation of Imines. *J. Am. Chem. Soc.* **2022**, *144* (43), 19861−19871.
(11) Eschmann, C.; Song, L.; Schreiner, P. R. London Dispersion Interactions Rather than Steric Hindrance Determine the Enantioselectivity of the Corey−Bakshi−Shibata Reduction. *Angew. Chem. Int. Ed.* **2021**, *60* (9), 4823−4832.
(12) Thomas, A. A.; Speck, K.; Kevlishvili, I.; Lu, Z.; Liu, P.; Buchwald, S. L. Mechanistically Guided Design of Ligands That Significantly Improve the Efficiency of CuH-Catalyzed Hydroamination Reactions. *J. Am. Chem. Soc.* **2018**, *140* (42), 13976−13984.
(13) Xi, Y.; Su, B.; Qi, X.; Pedram, S.; Liu, P.; Hartwig, J. F. Application of Trimethylgermanyl-Substituted Bisphosphine Ligands with Enhanced Dispersion Interactions to Copper-Catalyzed Hydroboration of Disubstituted Alkenes. *J. Am. Chem. Soc.* **2020**, *142* (42), 18213−18222.
(14) London, F. Zur Theorie und Systematik der Molekularkräfte. *Z. Phys.* **1930**, *63* (3−4), 245−279.
(15) London, F. The General Theory of Molecular Forces. *Trans. Faraday Soc.* **1937**, *33*, 8b−26.
(16) Domanski, M. H. J.; Fuhrmann, M.; Schreiner, P. R. London Dispersion as a Design Element in Molecular Catalysis. *J. Am. Chem. Soc.* **2025**, *147* (33), 29611−29623.
(17) Grimme, S.; Huenerbein, R.; Ehrlich, S. On the Importance of the Dispersion Energy for the Thermodynamic Stability of Molecules. *ChemPhysChem* **2011**, *12* (7), 1258−1261.
(18) Strauss, M. A.; Wegner, H. A. Molecular Systems for the Quantification of London Dispersion Interactions. *Eur. J. Org. Chem.* **2019**, *2-3*, 295−302.
(19) Elmi, A.; Cockroft, S. L. Quantifying Interactions and Solvent Effects Using Molecular Balances and Model Complexes. *Acc. Chem. Res.* **2021**, *54* (1), 92−103.
(20) Johnson, A. W.; LaCount, R. 9-Dimethylsulfonium fluorenylide. *Chem. Ind.* **1958**, 1440−1441.
(21) Johnson, A. W.; LaCount, R. B. The Chemistry of Ylids. VI. Dimethylsulfonium Fluorenylide—A Synthesis of Epoxides1. *J. Am. Chem. Soc.* **1961**, *83* (2), 417−423.
(22) Corey, E. J.; Chaykovsky, M. Dimethylsulfonium methylide, a reagent for selective oxirane synthesis from aldehydes and ketones. *J. Am. Chem. Soc.* **1962**, *84* (19), 3782−3783.
(23) Corey, E. J.; Chaykovsky, M. Dimethyloxosulfonium Methylide ($(CH_3)_2SOCH_2$) and Dimethylsulfonium Methylide ($(CH_3)_2SCH_2$). Formation and Application to Organic Synthesis. *J. Am. Chem. Soc.* **1965**, *87* (6), 1353−1364.
(24) Aggarwal, V. K.; Alonso, E.; Fang, G.; Ferrara, M.; Hynd, G.; Porcelloni, M. Application of Chiral Sulfides to Catalytic Asymmetric Aziridination and Cyclopropanation with In Situ Generation of the Diazo Compound. *Angew. Chem. Int. Ed.* **2001**, *40* (8), 1433−1436.
(25) Shorokhov, V. V.; Chabuka, B. K.; Nikolaeva, A. A.; Zhokhov, S. S.; Andreev, I. A.; Ratmanova, N. K.; Trushkov, I. V.; Ivanova, O. A.; Alabugin, I. V. New mode of sulfur ylides reactivity: stereoelectronic control provides C−C bond insertion before cyclopropanation/epoxidation directly affording homologated three-membered rings. *Org. Chem. Front.* **2025**, *12* (24), 6852−6863.
(26) Aggarwal, V. K.; Alonso, E.; Hynd, G.; Lydon, K. M.; Palmer, M. J.; Porcelloni, M.; Studley, J. R. Catalytic Asymmetric Synthesis of Epoxides from Aldehydes Using Sulfur Ylides with In Situ Generation of Diazocompounds. *Angew. Chem. Int. Ed.* **2001**, *40* (8), 1430−1433.
(27) Aggarwal, V. K.; Richardson, J. The complexity of catalysis: origins of enantio- and diastereocontrol in sulfur ylide mediated epoxidation reactions. *Chem. Commun.* **2003**, No. 21, 2644−2651.
(28) Aggarwal, V. K.; Winn, C. L. Catalytic, Asymmetric Sulfur Ylide-Mediated Epoxidation of Carbonyl Compounds: Scope, Selectivity, and Applications in Synthesis. *Acc. Chem. Res.* **2004**, *37* (8), 611−620.
(29) Aggarwal, V. K.; Hebach, C. Carboxylate-stabilised sulfur ylides (thetin salts) in asymmetric epoxidation for the synthesis of glycidic acids. Mechanism and implications. *Org. Biomol. Chem.* **2005**, *3* (8), 1419−1427.
(30) Aggarwal, V. K.; Charmant, J. P. H.; Fuentes, D.; Harvey, J. N.; Hynd, G.; Ohara, D.; Picoul, W.; Robiette, R.; Smith, C.; Vasse, J.-L.; et al. Highly Enantioselective Synthesis of Glycidic Amides Using Camphor-Derived Sulfonium Salts. Mechanism and Applications in Synthesis. *J. Am. Chem. Soc.* **2006**, *128* (6), 2105−2114.
(31) Volatron, F.; Eisenstein, O. Theoretical study of the reactivity of phosphonium and sulfonium ylides with carbonyl groups. *J. Am. Chem. Soc.* **1984**, *106* (20), 6117−6119.
(32) Volatron, F.; Eisenstein, O. Wittig versus Corey-Chaykovsky Reaction. Theoretical study of the reactivity of phosphonium methylide and sulfonium methylide with formaldehyde. *J. Am. Chem. Soc.* **1987**, *109* (1), 1−14.
(33) Lindvall, M. K.; Koskinen, A. M. P. Origins of Stereoselectivity in the Corey−Chaykovsky Reaction. Insights from Quantum Chemistry. *J. Org. Chem.* **1999**, *64* (13), 4596−4606.
(34) Aggarwal, V. K.; Harvey, J. N.; Richardson, J. Unraveling the Mechanism of Epoxide Formation from Sulfur Ylides and Aldehydes. *J. Am. Chem. Soc.* **2002**, *124* (20), 5747−5756.
(35) Edwards, D. R.; Montoya-Peleaz, P.; Crudden, C. M. Experimental Investigation into the Mechanism of the Epoxidation of Aldehydes with Sulfur Ylides. *Org. Lett.* **2007**, *9* (26), 5481−5484.
(36) Edwards, D. R.; Du, J.; Crudden, C. M. Experimental Demonstration of Base-Catalyzed Interconversion of Isomeric Betaine Intermediates in the Corey−Chaykovsky Epoxidation. *Org. Lett.* **2007**, *9* (12), 2397−2400.

https://doi.org/10.1021/acs.joc.6c00154
J. Org. Chem. 2026, 91, 4829−4841

(37) Jadhav, P. D.; Lu, X.; Liu, R.-S. Gold-Catalyzed [5 + 2]- and [5 + 1]-Annulations between Ynamides and 1,2-Benzisoxazoles with Ligand-Controlled Chemoselectivity. *ACS Catal.* **2018**, *8* (10), 9697−9701.
(38) Annunziata, R.; Benaglia, M.; Cinquini, M.; Cozzi, F.; Tocco, G. A Poly(ethylene glycol)-Supported Quaternary Ammonium Salt: An Efficient, Recoverable, and Recyclable Phase-Transfer Catalyst. *Org. Lett.* **2000**, *2* (12), 1737−1739.
(39) Mohanty, A. D.; Bae, C. Mechanistic analysis of ammonium cation stability for alkaline exchange membrane fuel cells. *J. Mater. Chem. A* **2014**, *2* (41), 17314−17320.
(40) Krief, A.; Swinnen, D.; Billen, D. Stereocontrolled synthesis of [3.1.0]bicyclohexanones by cyclopropanation of enones with benzylidene sulfuranes. *Tetrahedron Lett.* **2002**, *43* (33), 5871−5873.
(41) Li, F.; Yang, S. I.; Ciringh, Y.; Seth, J.; Martin, C. H.; Singh, D. L.; Kim, D.; Birge, R. R.; Bocian, D. F.; Holten, D.; et al. Design, Synthesis, and Photodynamics of Light-Harvesting Arrays Comprised of a Porphyrin and One, Two, or Eight Boron-Dipyrrin Accessory Pigments. *J. Am. Chem. Soc.* **1998**, *120* (39), 10001−10017.
(42) Hwang, J.; Li, P.; Carroll, W. R.; Smith, M. D.; Pellechia, P. J.; Shimizu, K. D. Additivity of Substituent Effects in Aromatic Stacking Interactions. *J. Am. Chem. Soc.* **2014**, *136* (40), 14060−14067.
(43) Schweighauser, L.; Strauss, M. A.; Bellotto, S.; Wegner, H. A. Attraction or Repulsion? London Dispersion Forces Control Azobenzene Switches. *Angew. Chem. Int. Ed.* **2015**, *54* (45), 13436−13439.
(44) Hwang, J.; Li, P.; Smith, M. D.; Shimizu, K. D. Distance-Dependent Attractive and Repulsive Interactions of Bulky Alkyl Groups. *Angew. Chem. Int. Ed.* **2016**, *55* (28), 8086−8089.
(45) Schümann, J. M.; Wagner, J. P.; Eckhardt, A. K.; Quanz, H.; Schreiner, P. R. Intramolecular London Dispersion Interactions Do Not Cancel in Solution. *J. Am. Chem. Soc.* **2021**, *143* (1), 41−45.
(46) Solel, E.; Ruth, M.; Schreiner, P. R. London Dispersion Helps Refine Steric A-Values: Dispersion Energy Donor Scales. *J. Am. Chem. Soc.* **2021**, *143* (49), 20837−20848.
(47) Rummel, L.; Domanski, M. H. J.; Hausmann, H.; Becker, J.; Schreiner, P. R. London Dispersion Favors Sterically Hindered Diarylthiourea Conformers in Solution. *Angew. Chem. Int. Ed.* **2022**, *61* (29), e202204393.
(48) Liu, T.; Schneider, H.-J. Additivity and Quantification of Dispersive Interactions—from Cyclopropyl to Nitro Groups: Measurements on Porphyrin Derivatives. *Angew. Chem. Int. Ed.* **2002**, *41* (8), 1368−1370.
(49) Swierczynski, D.; Luboradzki, R.; Dolgonos, G.; Lipkowski, J.; Schneider, H.-J. Non-Covalent Interactions of Organic Halogen Compounds with Aromatic Systems − Analyses of Crystal Structure Data. *Eur. J. Org. Chem.* **2005**, *6*, 1172−1177.
(50) Riley, K. E.; Hobza, P. Investigations into the Nature of Halogen Bonding Including Symmetry Adapted Perturbation Theory Analyses. *J. Chem. Theory Comput.* **2008**, *4* (2), 232−242.
(51) Mayerhöffer, U.; Würthner, F. Halogen−Arene Interactions Assist in Self-Assembly of Dyes. *Angew. Chem. Int. Ed.* **2012**, *51* (23), 5615−5619.
(52) Riley, K. E.; Murray, J. S.; Fanfrlík, J.; Řezáč, J.; Solá, R. J.; Concha, M. C.; Ramos, F. M.; Politzer, P. Halogen bond tunability II: the varying roles of electrostatic and dispersion contributions to attraction in halogen bonds. *J. Mol. Model.* **2013**, *19* (11), 4651−4659.
(53) Riley, K. E.; Hobza, P. The relative roles of electrostatics and dispersion in the stabilization of halogen bonds. *Phys. Chem. Chem. Phys.* **2013**, *15* (41), 17742−17751.
(54) Schneider, H.-J. Dispersive Interactions in Solution Complexes. *Acc. Chem. Res.* **2015**, *48* (7), 1815−1822.
(55) Varadwaj, A.; Marques, H. M.; Varadwaj, P. R. Is the Fluorine in Molecules Dispersive? Is Molecular Electrostatic Potential a Valid Property to Explore Fluorine-Centered Non-Covalent Interactions? *Molecules* **2019**, *24* (3), 379.
(56) Solel, E.; Ruth, M.; Schreiner, P. R. London Dispersion Helps Refine Steric A-Values: The Halogens. *J. Org. Chem.* **2021**, *86* (11), 7701−7713.
(57) Aggarwal, V. K.; Calamai, S.; Ford, J. G. Additions of benzylsulfonium ylides to aldehydes and ketones: are they under kinetic or thermodynamic control? *J. Chem. Soc., Perkin Trans. 1* **1997**, No. 5, 593−600.
(58) Park, K.; Bae, G.; Moon, J.; Choe, J.; Song, K. H.; Lee, S. Synthesis of Symmetrical and Unsymmetrical Diarylalkynes from Propiolic Acid Using Palladium-Catalyzed Decarboxylative Coupling. *J. Org. Chem.* **2010**, *75* (18), 6244−6251.
(59) Yoshimine, M.; Hatch, M. J. Mechanism of the reaction of aqueous benzyldimethylsulfonium chloride and formaldehyde with sodium hydroxide. *J. Am. Chem. Soc.* **1967**, *89* (23), 5831−5838.
(60) Aggarwal, V. K.; Charmant, J. P. H.; Ciampi, C.; Hornby, J. M.; O'Brien, C. J.; Hynd, G.; Parsons, R. Additions of stabilised and semi-stabilised sulfur ylides to tosyl protected imines: are they under kinetic or thermodynamic control? *J. Chem. Soc., Perkin Trans.* **2001**, *1* (23), 3159−3166.
(61) Stein, M.; Winter, W.; Rieker, A. Hexakis(2,6-di-*tert*-butyl-4-biphenylyl)ethane—The First Unbridged Hexaarylethane. *Angew. Chem. Int. Ed.* **1978**, *17* (9), 692−694.
(62) Kahr, B.; Van Engen, D.; Mislow, K. Length of the ethane bond in hexaphenylethane and its derivatives. *J. Am. Chem. Soc.* **1986**, *108* (26), 8305−8307.
(63) Rösel, S.; Balestrieri, C.; Schreiner, P. R. Sizing the role of London dispersion in the dissociation of all-meta *tert*-butyl hexaphenylethane. *Chem. Sci.* **2017**, *8* (1), 405−410.
(64) Rösel, S.; Becker, J.; Allen, W. D.; Schreiner, P. R. Probing the Delicate Balance between Pauli Repulsion and London Dispersion with Triphenylmethyl Derivatives. *J. Am. Chem. Soc.* **2018**, *140* (43), 14421−14432.
(65) Rummel, L.; Schümann, J. M.; Schreiner, P. R. Hexaphenylditetrels − When Longer Bonds Provide Higher Stability. *Chem.—Eur. J.* **2021**, *27* (55), 13699−13702.
(66) Rösel, S.; Schreiner, P. R. Computational Chemistry as a Conceptual Game Changer: Understanding the Role of London Dispersion in Hexaphenylethane Derivatives (Gomberg Systems). *Isr. J. Chem.* **2022**, *62* (1−2), e202200002.
(67) Carter, P. J.; Winter, G.; Wilkinson, A. J.; Fersht, A. R. The use of double mutants to detect structural changes in the active site of the tyrosyl-tRNA synthetase (*Bacillus stearothermophilus*). *Cell* **1984**, *38* (3), 835−840.
(68) Adams, H.; Carver, F. J.; Hunter, C. A.; Morales, J. C.; Seward, E. M. Chemical double-mutant cycles for the measurement of weak intermolecular interactions: Edge-to-face aromatic interactions. *Angew. Chem. Int. Ed. Engl.* **1996**, *35* (13−14), 1542−1544.
(69) Becke, A. D. Density-functional thermochemistry. III. The role of exact exchange. *J. Chem. Phys.* **1993**, *98* (7), 5648−5652.
(70) Lee, C.; Yang, W.; Parr, R. G. Development of the Colle-Salvetti correlation-energy formula into a functional of the electron density. *Phys. Rev. B: Condens. Matter Mater. Phys.* **1988**, *37* (2), 785−789.
(71) Weigend, F.; Ahlrichs, R. Balanced basis sets of split valence, triple zeta valence and quadruple zeta valence quality for H to Rn: Design and assessment of accuracy. *Phys. Chem. Chem. Phys.* **2005**, *7* (18), 3297−3305.
(72) Grimme, S.; Antony, J.; Ehrlich, S.; Krieg, H. A consistent and accurate ab initio parametrization of density functional dispersion correction (DFT-D) for the 94 elements H-Pu. *J. Chem. Phys.* **2010**, *132* (15), 154104.
(73) Grimme, S.; Ehrlich, S.; Goerigk, L. Effect of the damping function in dispersion corrected density functional theory. *J. Comput. Chem.* **2011**, *32* (7), 1456−1465.
(74) Marenich, A. V.; Cramer, C. J.; Truhlar, D. G. Universal solvation model based on solute electron density and on a continuum model of the solvent defined by the bulk dielectric constant and atomic surface tensions. *J. Phys. Chem. B* **2009**, *113* (18), 6378−6396.
(75) Parrish, R. M.; Gonthier, J. F.; Corminboeuf, C.; Sherrill, C. D. Communication: Practical intramolecular symmetry adapted perturbation theory via Hartree-Fock embedding. *J. Chem. Phys.* **2015**, *143* (5), 051103.

https://doi.org/10.1021/acs.joc.6c00154
J. Org. Chem. 2026, 91, 4829−4841

(76) Pastorczak, E.; Prlj, A.; Gonthier, J. F.; Corminboeuf, C. Intramolecular symmetry-adapted perturbation theory with a single-determinant wavefunction. *J. Chem. Phys.* **2015**, *143* (22), 224107.
(77) Luu, D.; Patkowski, K. Overcoming Artificial Multipoles in Intramolecular Symmetry-Adapted Perturbation Theory. *J. Phys. Chem. A* **2023**, *127* (1), 356−377.

https://doi.org/10.1021/acs.joc.6c00154
J. Org. Chem. 2026, 91, 4829−4841

3. Danksagung

Zu guter Letzt möchte ich die Gelegenheit nutzen, dieser Dissertation noch einige persönliche Worte hinzuzufügen. Eine solche Arbeit entsteht nie durch die Hand einer einzelnen Person. Sie erfordert zwar viel Geduld, Hingabe und Durchhaltevermögen, vor allem aber ein besonderes Team, das einen auf diesem Weg begleitet, unterstützt und manchmal auch daran erinnert, warum man eigentlich angefangen hat. Allen, die zu dieser Dissertation und zu den vergangenen Jahren beigetragen haben, möchte ich an dieser Stelle von Herzen danken.

Prof. Dr. Peter R. Schreiner, PhD, danke ich für die einzigartige Möglichkeit, meine Dissertation in seiner Arbeitsgruppe anfertigen zu dürfen. Besonders dankbar bin ich für die Freiheit, eigene Forschungsideen zu verfolgen und selbstständig an Forschungsprojekten arbeiten zu können. Diese Freiheit hat mir nicht nur ermöglicht, mich wissenschaftlich weiterzuentwickeln, sondern auch persönlich zu wachsen.

Prof. Dr. Richard Göttlich danke ich für die Erstellung des Zweitgutachtens sowie dafür, ebenso wie **Prof. Dr. Bernd Smarsly** und **Prof. Dr. Siegfried Schindler**, Teil meiner Prüfungskommission zu sein und dem Interesse an dieser Arbeit.

Meinem ehemaligen Betreuer, **Dr. Lars Rummel**, möchte ich einen ganz besonderen Dank aussprechen. Mit dir habe ich bereits während meines Masters und anschließend während der Promotion viele gemeinsame Projekte verwirklicht, von deiner Erfahrung profitiert und viel von dir gelernt. Du hast mir den Weg in die wissenschaftliche Arbeit geebnet und den entscheidenden Grundstein für diese Arbeit gelegt. Ohne deine wissenschaftliche und didaktische Fähigkeit, deine Unterstützung und dein Vertrauen wäre diese Arbeit in dieser Form nicht entstanden. Dafür bin ich dir sehr dankbar.

Michaela Richter und Dr. Jörg Neudert danke ich für die stets schnelle, unkomplizierte und ausgezeichnete administrative Unterstützung.

Dr. Dennis Gerbig danke ich für die niemals endende Odyssee der Clusterwartung und für die geduldige und freundliche Unterstützung in allen computerchemischen Belangen.

Dr. Raffael C. Wende und dem gesamten analytischen Team danke ich für die stets reibungslose Analytik, selbst in Zeiten besonders hohen Probenaufkommens.

Dr. Heike Hausmann, Dr. Jonathan Becker und Ephrath Solel Moroshko, PhD danke ich für die großartige Zusammenarbeit und die Durchführung unzähliger NMR-

Messungen, Einkristallstrukturanalysen und computerchemischer Rechnungen. Ohne eure Unterstützung hätten viele der in dieser Arbeit zusammengeführten Projekte nicht erfolgreich abgeschlossen werden können.

Meinem Laborkollegen und Co-Autor Michael Fuhrmann danke ich für die vielen Synthesen, die du im Rahmen unserer gemeinsamen Projekte übernommen hast, sowie für dein umfangreiches synthetisches Wissen, das du nicht nur mit mir, sondern auch mit unseren Studierenden geteilt hast. Die Zusammenarbeit mit dir hat die Arbeit im Labor definitiv bereichert.

Saskia N. Krug, dir möchte ich ebenfalls noch einmal ganz persönlich danken. Vielen Dank für das Vertrauen, mit mir bereits während des Studiums an gleich zwei Projekten zu arbeiten, und für die vielen Synthesen, die du dafür durchgeführt hast. Ich hoffe, dass ich mein Wissen an dich Weitergeben konnte. Für deine nun beginnende Promotion wünsche ich dir viel Erfolg!

Ein besonderer Dank gilt auch der Vielzahl an Studierenden: **Anna Hof, Theo Engel, Nils F. Hacket, Valeria Malynych, Anna Shurando und Salome Wagner** für euer Interesse am Thema „London Dispersion“ mitzuwirken und mich während meiner Promotion zu unterstützen.

Charlotte E. Lauter und Jan M. Metzler danke ich für die erholsamen Mittagspausen, die vielen fachlichen Diskussionen und natürlich für eine unvergessliche gemeinsame Reise in die USA.

Meinen ehemaligen und aktuellen Kolleginnen und Kollegen am Organisch-Chemischen Institut der JLU, insbesondere **Dr. Henrik F. König, Dr. Finn M. Wilming, Dr. Bastian Bernhardt, Dr. Jan M. Schümann, Dr. „Maddie“ J. Sowden, Dr. Nikolaos Vagkidis, Dr. Akkad Danho, Oliver Pereira, Tom Kirschstein, Eliane Mitura und Benito Marazzi** danke ich für die schönen Jahre, die wir gemeinsam verbracht haben, für die vielen Freundschaften, die dabei entstanden sind, und für all die Dinge, die wir voneinander lernen durften.

Meiner Familie danke ich für die bedingungslose und immerwährende Unterstützung. Vom Studium über die Promotion bis zum heutigen Tag. Danke, dass ihr immer an mich geglaubt, mich unterstützt und mir den Rücken freigehalten habt.

Die letzten Worte gebühren **Judith K. Metz.** Dir habe ich zu verdanken, dass nicht nur die Promotion eine schöne und besondere Zeit war, sondern auch die Jahre, die wir währenddessen gemeinsam verbringen durften. Danke, dass du mich auf diesem Weg begleitet hast. Ich freue mich auf die Jahre, die noch gemeinsam folgen werden!